An analysis of ebullition dynamics in agricultural reservoirs using novel automated sensors

A Thesis Submitted to the College of
Graduate and Postdoctoral Studies
In Partial Fulfillment of the Requirements
For the Degree of Master of Environment and Sustainability
With the School of Environment and Sustainability &
the Global Institute for Water Security
University of Saskatchewan
Saskatoon, Canada

By

Richard E. J. Helmle

Permission to use

In presenting this thesis in partial fulfillment of the requirements for a Postgraduate degree from the University of Saskatchewan, I agree that the Libraries of this University may make it freely available for inspection. I further agree that permission for copying of this thesis in any manner, in whole or in part, for scholarly purposes may be granted by the professor or professors who supervised my thesis work or, in their absence, by the Head of the Department or the Dean of the College in which my thesis work was done. It is understood that any copying or publication or use of this thesis or parts thereof for financial gain shall not be allowed without my written permission. It is also understood that due recognition shall be given to me and to the University of Saskatchewan in any scholarly use which may be made of any material in my thesis.

Disclaimer

Reference in this thesis to any specific commercial products, process, or service by trade name, trademark, manufacturer, or otherwise, does not constitute or imply its endorsement, recommendation, or favoring by the University of Saskatchewan. The views and opinions of the author expressed herein do not state or reflect those of the University of Saskatchewan, and shall not be used for advertising or product endorsement purposes.

Requests for permission to copy or to make other uses of materials in this thesis/dissertation in whole or part should be addressed to:

Director
School of Environment and Sustainability
University of Saskatchewan
117 Science Place, Kirk Hall
Saskatoon, Saskatchewan, S7N 5C8, Canada

OR

Dean
College of Graduate and Postdoctoral Studies
University of Saskatchewan
116 Thorvaldson Building, 110 Science Place
Saskatoon, Saskatchewan, S7N 5C9, Canada

Abstract

Freshwater systems are an important component of biogeochemical processing within terrestrial landscapes. Only recently has the importance of these systems for contributions to atmospheric budgets of methane (CH_4), carbon dioxide (CO_2) and nitrous oxide (N_2O) been recognized at large spatial scales; however, fluxes of the gases remain poorly described. Smaller aquatic systems (≤ 1 ha) may have a greater role in global carbon (C) cycling than their larger counterparts, partly due to the large collective area of small water bodies. Constructed reservoirs — like the headwater reservoirs in South Tobacco Creek Watershed (STCW), Manitoba, investigated herein — are of particular interest as they, among other benefits, trap nutrients and terrestrial C. Trapped materials in these shallow lentic water bodies are subject to enhanced biogeochemical processing and can be released as greenhouse gases (GHG), including CH_4 dominated bubble release from sediments (ebullition). Measurement of ebullition using traditional and novel techniques demonstrated that these reservoirs are hotspots of CH_4 generation and release. Across eight reservoirs the mean littoral ebullitive CH_4 flux was 2.6 (0.1–6.9) mmol m^{-2} d^{-1} during the open-water period of 2017 and was stimulated by autochthonous C fixation — showing the strongest relationships with total ammonia nitrogen and chlorophyll *a*. This highlights the importance of nutrient export to, and eutrophication within, these systems for stimulating methanogenesis. Mean littoral ebullitive CH_4 flux increased significantly during the 2018 open-water season to 12.7 (0.6–40.5) mmol m^{-2} d^{-1}, and these interannual variations were linked to warmer water temperatures, a result of year to year differences in local hydroclimate. Ebullitive fluxes of CH_4 from these reservoirs are higher than reported for most other lentic freshwater systems globally, but interestingly the rates varied strongly both across and within reservoirs. The use of novel sensors allowed ebullition rates in deeper zones to be quantified, and these measurements demonstrated that pelagic fluxes were significantly higher than those from littoral zones — an artifact of reservoir morphology. High temporal resolution records from the sensors also permitted detection of diel variations of ebullitive flux, and was significantly synchronous with sediment temperature at that timescale. This work advances our ability to quantify ebullition fluxes through the use of new sensors by allowing more comprehensive investigations of fluxes than previously possible, and also provides a foundation for agricultural reservoir siting and management strategies to minimize trade-offs associated with CH_4 emissions while continuing to confer benefits in terms of nutrient retention and flood control.

Dedication

I would like to dedicate this thesis to my uncle, Tony C. Greenwood. He was truly the most environmentally appreciative and connected person I have known. Along with being a friend, role model, and father figure in my life, he gave me a chance and saw something in me when others did not. He instilled in me the joy that can arise from small things and the pride that can arise from hard work and dedication. He largely fueled my passion and determination for shaping my life towards environmental and sustainability sciences, while simultaneously having fun and enjoying life to the fullest. Words cannot describe how much he is missed. I would also like to dedicate this thesis to my close family and friends for their continual support, encouragement, and mental relief throughout — completion of this project would not have been possible without you all.

Acknowledgments

First and foremost, I would like to acknowledge my supervisor, Dr. Colin Whitfield, for providing invaluable knowledge, guidance, and support throughout the entire process. I am forever grateful for the opportunity and experienced gained working under him. Secondly, I would like to acknowledge my field partner, Carlie Elliott, for her work ethic, patience, and determination over both field seasons. A special acknowledgement to Dr. Nicholas Kinar, and the Smart Water Systems Laboratory, for assistance with the electronics developed for my research, and support throughout. I would also like to acknowledge Dr. Helen Baulch and the SaskWatChe lab group. A special thank you to the following individuals for helping with field expeditions, laboratory work, analyses, and support: Anthony Baron, Lisa Boyer, Emily Cavaliere, Lauren Dyck, Nicholas Dylla, Kimberly Gilmour, Amy Hergott, Cameron Hoggarth, Laura McFarlan, Magali Nehemy, Katy Nugent, Danielle Spence, Stephanie Witham, and Dr. Nora Casson's University of Winnipeg lab group (Hamza Amjad, Emily Kroft, Jeremy Leathers, and Kody Oleson). I would like to acknowledge Dr. Daniel Karran for assistance with data analysis, and Lorelei Ford for introducing and recommending me to the MES opportunity; along with both of their friendship and support throughout. I would like to acknowledge the Deerwood Soil and Water Management Association and, in particular, Les McEwan, Jim Pankiw and all other landowners of the STCW reservoirs. I would like to acknowledge: the grant from Agriculture and Agri-Food Canada (Agricultural Greenhouse Gases Program) and the Faculty Start-up Grant (USask) awarded to C.J. Whitfield for funding my research; as well as the Global Institute for Water Security and the School of Environment and Sustainability for the space and platform to perform. Lastly, I would like to acknowledge my committee members, Dr. Tim Jardine and Dr. Jean-Michel DeVink, for their time, advice, and constructive criticisms throughout.

Table of contents

List of tables

List of figures

List of abbreviations

AAFC	Agriculture and Agri-Food Canada
ADC	analog to digital conversion
AES	automated ebullition sensor
AESv1	automated ebullition sensor version 1
AESv2	automated ebullition sensor version 2
Ah	ampere hour
ANOVA	analysis of variance
BMP	beneficial management practice
BT	bubble trap
˚C	degrees Celsius
C	carbon
CH_3COOH	acetate
CH_4	methane
Chl *a*	chlorophyll *a*
cm	centimeter
CO_2	carbon dioxide
d^{-1}	per day
DO	dissolved oxygen
DOC	dissolved organic carbon
DSWMA	Deerwood Soil and Water Management Association
FFE	fresh forced ebullition
FID	flame ionization detection
GC	gas chromatography
GHG	greenhouse gas
GIWS	Global Institute for Water Security
GWP_{100}	Global Warming Potential over the next 100 years
H_2	dihydrogen
H_2O	water
H_2SO_4	sulphuric acid

ha	hectare
HDPE	high-density polyethylene
Hz	hertz
ID	inner diameter
IR	infrared detector
kPa	kilopascal
L	liter
L m^{-2}	liter per square meter
L^{-1}	per liter
LOI	loss on ignition
m	meter
m^{-2}	per square meter
mA	milliamp
MB	mean bias
MDL	method detection limit
mg	milligram
mg L^{-1}	milligram per liter
min	minute
mL	milliliter
mL m^{-2}	milliliter per square meter
mL m^{-2} d^{-1}	volumetric ebullitive flux
mm	millimeter
mmol	millimole
mmol m^{-2} d^{-1}	molar ebullitive flux (specific to individual greenhouse gas)
Mn^{4+}	manganese
mV	millivolt
N	nitrogen
N_2	dinitrogen gas
N_2O	nitrous oxide
NDIR	non-dispersive infrared
NH_3	ammonia

NH_4^+	ammonium
nm	nanometer
NO_2^-	nitrite
NO_3^-	nitrate
NRMSE	normalized root mean square error
OM	organic matter
P	phosphorus
Pa	pascal
PC1	principle component 1
PC2	principle component 2
PCA	principle components analysis
PCB	printed circuit board
PFRA	Prairie Farm Rehabilitation Administration
ppmv	parts per million by volume
PTFE	polytetrafluoroethylene
PVC	polyvinyl chloride
s^{-1}	per second
SO_4^{2-}	sulphate
STCW	South Tobacco Creek Watershed
TAN	total ammonia nitrogen
TCD	thermal conductivity detection
TCMW	Tobacco Creek Model Watershed
TOC	total organic carbon
V	voltage
WEBs	Watershed Evaluation of Beneficial Management Practices
µg	microgram
µm	micrometer

Chapter 1: General introduction

1.0 Introduction

Global atmospheric methane (CH_4) concentrations are of concern, as CH_4 is among the strongest biogenic greenhouse gases (GHG) and levels have significantly increased since the industrial age (Dlugokencky et al. 2011). With a 100-year global warming potential (GWP_{100}) 25 times that of carbon dioxide (CO_2) (IPCC 2014) and increased indirect warming effects due to atmospheric interactions (i.e. tropospheric ozone and stratospheric water vapour) (Hansen and Sato 2001), atmospheric CH_4 has the potential to strongly contribute to future global climate change. Anthropogenic activity since the industrial revolution, and arguably the period of intense landscape modification preceding it (Ruddiman 2005), has led to an ~2.5-fold increase in atmospheric CH_4 concentrations (Mitchell et al. 2013). Landscape manipulation (Keller et al. 1990), landfills (Themelis and Ulloa 2007), biomass burning (Hao and Ward 1993), waste-water treatment (Daelman et al. 2012), the extraction and utilization of fossil fuels (Kirschke et al. 2013; Schwietzke et al. 2016) and agricultural activity (Kirschke et al. 2013) all play a role. Agricultural practices differ, however, in that they are multi-faceted, involving multiple contributing factors (e.g. landscape manipulation, biomass burning, fossil fuel combustion, livestock aggregation, manure management, and nutrient re-distribution) (Environment Canada 2019). Despite agricultural activity being acknowledged as among the strongest sources contributing to increases in atmospheric CH_4, its contributions may be underestimated. Small lentic aquatic systems harbor ideal conditions for the creation of biogenic GHGs, and the underlying processes may be stimulated by nutrient additions reaching these waters as a result of agricultural practices (Tangen et al. 2015; Ollivier et al. 2019).

Generally overshadowed by larger systems, small aquatic systems ($\leq$ 1 ha) have the potential to be significant GHG sources (Downing 2010; Ollivier et al. 2019). Agriculturists often create small impoundments/reservoirs to aid agricultural practices (e.g. livestock watering, irrigation, soil moisture availability, water management [drainage]); biogeochemical processes necessary for GHG formation may be heightened here as a result of activity in the agriculturally-worked (e.g. cultivation, nutrient additions) contributing areas. Downing and Cole (2006) demonstrated that over 3% (~460 million ha) of the terrestrial landscape is occupied by water bodies — of which ~1.7% (~7.7 million ha) are low-tech small agricultural reservoirs. These

reservoirs are also estimated to occupy up to 6% of global agricultural land area, but are often not inventoried, and may be increasing in number (Downing and Cole 2006). Agricultural reservoirs need to be accurately quantified in terms of GHG production to enhance our understanding of their contribution to both agricultural, and therefore global, GHG budgets. One of the obstacles hindering progress in quantifying GHG budgets is the CH_4 dominated release pathway of ebullition — the release of gases produced in the sediments in the form of bubbles (Bastviken et al. 2011). Ebullition is highly variable, both spatially and temporally, and has proven very challenging to accurately measure (Ostrovsky 2003; Leifer et al. 2004; Wik et al. 2016). The proficiency of agricultural production, and utilization of water resources therein, in the face of growing global population and an impending water crisis (Schindler and Donahue 2006) is of increasing importance. During an era of climate shift and an uncertain climatic future it is critical to consider potential trade-offs associated with GHG emissions from all sectors, as this can yield holistic management or adaption strategies.

1.1 Freshwater systems and nutrient cycling

Freshwater systems — such as rivers, lakes, reservoirs, wetlands and estuaries — are hotspots for biodiversity and key habitat for organisms that metabolize, transform and excrete nutrients (Dudgeon et al. 2006). These systems interact with their surroundings by exchanging energy and water, including the atmosphere (Krinner 2003), and play an important role in the elemental cycles of carbon (C) and nitrogen (N). Notably, freshwaters act as zones of transport and receiving sites; which can result in transformation and storage of materials. Nitrogen and allochthonous C, incorporated into terrestrial biomass via biological fixation (Falkowski 2000), can be carried from the land to aquatic systems (e.g. via fluvial load, wet and dry deposition) and represent a major input of organic material to freshwater systems. Lotic transport of this material may end up trapped or contained in standing or low-flow (lentic) aquatic environments. Terrestrial-freshwater interfaces, and the convergence of different hydrologic flow paths at the margins of lentic systems, are known to be biogeochemical hot spots having intermittent hot moments (McClain et al. 2003). Lentic systems (lakes, stream pools, reservoirs, impoundments, wetlands) are depositional zones for suspended sediments and nutrients, and internal cycling of this material can stimulate GHG production and release (Cole et al. 2007; Maeck et al. 2013). In

other systems, GHG emissions from lentic waters can be sustained by inputs of water supersaturated with GHG (Whitfield et al. 2010; Weyhenmeyer et al. 2015).

Nitrogen is a fundamental, but often limiting, nutrient in natural systems, and therefore can be an important determinant of primary production in the terrestrial biosphere (Phoenix et al. 2003). The availability of N in aquatic systems has increased with human activity, partly due to the application of N fertilizer to bolster crop yields (Galloway et al. 1996). A significant amount of this N can be lost to water systems via runoff, groundwater leaching, or direct entry (Carpenter et al. 1998). Nitrogen inputs to freshwaters can be stored in the sediments, biologically assimilated, emitted to the atmosphere as gaseous nitrogen (N_2 and N_2O) produced via denitrification, or removed via fluvial transport from the water body (Harrison et al. 2009). In addition to the potential to increase GHG release from aquatic systems, detrimental effects of increased N loads to receiving waterbodies include eutrophication and decreased water quality (Schindler et al. 2012). Both N and C are essential for the metabolic processes of many organisms, presenting opportunities for the biogeochemical cycles of these elements to interact in freshwater systems. While N and phosphorus (P) are critical for productivity and C sequestration in lentic systems, the focus herein will be on C dynamics, specifically CH_4, as it is the dominant ebullitive gas.

The storage, transformation and transport of C within the continents is complex. Lentic surface waters receive and store allochthonous C, but in productive aquatic systems, biological fixation of C via photosynthesis (autochthonous C) can be important for C inputs (Dean and Gorham 1998). Carbon that is assimilated via primary production in these systems may decompose and be deposited as sediment — potentially released to the atmosphere as CO_2 (Kling et al. 1991) or CH_4 (Bubier and Moore 1993) — or also exported via discharge. The annual amount of C that reaches inland freshwater systems (lakes, rivers and reservoirs) is nearly twice as much as the riverine flux to the ocean (Cole et al. 2007), suggesting the importance of freshwater systems for C storage, and release back to the atmosphere. Constructed water bodies are particularly important for inland C cycling (Soumis et al. 2004). Generally, where these structures are implemented by damming a stream to store water, the hydrologic regime and processes that affect C cycling in these systems are altered. Heightened particle trapping in constructed reservoirs results in considerably higher sedimentation rates shortly after

construction (Stallard 1998). Carbon that was destined for transport elsewhere can instead have a short-term (release to atmosphere) or long-term (burial in the sediments) fate.

Although lentic systems can be an active site for C cycling processes, the importance of different processes for C release to the atmosphere remains poorly understood, particularly for small water bodies. It has long been thought that large amounts of both allochthonous and autochthonous forms of C are processed and stored within lentic systems (Mulholland et al. 1982; Kempe 1984). Despite this knowledge, global C budgets are generally based on data from the largest lakes and rivers only (Schimel 1995), wherein the contribution of small bodies has been assumed negligible. Recent work has advanced our understanding of the frequency and distribution of small water bodies (Downing and Cole 2006; Downing et al. 2012). Small water bodies have been both underestimated in quantity historically, and are increasingly thought to represent an important component of the global C cycle (Downing 2010; Premke et al. 2016). The role of smaller freshwater systems in global C budgets remains a knowledge gap — one that limits efforts to quantify and predict climate feedbacks (Cole et al. 2007; Battin et al. 2009; Bastviken et al. 2011).

1.2 Reservoir greenhouse gas dynamics

Constructed reservoirs are created for a number of reasons: hydroelectric power generation, flood and erosion mitigation, drought relief, a tool supporting agricultural practices, and recreation, among others. Filling reservoirs with water often floods riparian and terrestrial landscapes, killing plants and other organisms, reducing their capacity to assimilate CO_2 from the atmosphere, and allowing microbial decomposition to transform this organic material to CO_2, CH_4 and N_2O (Kelly et al. 1997; Venkiteswaran et al. 2013). Notably different from natural systems, hydroelectric reservoirs are considered by some as a zero-emission source of energy, but this energy production has a tradeoff in the form of enhanced aquatic GHG emissions (Rudd et al. 1993; Tremblay et al. 2004). Emissions can vary greatly between reservoirs over different spatial scales depending on a number of factors, such as the size of flooded land area, availability of labile organic material and various physicochemical conditions. The amount of organic C flooded can be proportional to the short-term flux of gaseous C emissions (St. Louis et al. 2000). Reservoir age can affect GHG flux as newly immobilized C is more efficiently decomposed

(Abril et al. 2005). Thus, following construction this flux can be enhanced as the initial flooded biomass is subject to biogeochemical processing and emission, eventually declining until a balance is achieved by processing new C inputs (St. Louis et al. 2000; Barros et al. 2011). In large reservoirs on agricultural landscapes, the C balance of reservoirs can shift at sub-annual timescales from being a sink to a source — a large pulse of water from a storm event or hydrologic turnover can promote GHG emissions (Jacinthe et al. 2012). The processes controlling GHG flux are not well understood and evidently sensitive in lentic systems, and managing these reservoirs can be important to GHG release (Harrison et al. 2017). Developing accurate GHG budgets for these systems is complicated; consequently, annual budgets of agricultural reservoirs are uncertain — partly because the CH_4 dominated emission pathway of ebullition is highly variable, may be event driven, and is rarely quantified in detail.

Being a globally relied upon and environmentally demanding practice, the management of both terrestrial and aquatic systems in agricultural landscapes is of increasing importance — particularly with respect to C mobilization and nutrient flux to reservoirs. Some agricultural practices are dependent on large quantities of water, and agriculturists often create small impoundments on their lands to address this need. In addition to particle trapping, agricultural activity in the surrounding contributing areas can contribute to these reservoirs receiving increased nutrient inputs — promoting aquatic primary production and, therefore, increased autochthonous inputs of C (Huttunen et al. 2003). Allochthonous C loads to these systems can also be high due to material redistribution via erosion associated with tillage practices (McCarty and Ritchie 2002). Thus, these reservoirs are often subject to much higher inputs of C than those in non-agricultural landscapes, making them a prime candidate for C-based GHG emissions. Agricultural GHG budgets have typically had a strong focus on terrestrial sources (i.e. manure management, fertilized soils, livestock, crop burning) (Environment Canada 2019) — overlooking the small reservoirs that are common in most agricultural landscapes. Low-tech small agricultural reservoirs bring many benefits to an operation and can be easily implemented. Prior to construction of the reservoirs, materials reaching these sites would have likely been processed in and emitted from downstream systems. While the overall effect of constructed reservoirs on net emissions is uncertain, the role of these landscape features for GHG emission is a critical unknown with respect to agricultural GHG budgets.

1.3 Methanogenesis and emissions

Constructed reservoirs disrupt lotic sediment loads, leading to rapid sediment accumulation (Syvitski et al. 2005). This sedimentation, along with autochthonous C deposition, results in benthic oxygen consumption as organic materials decompose — typically leading to an anaerobic environment rich in labile C. Lentic reservoirs harbour anaerobic conditions necessary for CH_4 production, resulting in an important source of atmospheric CH_4 (Cole et al. 2007; Bastviken et al. 2011; Deemer et al. 2016). Anaerobic zones at or just below the water-sediment interface are an ideal environment for the microbial production of CH_4 (Rudd and Hamilton 1978). Microorganisms called methanogens thrive in anoxic and highly reduced conditions to produce CH_4 as the end product of anaerobic respiration through two main reactions: (1) Hydrogenotrophic methanogenesis — the oxidation of dihydrogen (H_2) with CO_2 acting as the electron acceptor to produce H_2O and CH_4 (Horn et al. 2003); and (2) Acetoclastic methanogenesis — the breakdown of acetate (CH_3COOH) into CO_2 and CH_4 (Cicerone and Oremland 1988; Bridgham et al. 2013). Although there has been evidence of methanogenesis in aerobic aquatic conditions, it is rare and not fully understood (Bogard et al. 2014; Martins et al. 2017). The presence of competing electron acceptors, such as nitrate (NO_3^-) and sulphate (SO_4^{2-}), can restrict methanogenesis in anaerobic conditions (Zehnder and Stumm 1988; Segers 1998). Methane emissions have been shown to be significantly reduced in the presence of SO_4^{2-} (Pennock et al. 2010).

Typical pathways for emission of CH_4 are diffusion at the air-water interface, plant-mediated transfer, and ebullition, while turbulent flow in lotic waters may also contribute to degassing at some locations. Nonetheless, ebullition is the dominant pathway for the emission of CH_4 and other volatile species to reach the atmosphere in shallow systems (Baulch et al. 2011; Stanley et al. 2016) and can represent upwards of 90% of a system's total CH_4 flux (Keller and Stallard 1994; Walter et al. 2006). This flux pathway could be directly related to net sediment CH_4 production (Fendinger et al. 1992). In anaerobic sediments, resultant CH_4 bubbles from microbial degradation coalesce, eventually becoming buoyant enough to breach into the water column and ascend to the atmosphere (Boon and Mitchell 1995). Heightened production and subsequent release of CH_4 via ebullition can be expected with sediments of smaller particle size, rich in organic material (Sanders et al. 2007).

Not all CH_4 generated in sediments is released to the atmosphere through ebullition. Some CH_4 molecules can diffuse from a rising bubble into the water column; however, CH_4 has a significantly lower mole fraction solubility in water (2.81×10^{-5} at 20˚C) compared to CO_2 (7.07×10^{-4} at 20˚C) (Deemer et al. 2016) and freshwater systems are to a great extent supersaturated with CH_4 (Whitfield et al. 2011; Stanley et al. 2016), which may be indicative of strong source environments. Consumption of CH_4 by methanotrophs in aerobic waters also occurs (Rudd et al. 1976; Bastviken et al. 2004), but due to the rapid ascent of these bubbles through the water column, particularly in shallow systems, there is limited opportunity for consumption. Sediment bubbles are more easily released during an event of decreased atmospheric pressure (Tokida et al. 2007) or a drop-in water level (Harrison et al. 2017), as the force on the sediment layer is reduced. In temperate wetlands there can be heightened ebullitive emissions during early spring with higher labile C available and plant-root growth (Wilson et al. 1989), and late summer/early fall due to foliage inputs and hydrologic turnover in larger lakes (Riera et al. 1999). The winter production of CH_4 can accumulate during ice-covered periods and the release following spring thaw can represent an important fraction (up to 27% in lakes) of annual CH_4 emissions (Canelhas et al. 2016; Denfeld et al. 2018) in a very short time. Water temperature can affect how efficiently organic C is transformed into gaseous emission in these systems as increases in decomposition, as well as reaction rates, are associated with a rise in temperature (Kellner et al. 2006). Tokida et al. (2007), as well as Barros et al. (2011), linked C emissions with latitude and changes in atmospheric pressure. Because ebullition is an important pathway for atmospheric CH_4, understanding the drivers and dynamics of this process will enhance the ability to quantify the magnitude of this atmospheric C flux at larger scales.

1.4 Background information and study rationale

1.4.1 Tobacco Creek Model Watershed

The Tobacco Creek Model Watershed (TCMW) in south-central Manitoba, is a unique initiative — unifying academic efforts, local policy, and landowners — that aims to acknowledge and address the inter-related sustainability issues involved with agriculture (TCMW 2004). Referred to as a “living laboratory” the TCMW is one of nine watersheds used in Agriculture and Agri-Food Canada’s (AAFC) Watershed Evaluation of Beneficial Management

Practices (WEBs) program. The WEBs initiative is focused on assessing the environmental and economic performance of beneficial management practices (BMP) (AAFC 2007).

Water issues are long-standing in the region where clay-based soils result in considerably higher erosion and nutrient loading into streams and subsequent water quality issues for downstream stakeholders (TCMW 2004; Glozier et al. 2006). Periods of peak flow and fast drainage are often followed by droughts that put pressure on agriculturists (Hope et al. 2002). In 1979, a spring runoff event triggered a 50-year flooding event in the South Tobacco Creek Watershed (STCW). It was catastrophic for residents, and agricultural losses were estimated at more than $820,000 (TCMW 2004). To resolve these issues, in the 1980s the Deerwood Soil and Water Management Association (DSWMA) and local landowners began implementing a network of 50 small headwater reservoirs in the TCMW. Twenty-six of the 50 reservoirs are located on or near the Manitoba escarpment in the TCMW's westernmost sub-watershed, STCW.

The STCW is positioned directly on the Manitoba Escarpment, which drops ~ 60 m elevation in a < 3 km stretch (Tiessen et al. 2011). The terrain of the escarpment can result in local climate variations, with mean annual temperatures of 2.2˚C and 3.3˚C on the upper and lower reaches, respectively (Hope et al. 2002). Similarly, mean annual precipitation can be 590 mm above and 500 mm below the escarpment; 75% of which occurs as rainfall outside of the winter months (Hope et al. 2002). Early agricultural settlement in the region sparked intensive vegetation removal and wetland drainage (TCMW 2004) — which contributed to eventual implementation of the headwater reservoir network. The watershed drains 7,638 ha of agricultural land, of which ~ 70% has been under cultivation (Hope et al. 2002). Generally speaking, the implemented reservoirs studied herein were positioned and sheltered down in depressions, with the immediate landscape comprised largely of *Typha*, unmanaged grasses, and perennial woody vegetation — potentially acting as a buffer between the reservoir and surrounding agricultural landscapes (e.g. cultivated cropland, livestock pasture).

Along with providing water resources to aid agricultural practices, the reservoirs in STCW have demonstrated the ability to reduce peak flow during spring freshet and summer storm events and reduce nutrient loads carried in stream (Tiessen et al. 2011; Liu et al. 2014). These reservoirs exhibit high denitrification rates but are often NO_3^- saturated owing to high N loads (Gooding and Baulch 2017). Effectiveness of the small headwater dams were investigated by the Prairie Farm Rehabilitation Administration (PFRA) in 1996. Individual dams reduced

peak flow by up to 90%, while collectively the dam network in STCW was found to reduce overall downstream peak flow by 25% — comparable to that of larger dam structures (Yarotski 1996).

While successfully mitigating water-related issues faced in the STCW, these systems are trapping and storing large amounts of N and C. Recent and rapid sedimentation here provides ideal conditions for transformation of organic C to emittable gaseous forms — particularly CH_4 in the anaerobic sediments. The small dam network has shown to be an effective BMP for water management, but may provide the conditions for CH_4 production and release via ebullition. The identification of CH_4 dynamics in these reservoirs from this study can inform landowners on management strategies (e.g. water level control, construction morphology) of these reservoirs in a way that promotes the ecosystem and agricultural services they provide, while minimizing trade-offs associated with CH_4 emissions.

1.4.2 Significance and research rationale

The factors that control ebullitive emission of CH_4 from small agricultural reservoirs is an important knowledge gap; to date, the role of freshwater systems in agricultural GHG budgets remains largely unknown. Methods and techniques, including modelling approaches, typically used to quantify fluxes do not accurately incorporate the ebullitive contribution to CH_4 flux (Deemer et al. 2016). Ebullition is a challenging emission pathway to accurately measure as fluxes have high spatial and temporal variability (Wik et al. 2016). Ebullition often occurs in sporadic intermittent large events randomly across a water body and predicting the locations of these episodes is challenging (Walter et al. 2006). Collectively, the investigations performed in this study will allow analysis of the dynamics of ebullitive flux in these systems (i.e. the driving physicochemical characteristics, interannual variations of the reservoirs, spatial variations within the reservoirs). In addition, this work seeks to develop a sensor capable of measuring ebullitive flux at high temporal resolution in shallow lentic systems as a means of enhancing understanding of ebullition's sporadic nature in these systems and improving the capacity to quantify GHG fluxes. High temporal resolution measurement can provide insight into the factors driving ebullitive emissions, allowing connections to be made with other temporal records of physicochemical characteristics of these systems. Accurate quantification and CH_4 budgets

should be well understood prior to developing GHG mitigation strategies. Considering the complexity of chemical interactions that can occur within the water column, emissions via ebullition may be mitigated through improvements to reservoir management strategies. Therefore, studies targeting the processes that stimulate methanogenesis and subsequent bubble release can be particularly valuable. Furthermore, enhanced measurement of ebullitive flux rates from agricultural reservoirs during the open-water season will ultimately improve understanding of C cycling dynamics here, and clarify their role in agricultural GHG budgets.

Studying CH_4 dynamics in the STCW reservoirs presents an excellent opportunity to evaluate how these and similar systems contribute to C emissions within agricultural landscapes, and ultimately, enhance our understanding of how agricultural GHG budgets contribute to global C cycles. Accurate GHG budgets are useful for societies as they seek to better understand, adapt and respond to unpredictable future climate conditions during an era of population growth. Informing landowners of how to best manage agricultural reservoirs as a BMP can enhance the effectiveness of this tool. This can help to ensure these reservoirs continue to confer the numerous benefits (e.g. livestock watering, irrigation, erosion and flood control, nutrient retention) while also minimizing environmental effects (GHG emissions). The effort to establish new sensor technology for use in this study should eventually improve capacity to quantify ebullition through uptake of this tool by researchers elsewhere.

1.5 Thesis structure and research objectives

One purpose of this research was to first develop an automated sensor-based instrument that measures volumetric ebullitive flux at high temporal resolution in shallow waters, while also providing the capacity for convenient manual extraction of gas samples for laboratory analysis of GHG concentrations. A goal of the instrument design is to permit automated operation in both littoral reservoir zones to which sampling has been biased previously, as well as deeper (pelagic) zones where fluxes are typically unquantified. Secondly, the data from the automated sensors, along with other data collections methods were used to quantify the rate of CH_4 release via ebullition across eight agricultural reservoirs, and further analyze the dynamics of CH_4 ebullitive flux from these reservoirs in a number of ways.

This introduction is followed by two individual manuscript chapters, each aiming to address multiple objectives. The manuscript chapters (2 and 3) are followed by a general conclusions chapter, and list of references. Supporting information for each data chapter follows in appendices. Specifically, the objectives for chapters 2 and 3 are as follows:

Chapter 2: A novel sensor for automated high temporal resolution measurement of ebullition from shallow lentic systems

- Objective 1: Develop an automated sensor to measure the process of ebullition in shallow aquatic systems.
- Objective 2: Test and establish whether the sensors can reliably measure gas volumes under laboratory conditions.
- Objective 3: Deploy and field-validate operation of the sensors.

Chapter 3: Methane flux from agricultural reservoirs: rates and drivers of ebullition

- Objective 1: Quantify littoral ebullitive CH_4 fluxes from the study reservoirs in 2017.
- Objective 2: Identify the reservoir physicochemical parameters driving littoral ebullitive CH_4 flux across the study reservoirs.
- Objective 3: Determine if there is interannual variation in littoral ebullitive CH_4 flux from the study reservoirs (i.e. compare rates in 2017 to rates in 2018).
    - H_0: Ebullitive CH_4 flux rates do not vary interannually.
    - H_a: Ebullitive CH_4 flux rates do vary interannually.
- Objective 4: Identify whether ebullitive CH_4 flux from the study reservoirs is different between littoral and pelagic zones.
    - H_0: Ebullitive CH_4 flux rates do not vary between pelagic and littoral zones within a reservoir.
    - H_a: Ebullitive CH_4 flux rates do vary between pelagic and littoral zones within a reservoir.
- Objective 5: Identify whether ebullition fluxes are coherent with other reservoir parameters (i.e. pressure on sediment, water temperature, dissolved oxygen concentrations).

Chapter 2: A novel sensor for automated high temporal resolution measurement of ebullition from shallow lentic systems

R. E. J. Helmle[1,2,3], N. J. Kinar[1,2], and C. J. Whitfield[1,2,3]

Prepared for Submission: Limnology and Oceanography Methods

[1]Global Institute for Water Security, University of Saskatchewan, Saskatoon, Saskatchewan, Canada.

[2]Smart Water Systems Laboratory, University of Saskatchewan, Saskatoon, Saskatchewan, Canada.

[3]School of Environment and Sustainability, University of Saskatchewan, Saskatoon, Saskatchewan, Canada.

2.0 Abstract

Freshwater systems are important sites for biogeochemical transformations. Contributions of small water bodies to global greenhouse gas emissions may be larger than previously understood, with small systems (≤ 1 ha) potentially more important than larger systems. Ebullition can be an important pathway for methane (CH_4) release into the atmosphere, but as this process typically remains unquantified, its role remains uncertain. This study introduces and tests a novel automated sensor for measuring ebullitive fluxes in shallow aquatic environments at high temporal resolutions. This automated ebullition sensor (AES) consists of a floating deck mounted to the top of a submerged collection chamber attached to an inverted funnel. Pressure changes in the collection chamber resulting from the accumulation of gas released from benthic sediments are measured by a differential pressure sensor. The differential pressure sensor is part of a custom-built electrical circuit designed for data storage and energy efficiency. Two separate versions of this system allowed for up to six months of continuous operation on a single charge of a low-capacity battery (4.5 | 7 Ah). The result is a low-cost (~ $700) technique for automated, high resolution measurement of ebullitive flux in shallow lentic systems. Here, the AES is described, and its accuracy and precision is tested in the laboratory. Measurements obtained with the AES were compared to measurements from a manual bubble trap (BT), and human sampling errors were quantified by the use of multiple operators. The experiments demonstrated that, for volumes 81–98 mL, the AES sensor reliably measured known

quantities of manually-added air with an average mean-bias of 0.9 mL and average normalized root mean square error of 2.4%. It is then demonstrated, using data from field sites, how the AES sensor can be reliably used to detect ebullition events in these shallow systems. This instrument enhances the capacity to quantify ebullition fluxes, providing an opportunity to better understand the role of ebullition and its contribution to greenhouse gas emissions from open water systems.

2.1 Introduction

Large amounts of both allochthonous and autochthonous carbon (C) are stored and processed within lentic systems, potentially accounting for a portion of missing C in global budgets (Mulholland et al. 1982; Kempe 1984). Yet global C budgets are generally based on data from large lakes and rivers (Schimel 1995), whereas the contribution of small water bodies has been assumed to be relatively low. Small water bodies (≤ 1 ha) can also be challenging to quantify over large spatial scales — leading to underestimates in their abundance and consequently the total area of surface water within a region. Recent work has advanced our understanding of the frequency and distribution of small water bodies and shown that collectively small systems likely occupy a similar surface area to that of larger systems (Downing and Cole 2006; Downing et al. 2012). These water bodies likely represent an important component of the global C cycle (Downing 2010; Holgerson and Raymond 2016; Premke et al. 2016). Carbon cycling dynamics of small water systems like ponds (DelSontro et al. 2016) and beaver-ponds (Weyhenmeyer 1999) have been studied in some regions, alluding to their significance. Due to their varying nature, the role of small water bodies in global C budgets remains a critical unknown — hindering efforts to quantify and predict climate feedbacks (Cole et al. 2007; Battin et al. 2009; Bastviken et al. 2011).

The primary pathways related to emission of C-based biogenic greenhouse gases (GHG) are (1) diffusion through the water column, (2) plant-mediated transfer, and (3) the release of bubbles from sediment (ebullition). Sedimentation and deposition of organic material in reservoir benthic zones typically lead to oxygen consumption as organic materials decompose. This decomposition can lead to anaerobic conditions situated at or just below the water-sediment interface, with the presence of labile C providing an ideal environment for the microbial production of CH_4 (Rudd and Hamilton 1978). Resultant CH_4 bubbles from anaerobic microbial

degradation coalesce, eventually becoming buoyant enough to breach the sediment and ascend through the water column to reach the atmosphere (Boon and Mitchell 1995), or, in deeper systems, dissolve in the water column. Aquatic environments with sediments of small particle size that are rich in organic material can lead to heightened production and subsequent release of CH_4 via ebullition (Sanders et al. 2007). Ebullition is an important pathway for the emission of CH_4 and other volatile chemical species that reach the atmosphere (Baulch et al. 2011; Deemer et al. 2016; Stanley et al. 2016). Ebullition rates could be directly related to net CH_4 production in the sediments of aquatic systems (Fendinger et al. 1992).

Methods and techniques used to quantify CH_4 fluxes from water bodies include acoustics (Greinert and Nützel 2004; Ostrovsky et al. 2008; Frouzova et al. 2015), resistivity (Slater et al. 2007), surface deformations (Glaser et al. 2004; Comas et al. 2007), and eddy covariance (Schubert et al. 2012); however, they often focus on large spatial scales or do not accurately distinguish the contributions of individual pathways (Deemer et al. 2016). Ebullition is a challenging emission pathway to accurately measure, as fluxes (both volumetric and molar) have high spatial and temporal variability (Wik et al. 2016), making it difficult to predict the location of these sporadic and intermittent events (Walter et al. 2006). Analysis of the volume emitted via ebullition is also important, as it can vary greatly in chemical composition and in CH_4 concentration across large and small spatial scales (DelSontro et al. 2016). Ebullitive flux is commonly measured by manually-operated submerged funnel traps. These BTs are deployed for either a short period with high sampling frequency (Keller and Stallard 1994; Bridgham et al. 2013) or for long periods with low sampling frequency (Baulch et al. 2011; Venkiteswaran et al. 2013). Capturing ebullitive events over a short period of time can miss ebullition events entirely, potentially leading to a false representation of ebullitive contribution to a system's total C budget. Manual methods integrating ebullition fluxes over longer deployment periods are likely sampled less frequently. Consequently, these methods do not provide adequate detail in the processes driving ebullition. Automated techniques to measure ebullition at a high resolution present one solution thus far and have been focused on deep-water systems such as lakes (Varadharajan et al. 2010) and oceans (Washburn et al. 2001).

Existing automated techniques for quantifying ebullition are designed in such a way that precludes their use in shallow ($\leq$ 4 m) water bodies. Measuring ebullitive flux at a high temporal resolution in shallow lentic systems (e.g. shallow wetlands, ponds, and reservoirs) must address

several challenges, including limited water column height, a sufficient collection chamber volume to accommodate potentially large fluxes, and the logistics of mooring the sensors in these systems.

The purpose of this research is to develop and test instrumentation that can accurately measure volumetric ebullitive flux at a high temporal resolution in shallow water systems, while also providing the capacity to conveniently collect samples for analysis of gas concentrations. These collected concentration samples can be applied to the volumetric measurements — permitting analysis of molar ebullitive gas flux. Automated systems of this nature that collect high quality data will assist both in quantifying GHG emissions from these and similar systems and in enhancing understanding of the ebullitive process itself. The sensors introduced herein could improve the spatial resolution of ebullition within reservoirs by allowing deployment in pelagic zones, which are often unsuitable for manually-operated or deep-water systems, thereby improving the ability to quantify and ultimately enhance our knowledge of ebullition in these systems. The design and use of two different sensor instrument types are described in detail herein, including laboratory performance tests, calibration procedures, operational details, and field performance. These sensors provide temporal data at a high resolution that can aid identification of the processes driving release of gas by ebullition at a number of different time scales and offer considerable advances over other automated systems for which published descriptions are available.

2.2 Methods

Automated ebullition sensors (AES) were developed specifically for sampling ebullition in shallow aquatic systems, such as ponds, wetlands, and agricultural reservoirs. The AES sensor design is based on the deep-water sensor technology described by Varadharajan et al. (2010). However, the AES designed here is suitable for deployment in shallow aquatic systems. The AES intercepts bubbles ascending through the water column and stores them in a collection chamber under the water surface. Pressure changes are recorded digitally as gas accumulates in the collection chamber. The AES design also features a surface-accessible sampling port for extraction of air samples to provide for laboratory gas concentration analysis without the need to remove the device from the water. The result is a low-cost, submerged-funnel instrument, which

provides the capacity to quantify both the volume and concentration of gases released through the ebullitive pathway at a high temporal resolution over a deployment time of weeks to months.

2.2.1 Mechanical design

Two different versions of the AES were developed: AESv1 and AESv2, with the latter being an upgraded and enhanced version of the former. Both versions of the device feature the same general design and consist of a submerged inverted funnel attached to a gas collection chamber suspended below the water surface from a flotation deck. The flotation deck also allows access to the sampling port (a PVC ball valve) and supports the electronics enclosure. The collection chamber of both devices comprises a schedule 40 PVC pipe. All fittings are conjoined with appropriate schedule 40 PVC adaptors and fused together with standard PVC cement. The inverted funnel is constructed from 28-gauge galvanized steel, which is cut and folded into a cone (diameter 50 cm). The seam was metal bonded and riveted before being sealed with water-resistant caulking and painted with corrosion-preventing enamel. The cone was bolted and glued to a piece of solid PVC rod (5.0 cm length and 7.5 cm diameter), which was machine beveled to match the upper dimensions of the cone and hollowed out for attachment to the bottom of the collection chamber via PVC cement. The cone and collection chamber are suspended below a flotation deck composed of high-density polyethylene puckboard, match fitted with styrofoam insulation board and surrounded by buoyancy tubes or floats to keep the assembly afloat in the water.

2.2.1.1 Automated ebullition sensor v1 mechanical design

The first version of the sensor (AESv1) is the longest and largest of the two (Figure 2.1; Table 2.1). The small section directly above the inverted funnel of AESv1 is a 40 cm length of 2 cm inner diameter (ID) pipe. To accommodate the large ebullitive flux expected to occur in shallow bodies of water and permit longer deployment times without increasing the collection chamber length, the AESv1 has a collection chamber section with increased diameter. This section with expanded volume consists of a 30 cm length of 10 cm ID pipe. The AESv1 has a total height of 101 cm (from base to the flotation deck) and collection capacity of 2775 mL. Due to a finite capture capacity, air collected in the AESv1 needs to be manually expelled

periodically via the integrated sampling port. This port is also used to draw samples of captured air for gas concentration analysis in the laboratory.

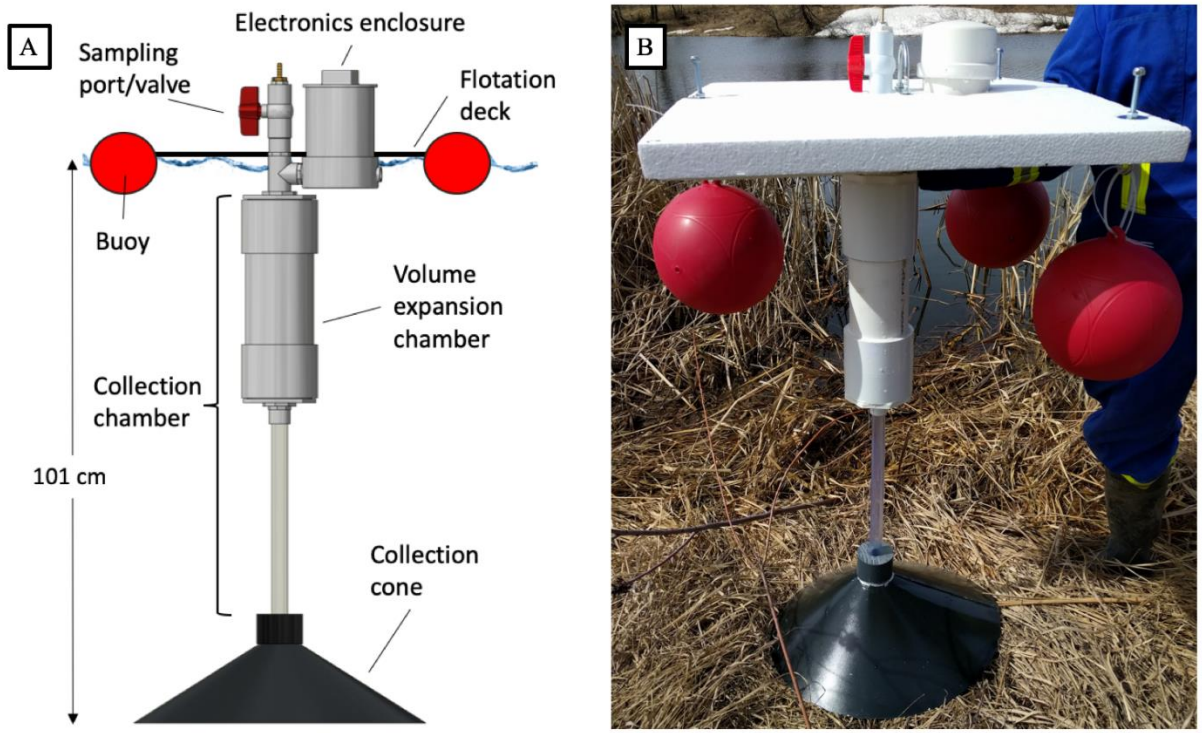

Figure 2.1: Conceptual diagram of automated ebullition sensor v1 (AESv1), deployed in water (A), and actual image of AESv1, prior to 2017 deployment in reservoir in south-central Manitoba, Canada (B).

2.2.1.2 Automated ebullition sensor v2 mechanical design

Improvements in the AESv2 design enhance the capability of the device to measure ebullitive fluxes by an automated purging of the collection chamber, thereby overcoming some limitations of the AESv1 (finite capture capacity, manual purging, higher potential for gas exchange via diffusion with underlying water). An electronic solenoid is integrated into the design to provide automated purging. The solenoid (Table 2) remains closed until a specified pressure is reached in the collection chamber. Once this threshold is reached, the solenoid opens momentarily before closing again after the air has been expelled from the chamber, at which point the next logging sequence is initiated. This allows the device to be smaller in both length (53 cm) and chamber volume (105 mL), thereby further mitigating depth restrictions, accommodating high rates of ebullitive flux, and limiting the need for frequent field visits. The

entire collection chamber on AESv2 in this study is a 30 cm length (although chamber length is flexible as desired) of 2 cm ID pipe, which should improve the accuracy of gas concentration samples collected from the collection chamber, owing to a much smaller water-air interface in the chamber. Although a 30 cm pipe was used in this study, the actual length can be flexible. The AESv2 also possesses an additional electronics enclosure to house additional sensors that supply measurements of atmospheric pressure and air temperature at the reservoir surface. Inclusion of these sensors allows a closer analysis of reservoir characteristics that drive the process of ebullition, as well as a larger battery to meet solenoid power demand.

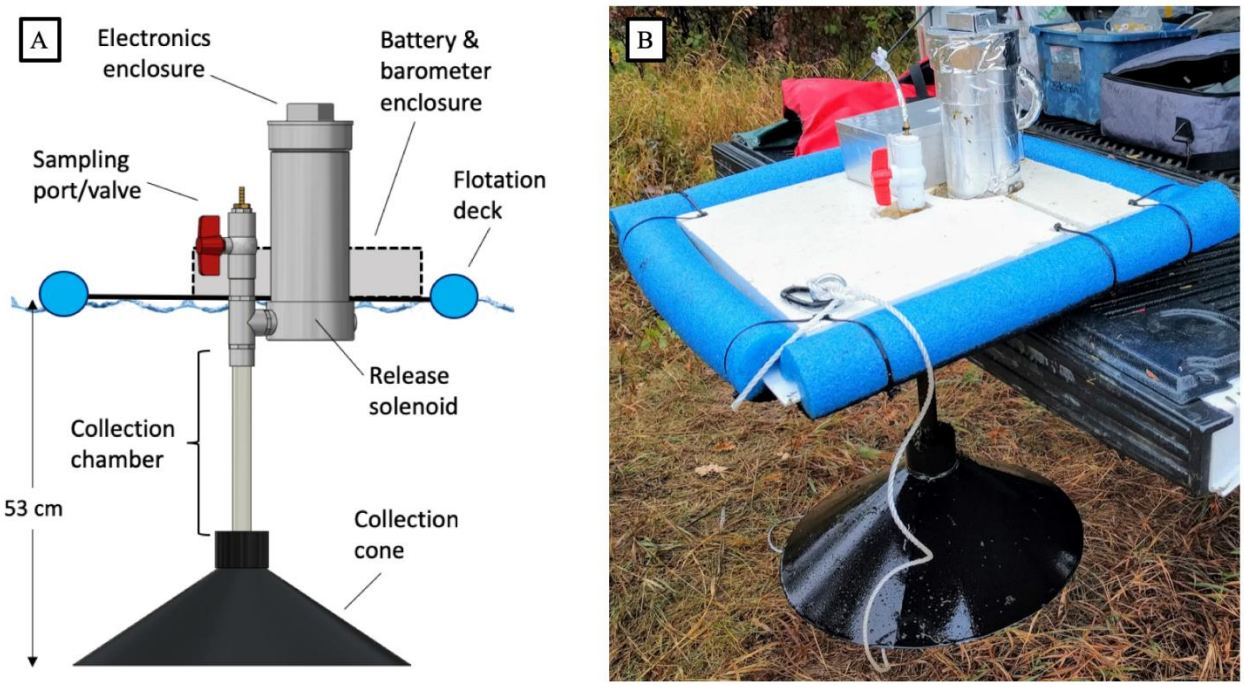

Figure 2.2: Conceptual diagram of automated ebullition sensor v2 (AESv2) deployed in water (A), and actual image of AESv2, during 2018 field campaign in South Tobacco Creek Watershed, Manitoba, Canada (B).

2.2.1.3 Electronics enclosure

Both versions of the AES feature a custom-fabricated enclosure to house the electronics. Constructed with a 10-cm ID PVC pipe, the enclosure(s) were custom-built to attach to the body of the AES and accommodate the pressure sensor ports. Enclosure lengths of 20 cm and 25 cm were selected to accommodate the entire circuit of AESv1 and the larger circuit board of AESv2, respectively. This enclosure was custom-built to attach to the body of the AES and accommodate

the pressure sensor ports. Barbed hose fittings mounted inside the electronics enclosure were used to conjoin the pressure sensor ports to the AES body using Tygon tubing (Figure 2.3). Both versions of the AES were designed so that the electronics enclosure is partially submerged, permitting one port of the differential pressure sensor to track pressure changes at the top of the collection chamber, whereas the other port was exposed to the water column. This configuration permitted a differential measurement of pressure as per Varadharajan et al. (2010). Following construction and prior to testing and deployment, both AES versions were leak tested to ensure an airtight seal throughout the body of the sensor.

The AESv2 used an additional outdoor water-resistant enclosure (24 cm long, 16 cm wide, and 9 cm high) to house additional components. This enclosure stores a larger battery, while also providing locations to mount additional sensors and an antenna for LoRa wireless communications technology.

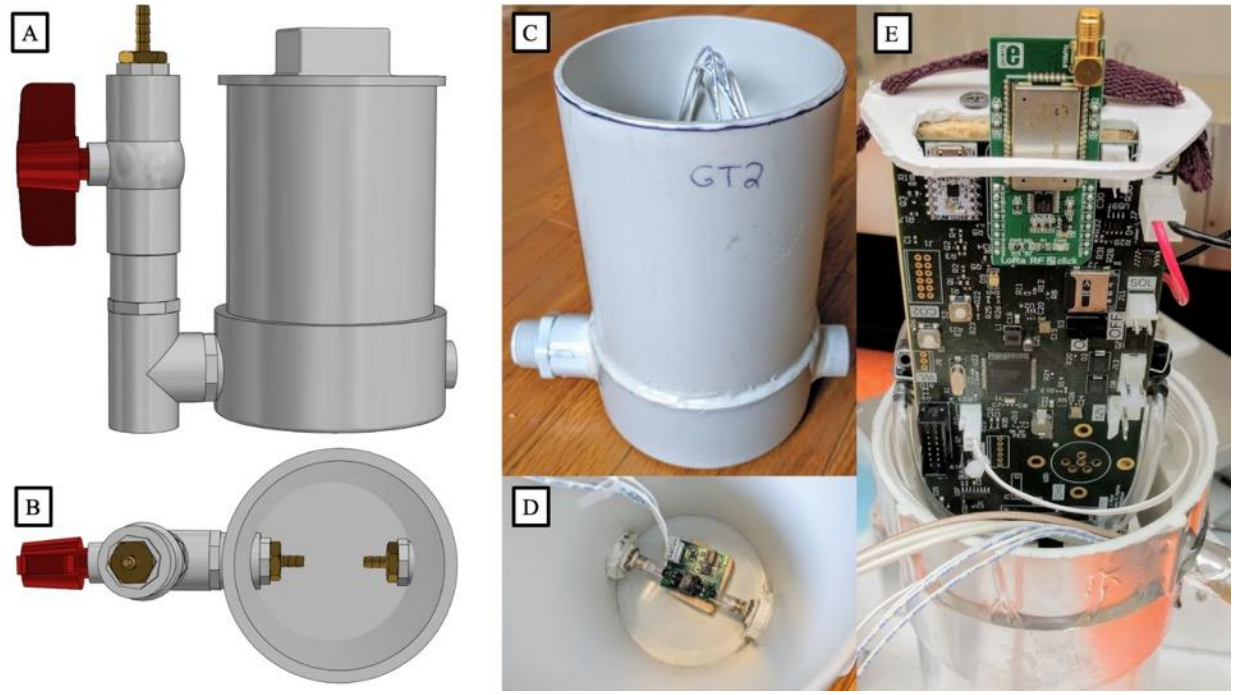

Figure 2.3: Modelled representation of the electronics enclosure and sample port/release valve design (A); internal view of the modelled electronics enclosure (B); photo of the actual electronics enclosure during testing (C); internal image of the actual AESv1 electronics enclosure with the circuit board conjoined (D); image of the AESv2 electronics enclosure with circuit board (E).

Table 2.1: Mechanical components and specifications for both versions of the automated ebullition sensors (AES).

Mechanical Components	AESv1	AESv2
Chamber Material	Schedule 40 PVC	Schedule 40 PVC
Collection Cone Material	28-gauge galvanized steel	28-gauge galvanized steel
Total Height*	101 cm	53 cm
Collection Cone Diameter	50 cm	50 cm
Chamber Diameter	2 cm	2 cm
Expansion Chamber Diameter	10 cm	NA
Total Capacity	2775 mL	105 mL

*Total height refers to depth of sensor bottom from the water surface (i.e. excluding the sampling port and electronics enclosure)

2.2.2 Electrical design and operation

Pressure change associated with the accumulation of ebullitive gas in the collection chamber was monitored in both versions of the AES using a differential pressure sensor (Table 2) mounted on a custom-designed printed circuit board (PCB).

2.2.2.1 Automated ebullition sensor v1 electrical design

The PCB for AESv1 amplifies changes in voltage associated with the pressure sensor so that these voltages can be recorded by an Onset HOBO datalogger (Table 2). The datalogger has a finite capacity, so the length of operation is determined by the desired resolution (e.g. 100.5 days at a resolution of 10 min). The datalogger also records temperature inside the electronics enclosure. These data were therefore used as a proxy of gas chamber temperature for final volume calculation (Section 2.2.4) in the absence of other water temperature measurement methods (as chamber temperature should be near that of the surrounding water) and assumed valid. Also required for final volume calculation is a measurement of atmospheric pressure (Section 2.2.4), which for AESv1, needs to be obtained from the nearest weather station in the absence of *in situ* measurements. The electrical system in AESv1 is powered by a rechargeable

lead-acid Powersonic battery (6V; 4.5 Ah), resulting in ~180 days of deployment on a single battery charge (theoretical). The datalogger has an analog to digital conversion (ADC) with a relatively low resolution (12 bit), and the maximum voltage that can be digitized is 2.5V, so the minimum voltage theoretically resolvable (step size) by the datalogger is 0.6 mV. The circuit for AESv1 follows Varadharajan et al. (2010), but some changes were made to resistor values to ensure that the PCB interfaces within the voltage operating range of the datalogger. The PCB, battery, and datalogger are placed inside the electronics enclosure.

2.2.2.2 Automated ebullition sensor v2 electrical design

The AESv2 is built on a completely redesigned custom PCB. The upgraded PCB provides a number of benefits, including an integrated gas release solenoid, microSD card support for flexible data storage capacity, increased energy efficiency, increased digital resolution (24 bit), and the ability to initiate remote communication via a LoRa wireless transmitter. In addition to increased efficiency, the redesigned sensor permits the addition of a solar panel to allow for longer deployment times. The electrical system in AESv2 has a quiescent current of less than 28 mA and is powered by a rechargeable lead-acid battery (12V; 7.0 Ah), thereby resulting in ~250 days of deployment (theoretical) on a single charge without the aid of a solar panel. The AESv2 PCB also has an extended thermistor that measures the temperature of the gas inside the chamber, which offers the advantage of enhanced accuracy of volume calculations (Section 2.2.4). Additionally, the AESv2 features an externally exposed digital barometer (Table 2.2) that supplies measurements of atmospheric pressure and air temperature at the water surface; these data permit a closer analysis of actual *in situ* environmental conditions at the AES — enhancing accuracy of volume calculations (Section 2.2.4).

Table 2.2: Electrical components and specifications for both versions of the automated ebullition sensors (AES).

Electrical Components	AESv1	AESv2
Pressure Sensor	Honeywell 26PCAFA6D	Honeywell 26PCAFA6D
Data Storage	Onset/ HOBO U12-013	MicroSD card
Data Extraction	HOBOware	Micro USB | SD card
Power Source	Powersonic PS-640-F1	Powersonic PS-1270-F1
Printed Circuit board Manufacturer	Alberta Printed Circuits	Beta Layout
Microcontroller	NA	Texas Instruments MSP430
ADC Resolution	12 bit	24 bit
Chamber Temperature	Proxy via HOBO logger	Via extended thermistor
Release Solenoid	NA	ZnDiy-BRY 2P2508
Digital Barometer	NA	TE Connectivity MS5806
Secondary Enclosure	NA	Bud Industries PN-1341
Wireless Transmitter	NA	LoRa RN2903 (not utilized)

2.2.3 Calibration technique

The relationship between the voltage output of the pressure sensor and the height of gas was determined by a laboratory experiment using a machine vision calibration technique based on measurements involving a digital camera. This technique extends the calibration procedure of Varadharajan et al. (2010). Water is added to a vertical cylinder connected to the differential pressure sensor (Figure 2.4). This cylinder is similar to the chamber used in the AES (Figure 2.4). Prior to the pressure sensor calibration procedure, the camera is calibrated to the cylinder using a checkerboard target, permitting real-world dimensions of the cylinder to be measured digitally. Coloured water is slowly added to the cylinder over the course of the calibration by squeeze bottle. Changes in the height of the column of water in the cylinder are recorded at a

sampling rate of 29.97 frames s^{-1}, while voltage measurements from the pressure sensor are recorded at 1 Hz. The height of fluid in the cylinder is determined by machine vision measurement algorithms and is related to the voltage output of the pressure sensor (Kinar, pers. comm. 2017).

The machine vision signal processing is used to determine calibration coefficients by linear curve-fitting:

$$h_g = mE + b \tag{2.1}$$

where h_g is the height of gas in the chamber (cm), m is the calibration coefficient (cm V^{-1}), E is the output voltage of the pressure sensor (V), and b is the calibration offset (cm). In this manner, sensor pressure measurements can be used to determine the height of gas in the collection chamber. The physical dimensions of the AES collection chambers and the height of gas from equation 2.1 are used to quantify the volume of gas collected.

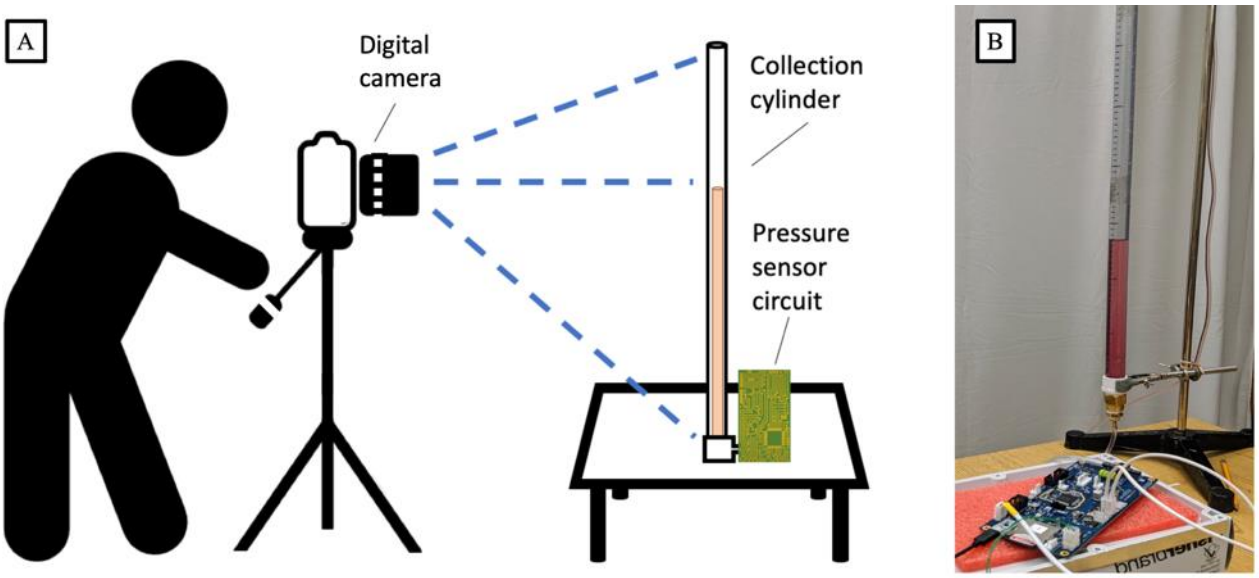

Figure 2.4: Conceptual diagram of setup for photo-visual calibration technique (A); photo of set-up during the actual photo-visual calibration at the University of Saskatchewan, Canada (B).

2.2.4 Data processing

Calculating the volume captured by the AES involves computing the height of gas h_g in the collection chamber (equation 2.1). A height offset value (σ) was used as a correction coefficient during volume calculations to compensate for non-ideal system effects associated with temperature offsets and differences between the output voltage during calibration and the output voltage associated with differential pressures recorded by the sensor. The height offset value σ ensures that $h_g = 0$ when no gas is present in the collection chamber. The offset value was selected by averaging the first two measurements immediately following launch. The volume of gas captured in the collection chamber (V_c) is thus calculated as follows:

$$V_c = (h_g - \sigma)A \tag{2.2}$$

where volume is in cm^3 and A is the cross-sectional area of the collection chamber (cm^2). The final volume of gas was then adjusted to standard conditions and corrected for any compression due to increasing pressure as the air-water interface extends below the water surface, using additional measurements from the circuit board and the combined gas law:

$$V_f = \frac{T_2 \; V_c \; (\rho_{water} \; g \; h_g \; + \; P_{atm})}{T_1 P_2} \tag{2.3}$$

where V_f is the adjusted volume in the collection chamber (cm^3 | mL), T_2 is standard temperature (273.15 K), V_c is the captured volume in the chamber (mL), ρ_{water} is the density of water (998 kg m^{-3}, g is acceleration due to gravity (9.81 m s^{-2}), h_g is the height of gas accumulated in the collection chamber (m), P_{atm} is atmospheric pressure at the water surface (Pa), T_1 is the temperature of the volume in the collection chamber (K), and P_2 is the standard pressure (101,325 Pa) at the standard temperature.

2.2.5 Laboratory experiment

Validation experiments were conducted in the laboratory to determine AES accuracy and precision. Each experiment was carried out by placing an AESv2 in a tank of water, thereby

simulating field deployment (Figure 2.5). A length of Tygon tubing was attached to the base of the collection cone to allow gas to be injected into the instrument. Initially, as the AES was deployed in the tank, the sampling port on the AES remained open, allowing the collection chamber to fill with water and the internal pressure to equilibrate. The other side of the Tygon tubing was capped with a Fisher Scientific 2-way luer valve accessible from outside the tank. Once the AES was in place the sampling port was closed, and the AES system was set to record measurements. Three trials of the experiment were conducted, with AES recording intervals set at 5 minutes for the first trial, and 4 minutes for trials two and three.

During the experiment, known and varying volumes of gas ranging from 2 mL to 20 mL were manually injected into the AES at random intervals using a 60 mL syringe, thereby simulating the spontaneity of ebullition. It should be noted that there may be manufacturing errors with respect to stamping/printing of measurement scale onto the syringe body, and so these injections are taken as a baseline for comparison and not assumed to provide highly accurate volumetric injections. To mitigate error, all injections were performed with the same new syringe. Immediately after each individual air injection, the Tygon tubing was flushed with water to purge any residual gas from the line into the AES collection chamber. The total volume of the Tygon tubing was less than 60 mL so that it could be fully flushed with water from a single 60 mL syringe, ensuring the entire gas volume reached the AES collection chamber. Following the experiment, the data were extracted and processed as outlined above to calculate the volume of gas collected by the AES.

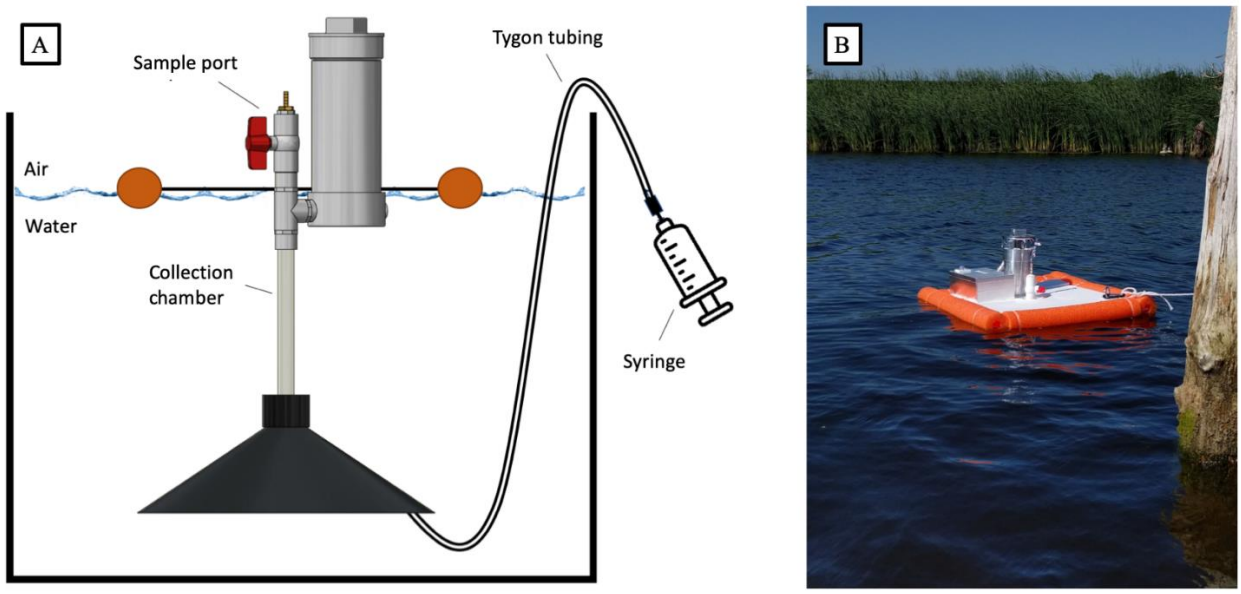

Figure 2.5: Conceptual diagram of automated ebullition sensor validation experiment (A); and photo of AESv2 deployed in the field in the South Tobacco Creek Watershed, Manitoba, Canada (B).

2.2.6 Bubble trap error comparison experiment

Experiments were conducted in the laboratory to assess typical operator errors associated with the manually-operated BTs — to compare them with AES operation errors. The use of manually-operated BTs (Baulch et al. 2011; Venkiteswaran et al. 2013) is a simple technique to measure ebullitive flux. These BTs are designed to capture ascending ebullition bubbles before they reach the atmosphere, allowing a cumulative volume of ebullition to be manually measured by an operator via syringe. The BTs used here are constructed of open-bottom Culligan® water cooler jugs, of known-diameter, that can be mounted to a fixed post within littoral zones (Figure 2.6). The BTs are deployed at a site such that the jugs are submerged, completely filled with water, and capped with rubber or neoprene septa fitted with Tygon tubing and a luer valve to act as a sampling port. The ebullitive volume accumulated in BTs over the time between site visits is measured manually via a syringe. The BTs are manually purged of gas after each site visit.

The experiment was carried out by placing a manual ebullition BT in the same receptacle of water used for the AES. Initially the BT was completely filled with water and the sampling port sealed. An additional length of Tygon tubing was positioned to allow gas to be injected through the open bottom of the BT. The Tygon tubing was capped with a Fisher Scientific 2-way

stopcock accessible from outside the tank. Known volumes of gas ranging from 18 mL to 205 mL were then injected into the BT at random using a 60 mL syringe. As above, to mitigate error, all injections and operator extractions were performed with the same new syringe. Immediately following each injection of gas, the Tygon tubing was fully flushed with water to purge any residual gas from the line, ensuring that the entire added gas volume reached the BT. Five different operators were invited to measure the quantity of gas in the BT using a 60 mL syringe and report the measurement of volume in the chamber. Different operators were used to quantify human errors associated with the BT measurements and help contextualize errors associated with AES.

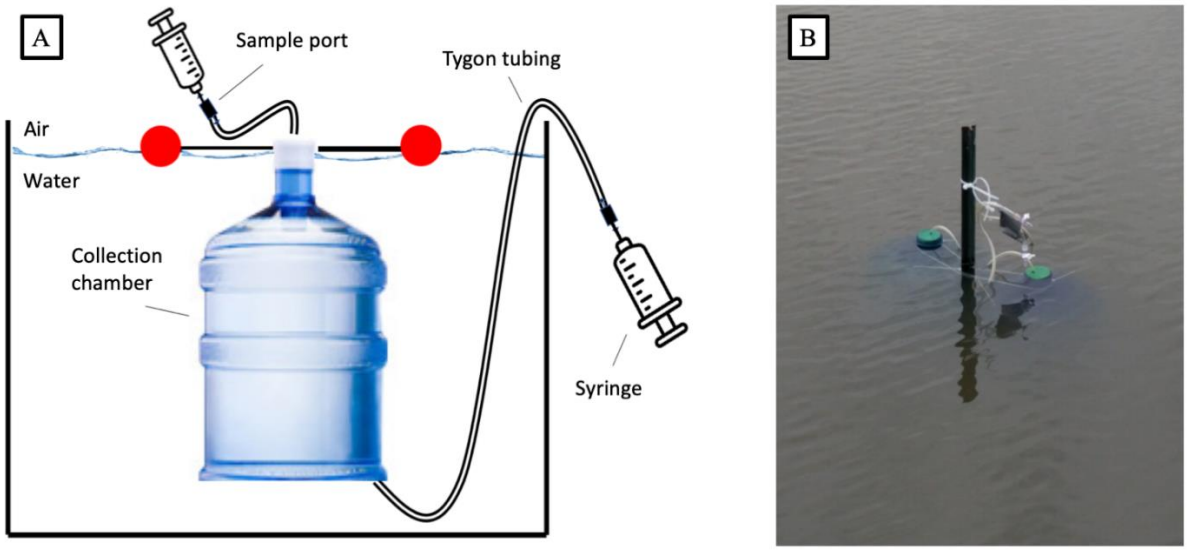

Figure 2.6: Conceptual diagram of bubble trap (BT) operator error experiment (A); photo of BT deployed in field in the South Tobacco Creek Watershed, Manitoba, Canada (B).

2.2.7 Field testing

Initial field tests of both AES versions were conducted during the open-water seasons of 2017 and 2018 in three small reservoirs located in the South Tobacco Creek Watershed (STCW) to illustrate field performance of the AES instruments. TCR04 is an ephemeral, shallow reservoir (max depth of ~1.4 m; April 2017) that was selected to test the operation of the shorter AESv2; this allowed comparison with BTs deployed at similar depths. The longer AESv1 was tested in deeper waters of TCR05 (max depth of ~3.7 m; April 2017) and TCR08 (max depth of ~2.6 m;

April 2017). The AESv2 was also deployed at TCR05 and TCR08, permitting a comparison of gas samples collected via multiple methods at a single site to evaluate whether AES design influences CH_4 concentration of air in the chamber.

In order to test the AES's ability to provide gas samples for concentration analysis, gas samples were extracted from the AES during each visit via syringe and subsequently transferred to an exetainer. For comparison, fresh forced ebullition samples (FFE) were also extracted from the reservoirs by wading in littoral zones and physically disturbing sediments to capture the immediate release of bubbles with a submerged funnel and inverted syringe, before transferring the bubbles to an exetainer. Both the FFE and AES samples were analyzed for CH_4 via gas chromatography (GC) using a Bruker Ltd. Scion 456 GC, at the Global Institute for Water Security (GIWS), University of Saskatchewan. Along with analyzing AES concentration sample reliability, this allows analysis of ebullitive GHG concentration variability both temporally in one location as well as spatially within reservoirs by observing measurements from two or three different locations (where permitted).

2.2.8 Data analysis

For all AES verification experiments, the BT operator experiment, and the field deployment data, the data were visualized, statistics analyzed, and results calculated using R: A Language and Environment for Statistical Computing, 2017 (R Core Team 2018; version 3.5.1).

The AES output data (at standard conditions) from the laboratory experiments were smoothed via a median filter, with a window size of three, to smooth-out voltage transients (package: 'stats'; function: 'runmed'). The cumulative manually added volume data was similarly converted to standard conditions using the combined gas law to enable comparison of the data. Three different techniques were used to determine how closely the AES calculated volume was to the manually added (known) volume. For the experiments, the injected volume recorded by the experimenter was assumed to be the known and correct benchmark for comparison.

Mean Bias (MB) was used to analyze the tendency of the AES to under- or over-estimate measurements of volume (Janssen and Heuberger 1995; Gupta et al. 2009). Reported in the same physical units (mL), a positive or negative MB indicates the degree of over or under estimation

of output values relative to the known values, respectively. Mean Bias was used on the data from each AES experiment (package: 'hydroGOF'; function 'me'), and is computed as follows:

$$MB = \frac{1}{n} \sum_{i=1}^{n} (x_o - x_k) \tag{2.4}$$

where n is the number of observations, i refers to the index of observations, x_o is the AES calculated volume, and x_k is the manually added known volume.

The Normalized-Root-Mean-Square-Error (NRMSE) (Janssen and Heuberger 1995) was used to compare output values (AES calculated) with known values (manually added). Normalized-Root-Mean-Square-Error is reported as a percent. A higher NRMSE indicates a greater difference between the output and known values, while an NRSME closer to 0 indicates the output more closely resembles the known values. An NRSME was used on the data from each AES experiment and is computed as follows:

$$NRMSE = \frac{\sqrt{\frac{1}{n} \sum_{i=1}^{n} (x_o - x_k)^2}}{\overline{x_k}} * 100 \tag{2.5}$$

where $\overline{x_k}$ is the mean of the manually added volume.

Operator error for volume measurements reported by operators for the BT experiment was described using relative percent error:

$$Error\ (\%) = \left(\frac{y_o - y_k}{y_k}\right) * 100 \tag{2.7}$$

where y_o is the volume reported by the operator, and y_k is the known volume added. The percent of error was calculated for all operators and then averaged.

To compare concentration samples extracted from both AESv1 and AESv2 with the FFE at TCR05 and TCR08, the data were first determined to be normal via visual inspection of histograms. As a result of the visual inspection of the data distribution indicating normality, a

parametric between-groups analysis of variance (ANOVA) (package: ‘stats’; function: [aov]) was performed on the CH_4 concentration data acquired via each sampling technique (AESv1, AESv2, and FFE). This is a necessary check, as storage of gas in the chamber could undergo compositional changes should individual gases diffuse into or out of the chamber prior to sampling. The residuals from the ANOVA tests were then also checked for normality via visual inspection of histogram and quantile-quantile plots, and determined to be normal (package: ‘stats’; function: [qqnorm]). The data residuals were also checked for homogeneity of variance (homoscedasticity) via Levene’s Test (package: ‘car’; function: [leveneTest]), where a p-value > 0.05 confirmed homoscedasticity. These statistical tests were selected based on the underlying assumption that CH_4 production as a component of ebullition is similar in both littoral and pelagic zones. A post-hoc TukeyHSD test (package: ‘stats’; function: [TukeyHSD]) was subsequently carried out on the ANOVA tests run on sampling techniques at TCR05 and TCR08, to identify differences between individual techniques within these sites. All p-values were Bonferroni corrected to provide each individual comparison with a 95% confidence interval. Due to the shallow nature of TCR04, this site was only equipped with an AESv2, so to compare AESv2 sensor concentration samples with FFE here, the data were similarly checked for normality, but determined to be nonparametric. As a result, a Mann-Whitney-Wilcox test (package: ‘stats’; function: [wilcox.test]) was performed.

2.3 Results

2.3.1 Automated ebullition sensor volume measurement

In the laboratory experiments, the volume of injected air quantified using the AES closely agreed with manually added volumes during each experiment. An MB of each experiment (volumes 81–98 mL) demonstrated that the AES slightly over-estimated total volume on average by 0.9 mL with a range of 0.2 mL to 1.8 mL. This apparent overestimation by the AES may be due to combined errors associated with syringe precision of operator injections. The NRMSE for each experiment showed that on average the sensors deviated from the known values by 2.4% (1.4–3.6%). All three experiments showed close linearity when the AES output values were compared directly with the known values (Figure 2.7).

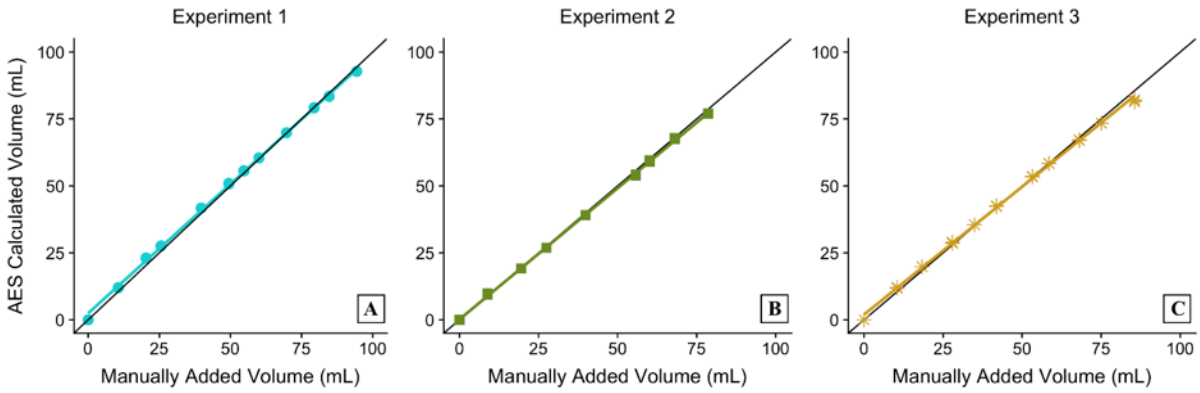

Figure 2.7: Direct comparison plot of the manually added volume (mL) with the AES calculated volume output (mL) over the duration of trials one (A), two (B), and three (C). The black line represents a 1:1 relationship, the coloured line is a line of best fit for each individual experiment, and the points represent the observations.

2.3.2 Bubble trap volume measurement error

The results of the BT operator experiment resulted in an average error of 1.3% and ranged from –1.1 to 5.6% (Table 2.3). The reliability of each operator varied throughout their respective trials, with only one individual (Operator 4) failing to report a correct (the known added) volume at least once. Operator 2 performed the best with an average error of 0.7% (0–1.5%), while Operator 4 performed the worst with an average error of 2.4% (0.7–5.6%). There was an overall tendency for Operators to overestimate the volume in chamber throughout the 20 trials performed, with only one underestimation by Operator 4. All volumes less than 51 mL, except for one (18 mL), were perfectly measured (to the nearest mL) — indicating that operator error may be compounded for BTs deployed where ebullition fluxes are high, or where lower fluxes are sampled less frequently (i.e. more aliquots required to complete the total gas measurement).

Table 2.3: Table of bubble trap operator percentage error experiment.

Sampler	Vol Added (mL)	Vol Measured (mL)	Difference (mL)	Error (%)
Operator 1	26	26	0	0
Operator 1	136	137	1	0.7
Operator 1	152	154	2	1.3
Operator 1	71	73	2	2.8
Operator 2	37	37	0	0
Operator 2	49	49	0	0
Operator 2	80	81	1	1.2
Operator 2	205	208	3	1.5
Operator 3	19	19	0	0
Operator 3	65	66	1	1.5
Operator 3	72	74	2	2.8
Operator 3	109	113	4	3.7
Operator 4	88	87	–1	–1.1
Operator 4	135	136	1	0.7
Operator 4	194	198	4	2.1
Operator 4	18	19	1	5.6
Operator 5	51	51	0	0
Operator 5	135	135	0	0
Operator 5	101	102	1	1
Operator 5	148	152	4	2.7

2.3.3 Concentration sample comparison

Comparison of the AES and FFE samples revealed that the AES provides samples with satisfactory CH_4 concentrations. Concentration ranges from the AES were similar to FFE concentrations (Figure 2.8), and the AESv2, when compared with FFE, demonstrated CH_4 concentrations that are not significantly different from each other ($p > 0.05$ at all three sites). The AESv1 also yielded CH_4 concentrations that were not significantly different from either AESv2 or FFE at TCR08. The only exception in the comparisons was AESv1 deployed in the deepest region (~3.7 m) of the larger TCR05. This region was deepest of all AES deployment in the three study reservoirs. The CH_4 concentrations of samples extracted from AESv1 at TCR05 were

significantly higher when compared to FFE samples (ANOVA $F(2,107) = 35.31$, $p = 0.001$; TukeyHSD < 0.001) and to those extracted from an AESv2 (ANOVA $F(2,107) = 35.31$, $p = 0.001$; TukeyHSD < 0.001), which was deployed for only a short period in 2017 in a shallower region (~2 m) of the reservoir.

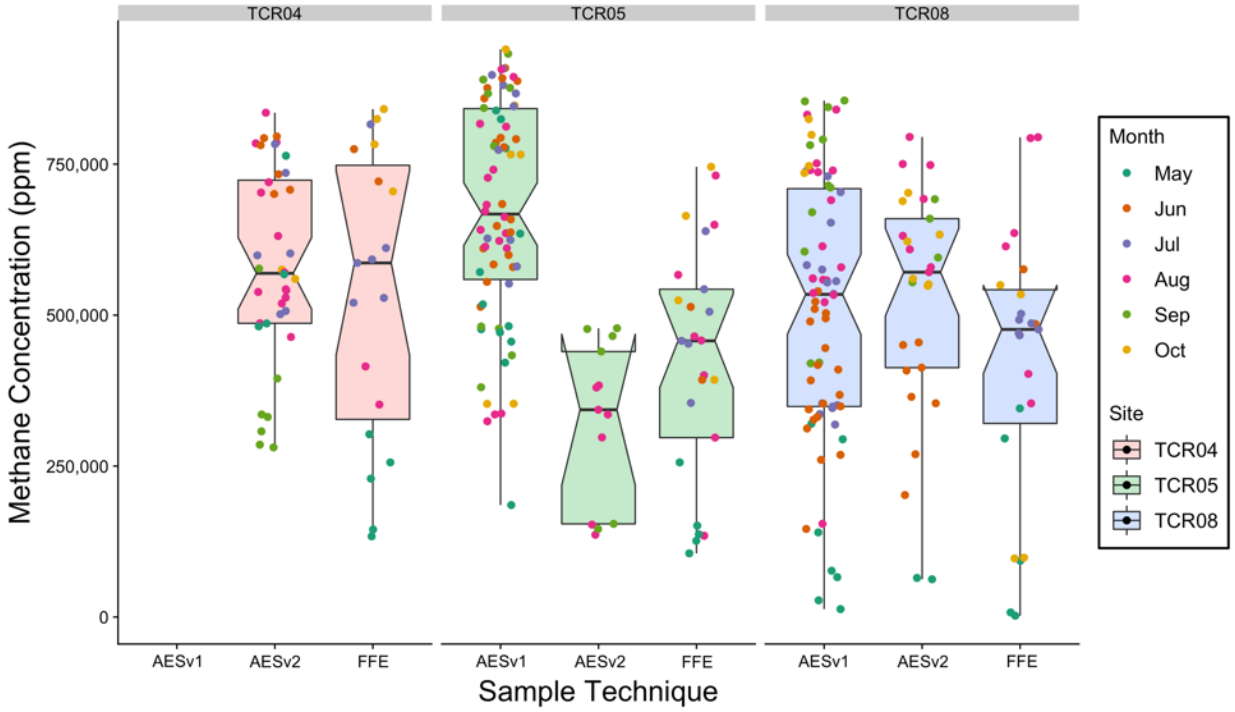

Figure 2.8: Boxplot comparison of CH_4 concentrations from bubble samples collected by the sensors (AESv1 and AESv2) and fresh forced ebullition (FFE) from 2017 and 2018 field seasons. Overlaying points allow observation of when during the season the samples were extracted. The boxplot displays data distribution (median, two hinges [25th and 75th percentiles], and two whiskers [max and min range]).

2.4 Discussion

The results of the laboratory experiment demonstrated that AES provides a robust measurement of gas volume accumulating in the collection chamber. Errors were low (NRMSE = 2.4%) and comparable to errors associated with manually-operated BTs (avg. error = 1.3%). Nonetheless, the errors associated with the AES measurements may be overstated, as the injected volumes are measured with a plastic syringe, rather than with a highly accurate method. Manual measurements of air in the BTs had a tendency to overestimate the actual volumes present. While the average error was small for volumes < 60 mL, errors could be more consequential during

periods of high flux, when measurement of accumulated volumes would require increased withdrawals with the syringe. Because the syringe draws a vacuum from the BT, untrained operators may have a tendency to close the sampling port and expel the air from the syringe prematurely (i.e. before the syringe reaches equilibrium pressure). These actions could lead to imprecise measurement of ebullition fluxes from these traps in the field and may explain the bias observed during our laboratory testing.

2.4.1 Field operation

Field tests of the AES systems deployed in the TCMW reservoirs demonstrated that the AES operated in the field as expected and reliably captured and measured the ebullitive flux over the deployment period. The AESv1 was deployed several weeks after ice-out and operated for the remainder of the 2017 open-water period, minus a ~4-day window mid-way through the season when the datalogger memory capacity was exhausted (Figure 2.9). The sensor recorded the volume as it accumulated in the chamber until concentration samples were drawn and the AESv1 was manually purged by a technician, initiating the next logging period. Captured volume exceeded the 2775 mL capacity in the PVC collection chamber, thereby breaching into the cone region and resulting in unusable data from this point until the AESv1 was manually purged.

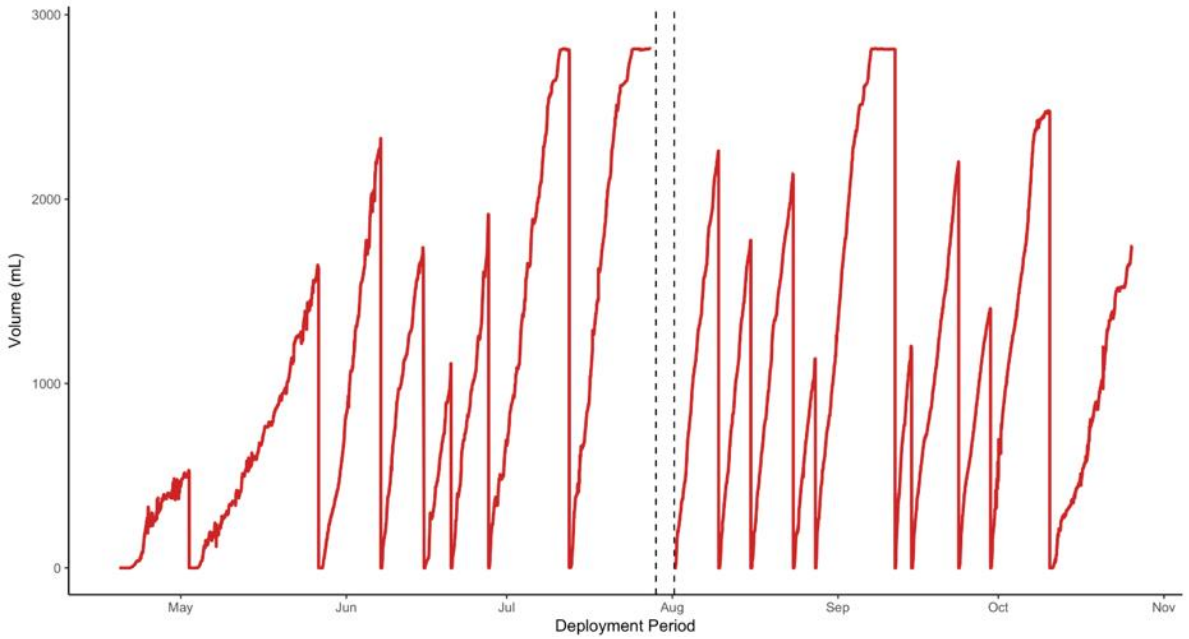

Figure 2.9: Plot of AESv1 volume from 2017 field deployment in South Tobacco Creek Watershed, Manitoba, Canada. Plot demonstrates volume accumulating (at 10-minute resolution), within and (on three occasions) exceeding the 2775 mL capacity, until manually evacuated during a field visit every ~1–2 weeks. Plot also demonstrates the gap of missing measurements (vertical dashed lines) due to datalogger capacity being exhausted.

Data provided by the AES can be used to analyze ebullitive flux in a number of ways for a particular location. The data presented above can be translated to visualize cumulative fluxes for this particular deployment period. However, the limitations of AESv1 deprive us of detail during the periods when gas breached the collection cone as well as the days that the datalogger memory was exhausted (Figure 2.10). Because of these gaps in the cumulative record, ebullitive flux will be underestimated; imputation may be used to reconstruct system behaviour during these gaps.

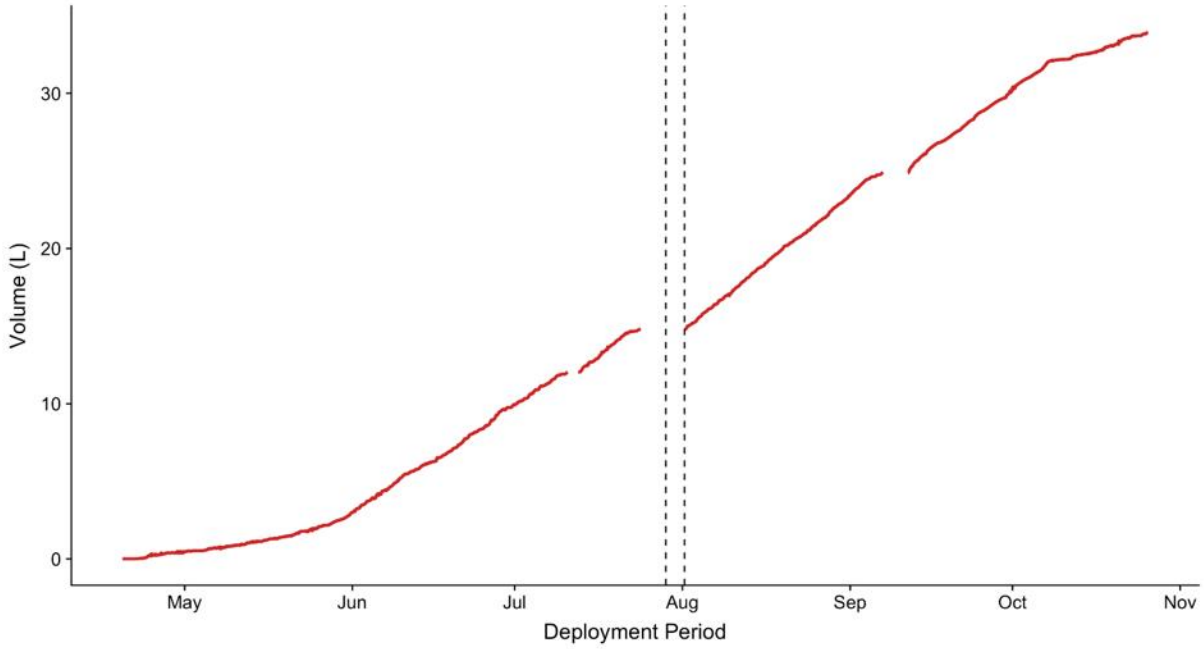

Figure 2.10: Plot of AESv1 field data demonstrating cumulative flux during the 2017 deployment period in South Tobacco Creek Watershed, Manitoba, Canada; breaks in the trend are due to periods when the gas breached beyond the max chamber capacity; vertical dashed lines indicate the period when datalogger memory was exhausted.

The limitations and challenges observed with AESv1 prompted the development and improved design of AESv2. The automated purging, larger battery, increased energy efficiency, and large data storage capacity of this sensor allowed continual operation over the deployment period without requiring site visits. As a result, the AESv2 overcomes the issues experienced with AESv1 and provides a more complete measurement series of ebullitive flux for a location during the deployment period. The AESv2 was deployed in late 2017 and operated for the entire 2018 open-water period, automatically purging captured volume when the chamber capacity was reached (Figure 2.11). Where deployed, the AESv2 therefore provided a complete cumulative flux record, as well as time resolution detail, during periods potentially missed by AESv1 (Figure 2.12).

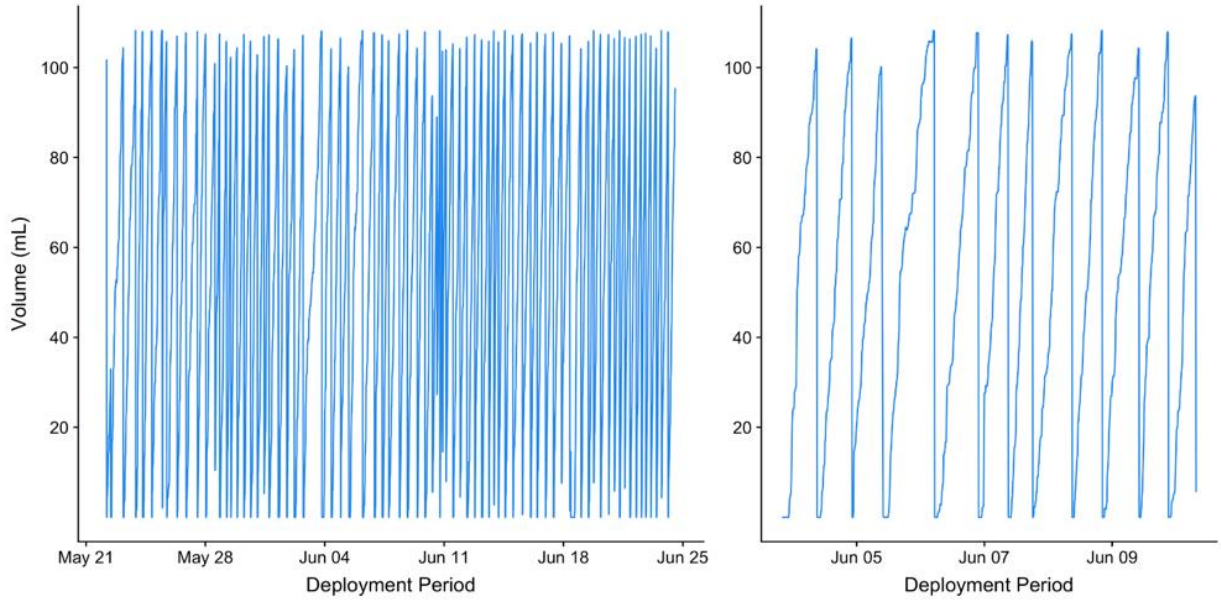

Figure 2.11: Plot of AESv2 field data (recording measurements at 10-minute intervals) from 2018 field deployment at TCR04 in South Tobacco Creek Watershed, Manitoba, Canada. Shown are a plot demonstrating volume (mL) accumulating and purging numerous times over a span of ~1-month (A), and a shorter (~1-week) subset of the data from plot A, demonstrating a closer look at the accumulation and subsequent automated purge event (B).

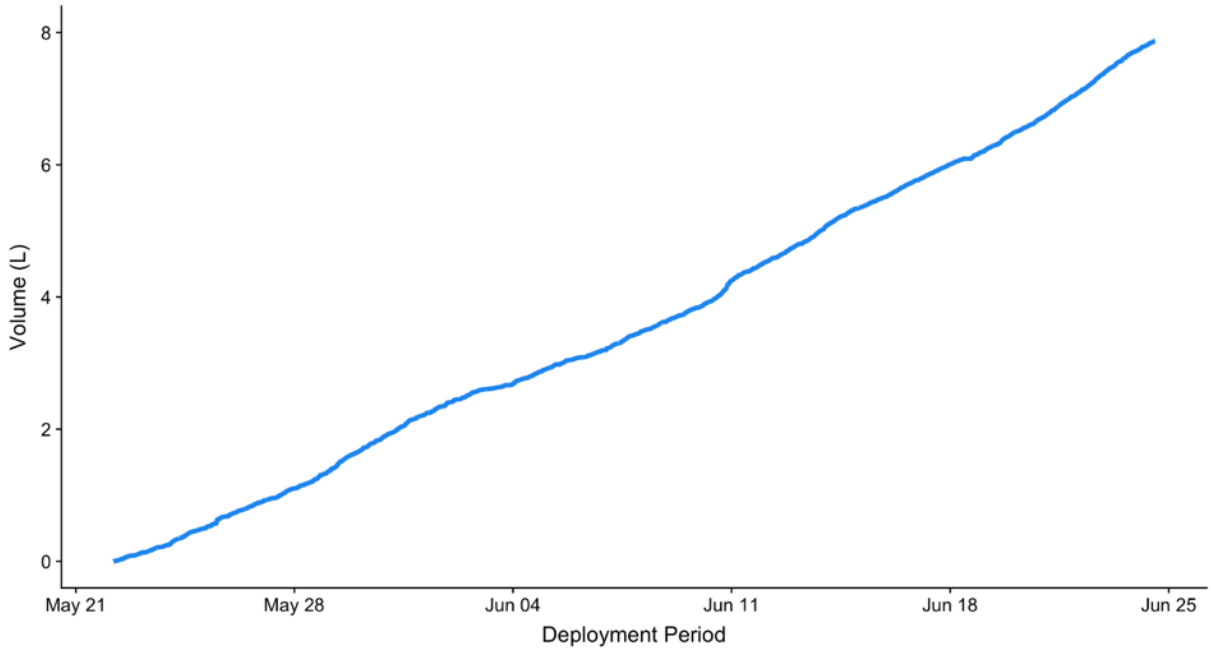

Figure 2.12: Plot of AESv2 field data (recording measurements at 10-minute intervals) over a span of ~1-month during 2018 field deployment in South Tobacco Creek Watershed, Manitoba, Canada demonstrating cumulative volume (L) accumulation over a span of ~1-month.

A closer look at the AESv2 data (Figure 2.11) shows that the AESv2 electronically purged around 1–2 times per day during early June, potentially resulting in missed opportunities for gas concentration sample extraction if a site visit occurs during or shortly after a purge event. Over the course of the 2018 season, the AESv2 deployed in the reservoirs were sampled for gas concentrations 94 times in total, out of which only five attempts were unsuccessful (sensor recently purged and contained less than the 20 mL required for gas concentration analysis). Out of the 89 successful extractions, 87 had sufficient volume (> 42 mL) for duplicate samples to be extracted. The large volume capacity of AESv1 increases the likelihood of sufficient volume being available for gas concentration samples to be extracted during field visits, provided frequency of site visits is not high.

There is potential for diffusion of CH_4 into the water column during storage of high CH_4 concentration air in the collection chambers. This was a concern with the AESv1 design, as this sensor has a larger air-water interface along part of its length, allowing for greater potential of molecular diffusion of captured gases back into the water (Delwiche and Hemond 2017). This effect could lead to potential inaccurate representation of gas concentrations collected using this instrument, particularly during sampling intervals that breached into the larger diameter cone region. In contrast, our analysis revealed higher concentrations in AESv1 deployed at TCR05 (Figure 2.8). As this was contrary to expectations for an AES with larger air-water interface, it suggests that CH_4 production in the pelagic zone is higher than in shallow parts of the reservoir where fresh bubbles were collected for analysis. Since the volume of gas accumulated in the AESv1 chamber reached the collection cone in most intervals, the air column was exposed to a larger air-water interface than in the chamber itself (Figure 2.1). Reasonable agreement between collection methods suggests that samples collected from AESv1 offer a robust characterization of CH_4 concentrations in ebullition. While ebullition is not the dominant pathway for CO_2 flux to the atmosphere, it does have notably higher solubility than CH_4. The same sampling technique comparison was also performed for carbon dioxide (CO_2) concentrations and demonstrated a similar pattern to that of CH_4, suggesting that the AES can be reliable for sampling gas concentrations of both these GHGs in ebullitive bubbles.

2.4.2 Advantages conferred by automated ebullition sensors

The BTs (described above) involve disturbing the sediment (with unknown consequences on the benthic community) upon installation and limit measurements to the littoral zones of a reservoir due to the nature of mounting requirements. In situations where water levels are dynamic, repositioning of the traps can also be necessary. In contrast, the AES are not restricted to reservoir littoral zones and were deployed in deeper parts of TCR05 and TCR08 to quantify emissions from pelagic zones, and to accommodate varying water levels over the season. To avoid disturbing the underlying sediments and depending on the reservoir structure in TCMW, the AES were moored in three different ways: (1) a short length of rope tethered the AES to a long length of rope reaching across the reservoir and secured on opposite banks; (2) the rope tethered the AES to standing deadwood near the desired location (e.g. Figure 2.5); (3), as a last resort, the AES was tethered to an anchored buoy. As deployment in this way permits some movement of the AES, ebullition measurements integrate across larger areas than if the collection cone were fixed in place, as is typical of BT deployment. In addition to pelagic deployment, the shorter AESv2 can also be deployed in reservoir littoral zones, but without the need to disturb sediments and benthic communities. In the shallow TCR04 reservoir an AESv2 was deployed adjacent to BTs to compare the two techniques over the same period. The AES data provided a satisfactory ebullitive flux rate relative to that provided by six manually-operated BTs in the reservoir (Figure 2.13).

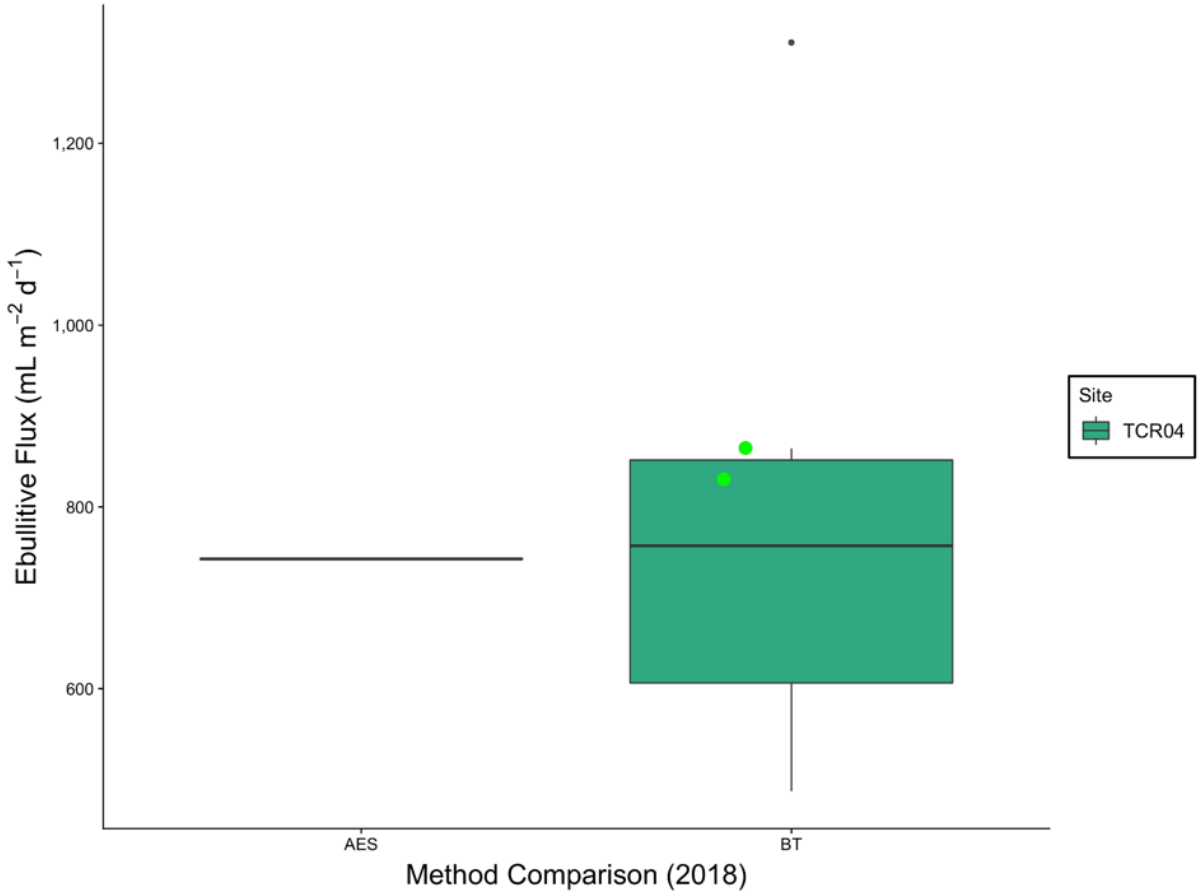

Figure 2.13: Comparison of flux estimates from a single AESv2 (AES) and six bubble traps (BT) deployed at similar depths at TCR04. The highlighted points on the BT boxplot represent BT deployed immediately adjacent to the AES, while other BTs were distributed throughout the reservoir. The boxplot displays data distribution (median, two hinges [25th and 75th percentiles], two whiskers [max and min range], and outlying points).

2.4.3 Possible sources of error

The reservoirs in TCMW displayed a high ebullitive flux, often exhausting the AESv1 volume capacity between site visits (~7–10 days). Depending on the time of year, productivity of the system, or feasibility of site access can present limitations on how long the AESv1 can be reliably deployed. Despite the weight of this larger sensor, the large chamber volume capacity (AESv1) could also result in buoyancy differences as volume accumulates, potentially impacting pressure/height in the chamber used to calculate volume. These potential errors due to buoyancy were simulated in the laboratory to quantify their effects on volume measurements. Similar to the AES laboratory experiment (outlined above), an AES sensor was launched in a tank of water, filled with air, and periodically had its position raised above the water surface in 1 cm

increments. These actions resulted in a ~1 mL decrease in total volume with every 1 cm increase. When it was visited in the field, AESv1 visually appeared to rise ~4 cm due to buoyancy when the chamber was full. Taking this difference in height into account resulted in a ~0.14 % error at maximum volume, which was considered negligible. The AESv2 did not experience similar buoyancy effects in the field, owing to a small chamber volume (100 mL) and larger battery (i.e. more weight) in the second electronics enclosure atop the flotation deck. This sensor could, however, due to the electronic purge solenoid, potentially underestimate flux during some recording intervals (i.e. if the chamber is full, near the purge point, and a large bubble flux enters the chamber that is greater than is needed to trigger a purge).

Reservoir characteristics can introduce additional challenges for measuring ebullitive flux in these and similar systems. In shallow reservoirs with large or sudden water level variation, the cone can make contact with the sediments, triggering bubble release. As these events shorten the reliable recording period, it is pragmatic to design AES with shorter collection chambers for use in these applications. This is entirely possible because the only disadvantages of such systems are the increased power requirements for more frequent activation of a solenoid and a lower likelihood of collecting gas samples. Over both field seasons (2017 and 2018) there was evidence of small birds and mammals mounting the sensors, which may result in the AES bobbing/sinking in the water, influencing chamber pressure and therefore the calculated volume (if this occurs during a logged measurement), similar to the previously mentioned buoyancy error. While our data processing steps (median filter) make these effects negligible, further consideration of this potential source of bias, including incorporation of wildlife deterrents on the flotation deck, may be worthwhile in systems with high animal activity. Due to the productive nature of some reservoirs in TCMW, some AES were subject to insects or small aquatic plants entering the device chamber and potentially clogging the access ports to the differential pressure sensor. In such systems the AES should be periodically removed and cleaned out to ensure the differential pressure sensor measurements are not impeded by obstructions. Prior to the 2018 field season, small mesh screens were added to the appropriate port openings to assist in mitigating this potential issue.

2.4.4 Future opportunities

All AESv2 are equipped for wireless data transmission using LoRa technology; however, testing its functionality did not come to fruition due to the project's time constraints. This technology would increase convenience for future field excursions because operation/data could be observed remotely and no field visits would be required, other than those to collect concentration samples if desired or to address potential technical malfunctions. All AESv2 are also equipped for the addition of on-board CH_4 and CO_2 sensors to measure the gas concentrations at the same temporal resolution as the volume; however, this feature was also not tested in this research. The small chamber (i.e. small air-water interface) and frequent purging of AESv2 would provide these concentration sensors with continual fresh ebullitive gas to measure for enhanced insights into the temporal nature of CH_4 production within the sediments. The AESv2 with an integrated solar panel, large data storage capacity, essentially limitless volume capture capacity, *in situ* concentration measurement, along with wireless data transmission, would be beneficial for future research projects looking to study GHG dynamics of shallow aquatic systems, especially those in remote locations. Testing these additional features will be an avenue of future work with these sensors.

The AES may also be tested for use in lotic systems, provided the flow rate is low enough that the sensor body is not disturbed and that surface turbulence is minimal. The AES described here is not limited to shallow environments and could be deployed in deep water systems (e.g. lakes). Because inverted funnels deployed at depth require further data processing with models of bubble dissolution (Delwiche and Hemond 2017) to estimate actual efflux at the water surface, the AES are likely to provide more reliable ebullition estimates, even in these deeper systems.

Current techniques and methods used to quantify GHG flux from water bodies can be costly; eddy covariance or autonomous surface vehicles, like those demonstrated by Dunbabin and Grinham (2010), could be used to detect GHG flux (although they would provide little detail on the ebullitive process directly). The manually-operated BTs, like those demonstrated here, are a cost-friendly method to measure ebullitive flux in shallow systems, but these require increased field visits to enhance the level of detail they can provide. Being deployed in the same system, the AES functioned similarly to manually-operated BT, while significantly enhancing our ability to analyze the process of ebullition. The components required to build the AES presented in this

work are total cost estimated to be ~ $500 for AESv1 and ~ $700 for AESv2. While the BTs themselves cost less (~ $30) than the AES, when considering personnel costs, the AES are likely to confer substantial savings depending on study site location/access.

2.5 Conclusions

We developed and tested an automated ebullition sensor for measuring ebullition flux in shallow lentic aquatic systems. In both experimental and field settings the AES proved to be an effective device to measure, at a high temporal resolution, the volume released through the process of ebullition in shallow aquatic systems. The AES demonstrated a volume measurement error that is less than or similar to operator errors (conducted in a controlled setting) associated with manually-operated BTs often used to measure ebullition. During field deployment the AES provided satisfactory volumetric records and gas concentration samples comparable to those extracted from traditional sediment gas concentration sampling techniques. The measurements made possible by both AESv1 and AESv2 can be used to observe GHG dynamics of water systems more generally. These systems provide advantages in characterizing the spatial and temporal nature of ebullition, while also improving our ability to quantify fluxes of specific gases when compared to existing methods. In the systems presented here and in similar systems the low-maintenance AESv2 (with its ability to self-purge, energy efficiency, and wireless data transmission potential) could be a relatively cost-friendly option for measuring ebullitive flux with greater detail than previous techniques.

2.6 Acknowledgments

I would like to acknowledge the entire SaskWatChE (Saskatchewan Water Chemistry and Ecology) lab group, for their help and support with laboratory analysis, field expeditions and experiments. I would like to thank my field partner, Carlie Elliott for her hard work, determination and patience throughout both field seasons; as well as additional field assistance from Lauren Dyck and Stephanie Witham. I would like to acknowledge the Deerwood Soil and Water Management Association and, in particular, Les McEwan, Jim Pankiw and all landowners of the STCW reservoirs; for their guidance, use of study reservoirs and providing local knowledge. Funding for this work was provided through a grant from Agriculture and Agri-Food Canada (Agricultural Greenhouse Gases Program) and a Faculty Start-up Grant (USask) awarded to C.J. Whitfield.

2.7 Author contributions

The shallow system AES concept and mechanical design was generated and built by R.E.J Helmle, while the electrical design was led by N.J. Kinar and assisted by R.E.J Helmle. The AES laboratory and field experiments were conducted by R.E.J Helmle. R.E.J Helmle carried out the data analyses and was lead author on the manuscript, with guidance from C.J. Whitfield.

Chapter 3: Methane flux from agricultural reservoirs: rates and drivers of ebullition

R. E. J. Helmle[1,2,3], N. J. Kinar[1,2], and C. J. Whitfield[1,2,3]

Prepared for submission

[1]Global Institute for Water Security, University of Saskatchewan, Saskatoon, Saskatchewan, Canada.

[2]Smart Water Systems Laboratory, University of Saskatchewan, Saskatoon, Saskatchewan, Canada.

[3]School of Environment and Sustainability, University of Saskatchewan, Saskatoon, Saskatchewan, Canada.

3.0 Abstract

Freshwater systems are key locations for biogeochemical processing. Often overshadowed by larger systems, small lentic systems (≤ 1 ha) may exhibit notable greenhouse gas emissions, but this has not been well quantified. In particular, ebullition can be an important pathway for methane (CH_4) release to the atmosphere, but is rarely measured in detail. The following study investigates ebullition fluxes in eight small constructed reservoirs in agriculturally-dominated southern Manitoba. These reservoirs were implemented as a beneficial management practice (BMP); they demonstrate significant nutrient retention, ultimately improving downstream water quality. In this study, open-water season ebullition rates were quantified, as were interannual and within-reservoir variability, and the role of reservoir characteristics was explored. Additionally, wavelet transforms were used on high temporal resolution data sets from novel automated ebullition sensors (AES) to identify synchronicity with variables driving the process of ebullition at a number of time scales. Across eight reservoirs the mean littoral ebullitive CH_4 flux was 2.6 (0.1–6.9) mmol CH_4 m^{-2} d^{-1} during the open-water period of 2017 and appears to be correlated with autochthonous carbon (C) fixation — showing the strongest relationships with total ammonia nitrogen and chlorophyll *a*, which are indicative of productivity. Mean littoral ebullitive flux increased significantly in the 2018 open-water season to 12.7 (0.6–40.5) mmol CH_4 m^{-2} d^{-1}, and these interannual variations were correlated with warmer water temperatures, likely a result of year to year differences in local hydroclimate. Spatial variability within reservoirs was analyzed over both 2017 and 2018 open-water seasons,

and the ebullitive flux from the pelagic zone of the reservoirs was significantly greater on average (16.3 mmol CH_4 m^{-2} d^{-1}) than rates from the littoral zone (6.0 mmol CH_4 m^{-2} d^{-1}); the heightened pelagic flux was correlated to higher organic matter content in the sediments of those zones. Furthermore, the wavelet analysis showed that bubble release demonstrated significant synchronous relationships with drops in pressure head on short time scales, and reservoir temperature at both short (diel) and long (seasonal) time scales. High resolution analysis of ebullition permits an enhanced understanding of the physical process of bubble release, and understanding ebullitive contributions to greenhouse gas release from these systems enhances the capacity to quantify atmospheric greenhouse gas fluxes from aquatic systems receiving water from agricultural lands.

3.1 Introduction

Freshwater systems — such as rivers, lakes, reservoirs, wetlands and estuaries — are hotspots for biodiversity and key habitat for organisms that metabolize, transform and excrete nutrients (Dudgeon et al. 2006). These systems are important for energy and water exchange with the atmosphere (Krinner 2003), and also play a role in greenhouse gas (GHG) exchange with the atmosphere. Freshwater systems play an important role in the elemental cycles of C and N by acting as receiving sites (from terrestrial systems), transportation mechanisms, and zones of both transformation and storage. Nitrogen and allochthonous C, incorporated into terrestrial biomass via biological fixation (Falkowski 2000), can be carried from the land to aquatic systems (e.g. via fluvial load, wet and dry deposition) and represent a major input to freshwater systems. It is believed that the annual amount of C that reaches freshwater systems is nearly twice as much as the riverine flux to the ocean (Cole et al. 2007). Terrestrial-freshwater interfaces, and the convergence of different hydrologic flow paths at the margins of lentic systems, are known to be biogeochemical hot spots and demonstrate intermittent hot moments (McClain et al. 2003). Depositional zones can be one such facet, with internal cycling of available material stimulating GHG emissions (Cole et al. 2007; Maeck et al. 2013). In some lentic systems, inputs of surface water supersaturated with GHG via runoff can sustain the GHG flux (Whitfield et al. 2010; Weyhenmeyer et al. 2015). In productive lentic systems, biological fixation of C via photosynthesis (autochthonous C) can also be important for C inputs (Dean and

Gorham 1998). Carbon that has been fixed through primary production or transported to these systems may be stored in sediments, mineralized and released to the atmosphere as CO_2 (Kling et al. 1991) or CH_4 (Bubier et al. 1993), or be exported via discharge.

Constructed water bodies, such as reservoirs, are particularly important for inland C cycling (Soumis et al. 2004). Generally, where these structures are implemented by damming a stream to store water, the hydrologic regime and processes that affect C cycling in these systems are altered. Heightened particle trapping in constructed reservoirs results in considerably higher sedimentation rates shortly after construction (Stallard 1998). Carbon that was destined for lotic transport downstream can instead have a short (release to atmosphere) or long-term fate (burial in the sediments). Reservoirs are created for a number of reasons: hydroelectric power generation, flood and erosion mitigation, drought relief, agricultural irrigation, and recreation, among others. Filling reservoirs by flooding terrestrial landscapes kills plants and other organisms, reducing their capacity to assimilate CO_2 from the atmosphere, and allowing microbial decomposition to convert this organic material to CO_2, CH_4 and N_2O (Kelly et al. 1997; Venkiteswaran et al. 2013). Emissions can vary greatly between reservoirs over different spatial scales depending on a number of factors, such as the size of flooded land area, availability of labile organic material, and physicochemical conditions. In large reservoirs on agricultural landscapes, the C balance of reservoirs can shift at sub-annual timescales from being a sink to a source — a large pulse of water from a storm event or hydrologic turnover can stimulate GHG emissions (Jacinthe et al. 2012). The role of these landscape features for GHG emission is a critical unknown with respect to agricultural GHG emissions.

Agricultural practices are dependent on a large quantity of water, and it is common for agriculturists to create small impoundments on their lands to help meet this demand. In addition to particle trapping, agricultural reservoirs can receive high inputs of dissolved nutrients, which can promote aquatic primary production and, therefore, increased autochthonous inputs of C (Huttunen et al. 2003). Because worked lands are often tilled and thus more susceptible to erosion, significant C redistribution can also occur on these landscapes (McCarty and Ritchie 2002). These reservoirs may feature much higher inputs of C than those in non-agricultural landscapes. Nonetheless, agricultural GHG budgets have typically focused only on terrestrial sources — overlooking the small impoundments that are commonly implemented in most agricultural landscapes, and emissions in downstream systems that are stimulated by elevated

nutrient export associated with agricultural practices. Low-tech small reservoirs are easily implemented, and can bring many benefits to an agricultural operation; while often not inventoried they are thought to be increasing on these landscapes (Downing and Cole 2006). Recent investigations have shown that small impoundments in agricultural landscapes can unpredictably sequester large amounts of N_2O (Webb et al. 2019). Conversely, these systems can also contribute significant fluxes of CO_2 and CH_4 to the atmosphere (Ollivier et al. 2019).

The primary pathways for emission of CH_4 from aquatic systems are diffusion through the water column, plant-mediated transfer and the release of bubbles out of the sediment (ebullition). Ebullition is a very important pathway for the emission of CH_4 and other volatile species to the atmosphere (Baulch et al. 2011; Stanley et al. 2016) and can represent upwards of 90% of a system's total CH_4 emissions (Keller and Stallard 1994; Walter et al. 2006). This flux pathway could be directly related to net sediment CH_4 production (Fendinger et al. 1992). Water temperature can affect how efficiently organic C is transformed into CH_4 and CO_2 in these systems, as increases in decomposition, as well as reaction rates, are associated with a rise in temperature (Kellner et al. 2006). Bubbles of these gases forming in the sediments are more easily released during an event of decreased atmospheric pressure or a drop in water level (Harrison et al. 2017), as the force on the sediment layer is reduced (Tokida et al. 2007). Understanding the drivers of ebullition will enhance the ability to quantify the magnitude of this atmospheric C flux at larger scales. Developing accurate GHG budgets for these systems is complicated; consequently, annual budgets of agricultural reservoirs are uncertain — partly because ebullition is episodic, and is rarely quantified in detail.

Enhanced measurement of ebullitive flux from agricultural reservoirs during the open-water season will contribute to an improved understanding of the ebullitive process itself and simultaneously permit analysis of C cycling dynamics in these systems — helping describe their role in agricultural GHG budgets. In this study, open-water season ebullition rates for eight agricultural reservoirs were quantified. Specifically, reservoir physicochemical parameters (water chemistry, sediment characteristics) were investigated to identify linked to littoral ebullition rates, and if there are significant differences in interannual fluxes over two open-water seasons. Furthermore, spatial heterogeneity within reservoirs was also analyzed — comparing littoral and pelagic fluxes, using a novel AES. Finally, via high temporal resolution records of pelagic ebullitive flux, additional drivers of temporal ebullition patterns were analyzed using

high resolution records of *in situ* pond temperature, dissolved oxygen concentrations, and hydrostatic pressure.

3.2 Materials and methods

3.2.1 Study area and site description

The Tobacco Creek Model Watershed (TCMW) is an agriculturally-dominated watershed located ~100 km southwest of Winnipeg, Manitoba (Figure 3.1), in the Red River Basin. The TCMW is largely comprised of the lower Manitoba Plain ecoregion but also reaches to the higher elevation Interior Plains. This transition is due to the large east-sloping Manitoba Escarpment — dropping ~ 60 m elevation in a < 3 km stretch (Tiessen et al. 2011). The TCMW's westernmost sub-watershed, South Tobacco Creek Watershed (STCW) lies on the escarpment and drains 7,638 ha of agricultural land, of which ~ 70% has been under cultivation (Hope et al. 2002). The terrain of the escarpment can result in local climate variations, with mean annual temperatures of 2.2˚C and 3.3˚C on the upper and lower reaches, respectively (Hope et al. 2002). Similarly, mean annual precipitation can be 590 mm above and 500 mm below the escarpment; 75% of which occurs as rainfall outside of the winter months (Hope et al. 2002). Early agricultural settlement in the region sparked intensive vegetation removal and wetland drainage (TCMW 2004). Historical landscape manipulation, along with predominantly clay-based soils laid by the ancient glacial Lake Agassiz, can result in periods of peak flow and fast drainage contributing to considerably higher erosion and nutrient loading into streams — leading to water related issues in the region (TCMW 2004; Glozier et al. 2006). South Tobacco Creek Watershed, and the larger TCMW, feed into the Morris River and later the Red River, ultimately transporting nutrients to Lake Winnipeg and contributing to its eutrophication (Schindler et al. 2012). To address these issues, in the early 1980s the Deerwood Soil and Water Management Association (DSWMA) and local landowners began implementing a network of 50 small reservoirs in the TCMW — 26 of which are located in the headwaters of STCW.

The reservoirs in STCW are a result of three different constructed dam types: dry flood-control dams, back-flood dams and multi-purpose dams. Dry-dams are flood control structures that decrease peak flow during spring freshet and rainstorm events by holding back water for a short period of time. Back-flood dams trap and spread out water over a large area at a shallow

depth, for ~two weeks, to increase soil moisture. Similar to dry-dams, multi-purpose dams are designed to reduce peak flow, but also store water for use during dry periods for livestock watering, small-scale irrigation and groundwater recharge. The multi-purpose dams were constructed in such a way that they slowly release water, with the rate controlled at the landowner's discretion, but retain ~ 50% of reservoir storage capacity for use during drier periods of the year (TCMW 2004).

In this study, ebullition rates were measured in eight reservoirs; either dry or multi-purpose dams, all located just west of Miami, Manitoba (Table 3.1; Figure 3.1). Together the reservoirs span the geographic extent of the STCW and represent most of the Manitoba escarpment elevation range. The reservoirs were selected based on landowner permission, feasibility of access, probable length of water storage, and outlet gate condition (i.e. sufficient depth to accommodate ebullition sensor deployment). The sites were also selected to encompass some of the heterogeneity among reservoirs in the region, including reservoir size. One ephemeral reservoir (TCR03), one long-studied reservoir (TCR05), and one receiving tile drainage (TCR07) were selected to cover a range of land-use practices in the immediate contributing area, such as cropland, livestock pasture, livestock watering and being adjacent to roadways. Another site, TCR04, can be considered ephemeral (Les McEwan; DSWMA, pers. comm. 2017), with water levels only dropping to lower than required for AES instrumentation in late summer — due to a damaged outlet structure.

Table 3.1: Study reservoir locations and characteristics.

Site ID	Latitude	Longitude	Reservoir Type	Construction	Area ha	Depth * m
TCR01	49.395694	–98.342075	Dry	1997	0.73	4.6
TCR02	49.384766	–98.331008	Dry	1988	0.23	2.3
TCR03	49.396058	–98.439675	Multi-purpose	1985	0.06	1.9
TCR04	49.397828	–98.369836	Multi-purpose	1988	0.31	1.4
TCR05	49.336322	–98.360550	Multi-purpose	1989	0.57	3.7
TCR06	49.387875	–98.335331	Dry	1990	0.37	3
TCR07	49.316397	–98.297469	Multi-purpose	1989	0.28	2.8
TCR08	49.331132	–98.332520	Multi-purpose	1986	0.38	2.6

**Maximum depth April 2017*

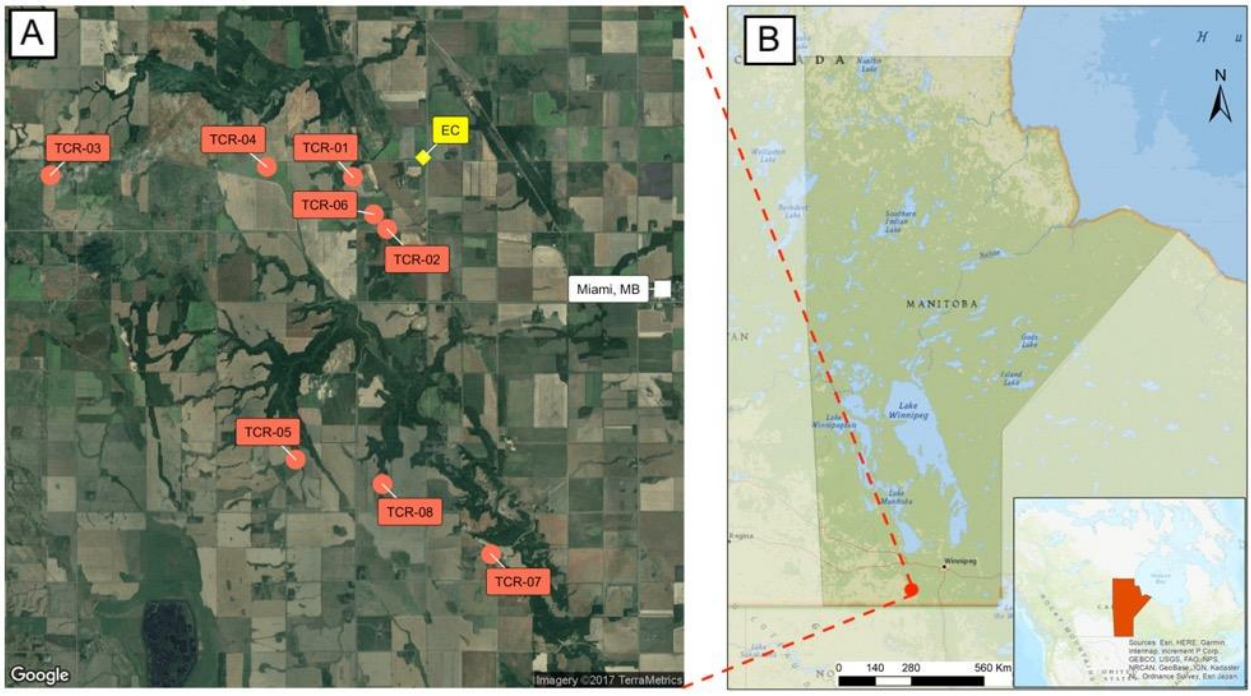

Figure 3.1: Map of study sites (red) and Environment Canada weather station #29886 (yellow) (A); location within the province of Manitoba and the Canadian prairies (inset) (B).

3.2.2 Field measurements

All reservoirs in this study were equipped with continuous measurement instruments (Section 3.2.2.1) shortly following ice-off (late April/ early May) that remained deployed until just prior to ice-on (late October), for both the 2017 and 2018 field seasons. The eight reservoirs were visited (at intervals of up to two weeks) for routine *in situ* sampling (Section 3.2.2.2) for the 2017 field season. After analyzing reservoir characteristics and trends in 2017, and to allow the opportunity for water level manipulation experiments, the number of study reservoirs was reduced to six (TCR03–TCR08) and the sampling frequency was increased to intervals of up to three weeks for the 2018 field season.

The instrumentation layout was similar at all reservoirs, with 2–3 pairs of manually-operated bubble traps (BTs) mounted in different locations of the littoral zone, and submerged loggers near the sediment-water interface in the deepest area of the reservoir. At select sites an AES was deployed in the pelagic zone near the center of the reservoir.

3.2.2.1 Continuous measurements

All reservoirs were equipped with 4–6 BTs (Baulch et al. 2011; Venkiteswaran et al. 2013). Bubble traps capture ebullitive gas before it reaches the atmosphere, and allow the volume to be measured. Bubble traps were deployed in pairs such that two open-bottom jugs, of known diameter, were mounted to a single post at several littoral locations. They are deployed such that the jugs are largely submerged, completely filled with water and capped with a rubber septum fitted with a sampling port — to capture ascending air emitted from sediments directly below. Ebullitive volume accumulated in BTs over the time between visits was measured from each BT via syringe, recorded and reset for the next interval. Where necessary due to dropping water level during the monitoring period, the BTs were repositioned and reset. Bubble traps were deployed in pairs to cover a range of the reservoir littoral zones (i.e. outlet, middle, or inlet), and additional BTs were deployed in larger reservoirs as necessary.

The AES (Chapter 2) were not restricted to littoral zones, and therefore deployed in a near-center location of the reservoirs to measure emissions from deeper profiles and accommodate varying water level over the season. An AESv1 was deployed at both TCR05 and TCR08 for the open-water period during both 2017 and 2018 field seasons. An AESv2 was

deployed at TCR02 in late July until ice-on in 2017. For the 2018 field season an AESv2 was deployed at TCR04 (a nearly uniformly shallow reservoir with no true pelagic zone) adjacent to a pair of BTs. The sensors were launched into the water and secured in place before sealing the sampling port to initiate the logging period.

A HOBO (U20L-04) water-level/ hydrostatic pressure logger and HOBO (U26-001) dissolved oxygen (DO) and temperature logger were deployed at each reservoir for the open-water period in both 2017 and 2018 field seasons. Loggers were calibrated according to HOBO specifications, fitted with anti-fouling copper tape and programmed to record measurements at half-hour or 10-minute intervals. The loggers were mounted and deployed on a submerged buoy to ensure that they maintained a consistent height above the sediments over the entire season (Figure 3.2). The submerged loggers were removed, on two separate occasions in the 2017 field seasons and once in the 2018 field season, for re-calibration and removal of any biofouling that may have developed. In the 2018 season, HOBO (UA-002-08) temperature pendant loggers were inserted directly into the sediments to demonstrate how accurately the water temperature records as a proxy represent temperatures of the actual sediments (Figure B.1).

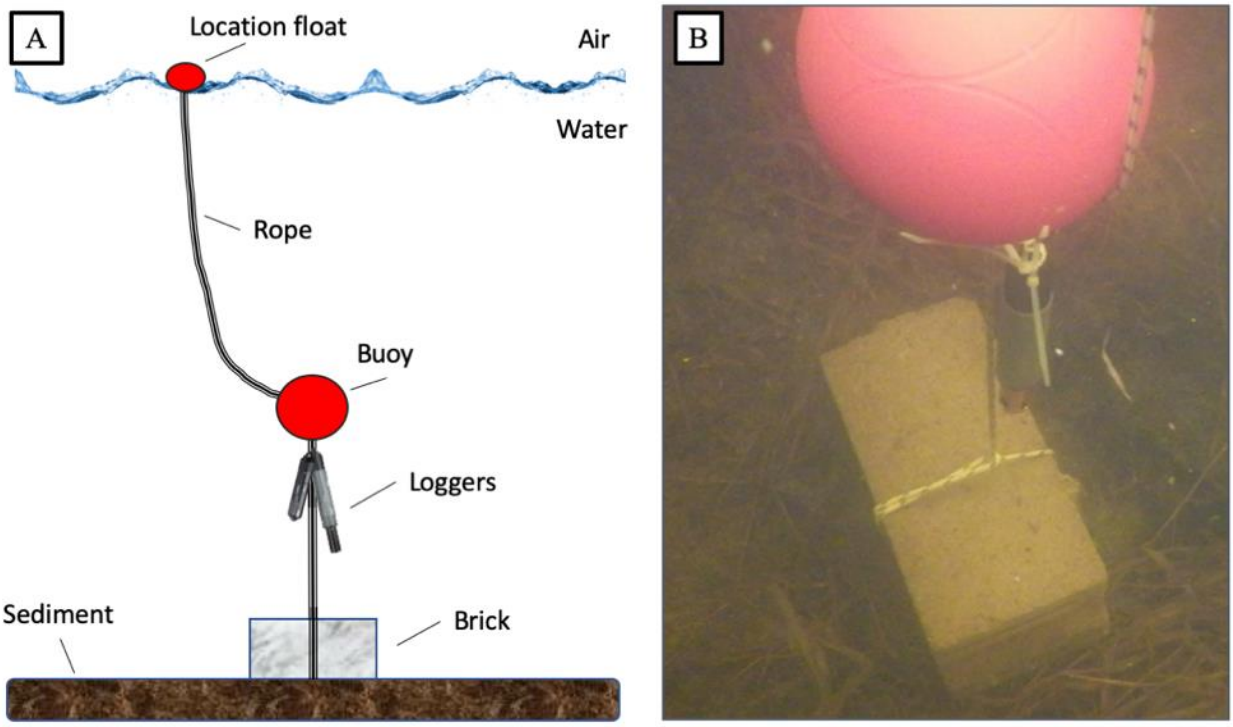

Figure 3.2: Image of submerged dissolved oxygen (U26-001) and Water-Level (U20L-004) HOBO loggers deployed at TCR03.

An Environment Canada Weather station (DEERWOOD RCS MB #29886) is located on the northeastern reach of STCW at Deerwood, Manitoba (e.g. Figure 3.1). Meteorological data (atmospheric temperature, precipitation, and atmospheric pressure) over the course of both 2017 and 2018 field seasons was used to characterize regional conditions.

3.2.2.2 *In situ* measurements and sample collection

During each site visit *in situ* pH of reservoir water was recorded using a multiparameter probe (Yellow Springs Instrument or Oakton PC Testr) at a depth of ~ 20 cm below the water surface. During each site visit, the volume of air accumulated in the manually-operated BTs was measured via 60 mL syringe. Additionally, during every other site visit water chemistry samples were collected in 1 L HDPE bottles at a depth of ~ 20 cm below the water surface via dip sampling. The water samples were subsampled, filtered, acidified, and stored according to their respective protocol (Table 3.2) for later laboratory analysis of total ammonia nitrogen (TAN), nitrate (NO_3^-), sulphate (SO_4^{2-}), dissolved organic carbon (DOC), and chlorophyll *a* (Chl *a*).

Table 3.2: Summary of preparation and storage of samples for water chemistry analysis.

Parameter	Treatment	Storage	Method
TAN	Filtered (0.45 µm nylon filter) and acidified with H_2SO_4	Frozen (–40 ºC)	NH_3K on SmartChem 170
NO_3^-	Filtered as above	Frozen (–40 ºC)	WNO_3 on SmartChem 170
SO_4^{2-}	Filtered as above	Frozen (–40 ºC)	SO_4K/ SO_4Z on SmartChem 170
DOC	Filtered as above	Refrigerated (4 ºC)	Catalytic Combustion to CO_2 and IR detection
Chl *a*	Filtered 50–500mL through GF/F filter	Frozen (–40 ºC)	Spectrophotometer

*Letters in methods refer to SmartChem technique (i.e. not compounds)

During every site visit over both field seasons, GHG concentration samples were extracted from the deployed AES via syringe from the sampling port. Prior to extracting the

sample, a syringe was first used to remove any residual atmospheric air from the sampling port, and then to mix ebullitive gas captured in the collection chamber by repeatedly drawing air from the chamber and reinjecting it. Samples were then collected and immediately injected into 6 mL gas Exetainers® (Labco Ltd, Lampeter, UK) sealed with a double-wadded (chlorobutyl septum + PTFE/Silicon) cap for storage. Exetainers® used during the 2017 field season were unevacuated (filled with 6 mL atmospheric air for predilution), and over-pressurized to 20 mL with 14 mL of ebullitive gas. In 2018, upgrades to laboratory equipment made it possible to analyze CH_4 concentrations > 100,000 ppmv without dilution. Thus Exetainers® used during the 2018 seasons were evacuated and filled with 20 mL ebullitive gas. After sampling, the AES was purged to reset for the next logging interval. During every other site visit, fresh forced ebullitive (FFE) gas concentrations were also collected by disturbing littoral zone sediments and capturing the ascending gas with a submerged funnel-syringe system before it reached the atmosphere (Venkiteswaran et al. 2013); 14 or 20 mL (in 2017 and 2018, respectively) of this gas was immediately injected through a hydrophobic filter into 6 mL Exetainers® (unevacuated in 2017 and evacuated in 2018, as described above).

Sediment samples were collected at all reservoirs using a standard Ekman Grab (Boon and Mitchell 1995) and stored in a new sealable plastic bag for later laboratory analysis. Samples were handled using new Fisherbrand® Nitrile powder-free medical gloves, and carefully collected from the center of the Ekman Grab extract — avoiding the perimeter where draining water may have washed away finer sediments. Sediment sampling in the littoral zone was collected by wading out to a location near BTs and placing the Ekman grab on undisturbed sediments. Sediment sampling during the 2017 field season took place on two occasions (mid-summer, and again on the last visit during site decommissioning). During the 2018 field season the frequency of sediment sampling was increased, with collection occurring nearly every other site visit. Sediment samples were similarly collected from the pelagic zone, via Ekman Grab and a kayak, during the 2018 field season.

3.2.3 Laboratory analysis

Total ammonia nitrogen, NO_3^-, SO_4^{2-}, and Chl *a* were all analyzed at the Global Institute for Water Security (GIWS), University of Saskatchewan, via SmartChem 170 auto-analyzer

(WestCo Scientific Instruments, Inc.) using appropriate methods (Table 3.2). Total ammonia nitrogen analysis (EPA 350.1) reports concentrations of both ammonia (NH_3) and ammonium (NH_4^+). The NO_3^- analysis (EPA 353.2) uses a small amount of nitrite (NO_2^-) in the colorimetric analysis technique; as a result, the NO_3^- reported in this study is $NO_2^- + NO_3^-$. Sulphate analysis (EPA 375.4) is performed by converting SO_4^{2-} to barium SO_4 suspension and stabilized via glycerin and sodium chloride to compare turbidity with a standard curve at 420 nm. Dissolved organic carbon (DOC) was analyzed at the University of Waterloo, using a Shimadzu TOC-L analyzer where samples were converted to CO_2 via combustion (at > 680˚C) and subsequently analyzed with non-dispersive infrared (NDIR) detectors (ASTM International 2018; Method D7573-18).

All GHG concentration samples were analyzed at the Global Institute for Water Security, University of Saskatchewan, via gas chromatography (GC) using a Bruker Ltd. Scion 456 GC with auto-sampler. Prior to sample analysis, the GC was calibrated according to specification with standards of known concentrations of CH_4 gas. Methane concentration of the samples were detected by flame ionization detection (FID), or by thermal conductivity detection (TCD) for concentrations > 100,000 ppmv. Inert argon functioned as the carrier gas, and sample response to the detection methods was compared to calibration values.

Sediment samples collected in the field were analyzed in the laboratory for particle size and organic matter (OM) content. Sub-samples of air-dried and disaggregated sediments were sieved to 2mm, weighed, and oven dried at 105˚C to vaporize residual water content. The samples were then weighed, combusted at 400˚C for 16 hours, and then reweighed to determine OM content according to loss-on-ignition (LOI) (EMASC-001; Schumacher 2002). These same subsamples were then analyzed in triplicate at Trent University via laser ablation using a Horiba Partica LA-950 to determine fractions of clay, silt, and sand (Goossens 2008), as well as the geometric mean particle size (Geomean).

3.2.4 Data & statistical analyses

Data visualizations, statistical analyses and calculated results were all performed using R: A Language and Environment for Statistical Computing, 2017 (R Core Team 2018; version 3.6.0).

Littoral ebullition rates were calculated by first quantifying the volumetric flux (mL m^{-2} d^{-1}) using the accumulated volume collected per BT chamber area over the length of the deployment period. Littoral CH_4 concentration values from FFE samples in the 2017 field season were pre-filled with atmospheric air, so these samples were corrected with a reference sample according to:

$$C_T V_T = C_1 V_1 + C_2 V_2 \tag{3.1}$$

where subscript T is the final volume (20 mL) of the exetainer and the concentration (ppmv) analyzed on the GC, while subscripts 1 and 2 refers to volumes and concentrations of the atmospheric and ebullitive gases, respectively. Fresh forced ebullition samples were taken at random locations, and an average littoral CH_4 molar concentration for each reservoir was determined, and applied to each BT volumetric flux using the ideal gas law:

$$PV = nRT \tag{3.2}$$

in order to calculate mean littoral ebullitive CH_4 flux for each of the reservoirs according to the measured ebullition volumes at that reservoir. The volumetric component of the ebullitive CH_4 flux (mmol CH_4 m^{-2} d^{-1}) was standardized to standard pressure (1 atm) and temperature (273.15˚K).

To compare the littoral ebullitive CH_4 flux emitted from all eight sites studied in 2017, the distributions of the data were first tested for normality using visual inspection of histograms. Subsequent to the confirmation of normality, a parametric between-groups analysis of variance (ANOVA) (package: ‘stats’; function: [aov]) was performed. The residuals from the ANOVA were then also checked for normality via visual inspection of histogram and quantile-quantile plots, and were determined to be normal (package: ‘stats’; function: [qqnorm]). The data residuals were also checked for homogeneity of variance (homoscedasticity) via Levene’s Test (package: ‘car’; function: [leveneTest]); where a p-value > 0.05 confirmed homoscedasticity. A post-hoc TukeyHSD test (package: ‘stats’; function: [TukeyHSD]) was subsequently carried out on the ANOVA test to identify differences between individual reservoirs, with p-values Bonferroni-corrected to provide each individual comparison with a 95% confidence interval.

Observations of reservoir physicochemical parameters over the open-water period were averaged to produce a single mean reservoir value. Observations of select analytes (TAN, NO_3^-, and SO_4^{2-}) that were less than the method detection limit (MDL) were set to half of the MDL prior to calculating mean values. To investigate these variables as predictors of littoral CH_4 ebullitive flux, the rates were tested for correlation (package: 'stats'; function: [cor.test]) with mean reservoir physicochemical characteristics (temperature, DO, pH, TAN, NO_3^-, SO_4^{2-}, DOC, Chl *a*, OM, Geomean, and clay, silt and sand contents). Bonferroni correction was used to provide each test with a 95% confidence interval. A principle components analysis (PCA) was conducted to highlight interactions between all mean physicochemical parameter values, in terms of CH_4 flux from the littoral zone (package: 'stats'; function: [prcomp]). The PCA demonstrates which variables are linked, and the strength of the relationships (i.e. closer vector length and angle).

To compare interannual variations in littoral ebullitive CH_4 flux, the data distributions were first determined to be nonparametric via visual inspection of histograms, and as a result a Mann-Whitney-Wilcox test (package: 'stats'; function: [wilcox.test]) was performed on the 2017 and 2018 data from each site. To compare interannual variations of explanatory variables, these data were similarly checked for normality, and parametric data (temperature) were compared using a t-test (package: 'stats'; function: [t.test]) while nonparametric data (TAN, Chl *a*) were compared using a Mann-Whitney-Wilcox test (package: 'stats'; function: [wilcox.test]).

Measurements of ebullitive CH_4 flux from the pelagic zone in the study reservoirs were provided by the AES. Volumetric rates of this flux were calculated as outlined in Chapter 2, and mean CH_4 concentrations (via samples from the AES collection chamber) were used to compute a pelagic ebullitive CH_4 flux (mmol m^{-2} d^{-1}). To compare how ebullitive CH_4 flux differs between the littoral and pelagic zones within reservoirs the data distributions were first determined to be nonparametric via visual inspection of histograms, and a Mann-Whitney-Wilcox test (package: 'stats'; function: [wilcox.test]) was performed. To explain within reservoir variations in CH_4 flux, sediment characteristics were checked for normality, and parametric data (OM) were compared using a t-test (package: 'stats'; function: [t.test]).

High temporal resolution data collected at select (based on most complete data records) reservoirs in 2017 was used to analyze volume released via ebullition (mL m^{-2}), and its potential drivers, at a number of different timescales. Wavelet transforms is a powerful approach for

analyzing time-series data (Percival and Walden 2000). The R package 'wsyn' (Reuman et al. 2019) was used to investigate synchronicity between different time-series records and detect at which timescales these correlations were significant. The package, and its functions, implement the Morlet wavelet transform to provide timescale specific information on the fluctuations expressed across multiple time-series records (Addison 2002; Sheppard et al. 2019). Moments of synchronicity between different wavelet transformed variables, at different timescales, can be detected using wavelet coherence (Sheppard et al. 2016, 2017). Wavelet coherence tests the relationship, with respect to timescale, of two wavelet transformed variables as they fluctuate over time and therefore can detect relationships where conventional correlation cannot (Sheppard et al. 2019).

In order to normalize the variables for comparison, full season cumulative ebullition records provided by the AES (10-minute intervals) were transformed to hourly ebullition fluxes. Wavelet transformations were performed on the hourly observations (ebullition, hydrostatic pressure, pond temperature, and DO (HOBO loggers near the sediment-water interface) (package: 'wsyn'; function: [wt]). The strength of synchronicity (ranging between 0 and 1) between wavelet-transformed variables was tested at various timescales (package: 'wsyn'; function: [coh]); where higher values indicate a stronger association, and coherence above the significant threshold of 0.95 can be considered as significant synchronous behaviour over that band of timescales. Reservoir TCR08 has its water manually drained by the landowner just prior to ice-on annually, so the data records measured at this reservoir were constrained to avoid inclusion of ebullitive release during these drainage periods.

3.3 Results

3.3.1 Littoral ebullitive flux from agricultural reservoirs

The 2017 littoral ebullitive CH_4 flux was significantly different among sites (ANOVA, $F[7,34] = 12.72$, $p = 0.001$; Figure 3.3). TCR04 demonstrated the highest mean littoral ebullitive CH_4 flux of all the reservoirs in the study (6.94 mmol m^{-2} d^{-1}) and was statistically higher than all reservoirs except TCR07. The lowest mean littoral ebullitive flux of all reservoirs in the study was 0.12 mmol m^{-2} d^{-1}, measured at TCR06. The CH_4 flux at reservoirs TCR01, TCR02, TCR03, TCR05 and TCR08 were comparable, with medians ranging from 1.35 to 2.96 mmol m^{-}

^{2} d^{-1}. The release of other GHGs (CO_2 and N_2O) was also investigated, but CH_4 dominated the ebullitive GHG flux (Figure B.2 and Figure B.3, respectively).

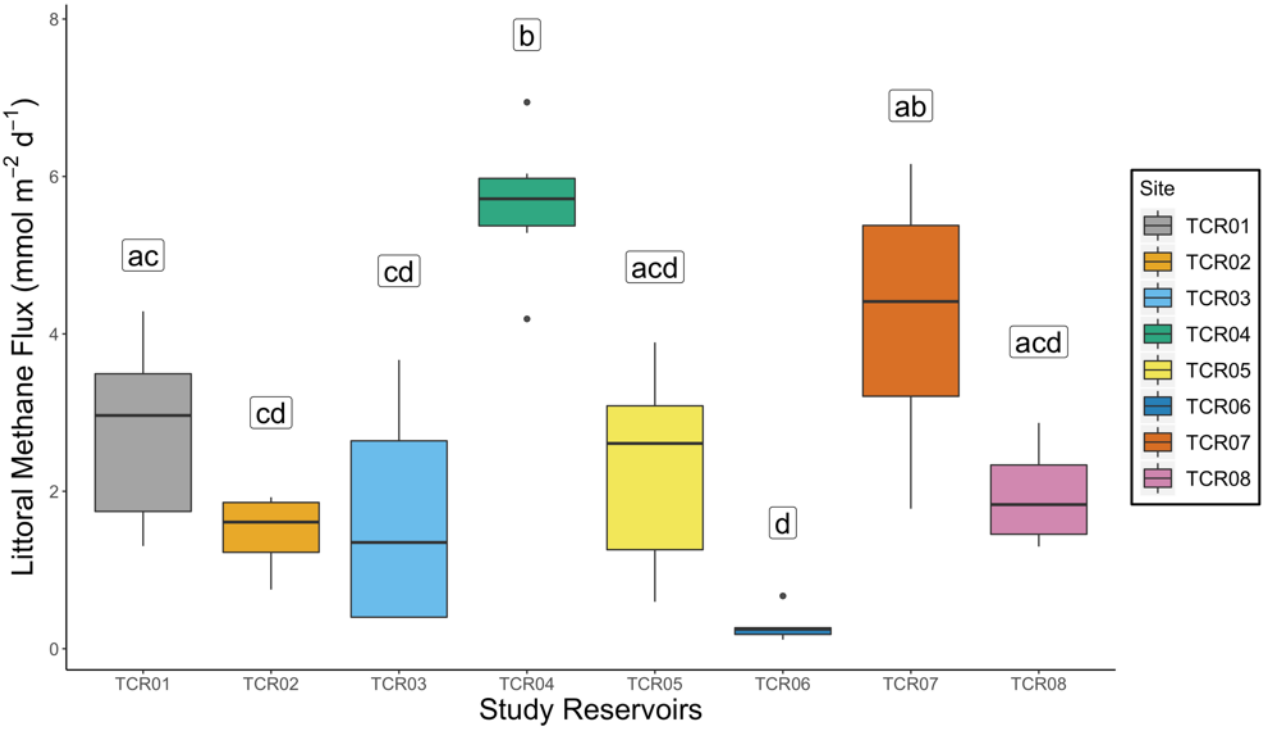

Figure 3.3: Boxplots of the range in total annual littoral CH_4 flux demonstrated in 2017. Sites with the same letters are not significantly different from one another. The boxplot displays data distribution (median, two hinges [25th and 75th percentiles], two whiskers [max and min range], and outlying points). Note that group labelling is generated in R and lettering is not sequential according to flux; reservoirs with the same labels are significantly similar to each another.

3.3.2 Relationships with reservoir physicochemical variables

The eight study reservoirs were all small (< 1 ha), but exhibited a range of depth (1.4–4.6 m) and chemical characteristics (Table 3.1, 3.3). In general, pH was circumneutral to slightly basic (7.2–8.6), and did not demonstrate much variation throughout the season. Average N levels, both as TAN and NO_3^- were generally low (< 1 mg L^{-1}), with the exception of higher NO_3^- concentrations at TCR07 and TCR06 (4.8 and 3.6, respectively). Chlorophyll *a* levels varied substantially across the sites (range: 6–80 µg L^{-1}), while DOC exhibited a similar pattern, but variation was less than 2-fold. Reservoirs TCR04, TCR05, TCR07 and TCR08 were visually

more productive reservoirs in comparison to the others — often partially or fully covered in duckweed (*Lemnoideae*). Sulphate, like Chl *a*, varied substantially among the sites, with values ranging by an order of magnitude (Table 3.3). Average open-water season water temperature near the sediments ranged from 9.0–14.3˚C, with five sites averaging greater than 13.4˚C. Two of the colder reservoirs (TCR02 and TCR08) were down in depressions and surrounded by large trees/shrubs. These sites held ice notably longer than most others during spring melt. The largest and deepest reservoir (TCR01) was also somewhat cooler. In contrast, the warmest reservoir, TCR04, was also the shallowest. This reservoir was on the uppermost bench of the escarpment where it received little shading from surrounding topography or surrounding vegetation, suggesting it was exposed to the most solar radiation. In general, reservoir water chemistry was relatively stable over the course of the season (Figure B.8), although DOC and Chl *a* were generally higher in late summer/early fall.

Table 3.3: Reservoir physicochemical characteristics including water temperature and chemistry (2017 only) and sediment organic matter (OM), and particle size (average of 2017 and 2018 samples). Values shown are averages with standard deviation below in parentheses.

Site ID	Temp	DO	pH	TAN	NO_3^-	SO_4^{2-}	DOC	Chl *a*	OM	Clay	Silt	Geomean
	˚C	mg L^{-1}		μg L^{-1}	mg L^{-1}	mg L^{-1}	mg L^{-1}	μg L^{-1}	%	%	%	μm
TCR01	12.3 (5.17)	2.80 (3.91)	8.05 (0.29)	54.1 (26.6)	0.377 (0.528)	404 (139)	10.2 (0.904)	19.1 (19.7)	9.32 (4.01)	4.92 (3.09)	65.5 (15.3)	28.2 (12.5)
TCR02	9.01 (3.24)	7.98 (5.09)	7.85 (0.31)	31.8 (39.1)	0.108 (0.12)	126 (51.2)	10.1 (2.57)	13.6 (18.6)	3.91 (NA)	16.6 (NA)	83.4 (NA)	3.36 (NA)
TCR03	13.4 (4.04)	1.65 (2.76)	7.75 (0.20)	35.7 (15.8)	0.0527 (0.0237)	49.8 (60.8)	9.15 (0.968)	6.27 (10.3)	12.0 (2.75)	3.44 (0.602)	72.3 (4.17)	20.7 (5.2)
TCR04	14.3 (3.70)	1.48 (2.92)	7.24 (0.43)	94.1 (86.4)	0.967 (1.56)	46.1 (52.5)	12.3 (5.34)	76.0 (101.2)	7.58 (2.22)	3.44 (1.35)	57.8 (9.16)	38.9 (15.7)
TCR05	13.8 (4.91)	4.23 (4.51)	8.07 (0.25)	46.2 (23.2)	0.623 (1.54)	85.6 (21.6)	15.8 (3.89)	48.7 (38.4)	10.6 (3.86)	2.41 (1.31)	54.5 (10.5)	43.4 (20.3)
TCR06	13.5 (5.27)	3.67 (4.14)	8.04 (0.24)	45.7 (33.4)	3.62 (4.53)	457 (179)	11.3 (3.44)	23.6 (25.2)	6.52 (1.35)	13.4 (10.8)	54.9 (10.4)	25.7 (20.3)
TCR07	13.8 (5.45)	5.96 (5.31)	8.58 (0.55)	110 (97.2)	4.81 (9.64)	83.3 (19.6)	15.2 (5.47)	80.0 (72.3)	6.51 (1.47)	2.94 (1.50)	68.4 (13.9)	33.2 (40.1)
TCR08	12.8 (4.09)	4.79 (4.89)	8.08 (0.47)	39.4 (21.5)	0.707 (1.73)	71.1 (24.7)	11.9 (3.44)	18.3 (17.6)	8.39 (1.79)	2.96 (1.79)	59.9 (13.7)	40.4 (29.6)

Temp & DO at depth
TCR02 sediment characteristics: n=1

To investigate explanatory relationships, mean littoral ebullitive fluxes of CH_4 were tested for correlations with water chemistry and sediment parameters. Ebullitive CH_4 flux rates were positively correlated with Chl *a* concentrations but lost significance after Bonferroni correcting (Pearson's product-moment correlation, R= 0.82, p = 0.007; Bonferroni corrected p = 0.079), as did TAN (Pearson's product-moment correlation, R= 0.84, p = 0.009; Bonferroni corrected p = 0.106) (Figure 3.4). These two variables can be linked to within-system productivity and were significantly correlated with each other (Pearson's product-moment correlation, R= 0.92, p = 0.002; Appendix; Figure B.4). Correlations between littoral ebullitive CH_4 flux and temperature, DO, pH, NO_3^-, SO_4^{2-}, DOC, OM, Clay, Silt, and Geomean were not significant.

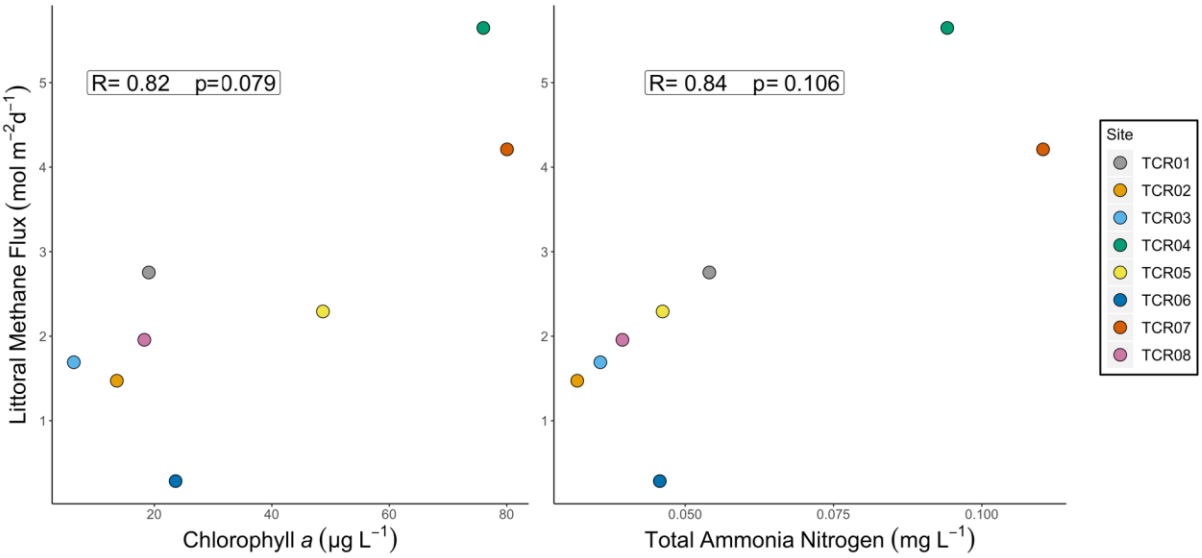

Figure 3.4: Scatterplots of littoral ebullitive CH_4 flux and select water chemistry parameters; chlorophyll a and TAN (p-values Bonferroni corrected).

The PCA highlights orientation of physicochemical parameters of the reservoirs in terms of mean CH_4 production (Figure 3.5) in two-dimensional space. Methane flux was loaded together with temperature and Geomean on principal component 1 (PC1). Variables which can contribute substrate necessary for methanogenesis — Chl *a*, DOC, and indirectly TAN — also plotted near CH_4 flux on PC1. Sulphate showed the opposite pattern to CH_4 flux.

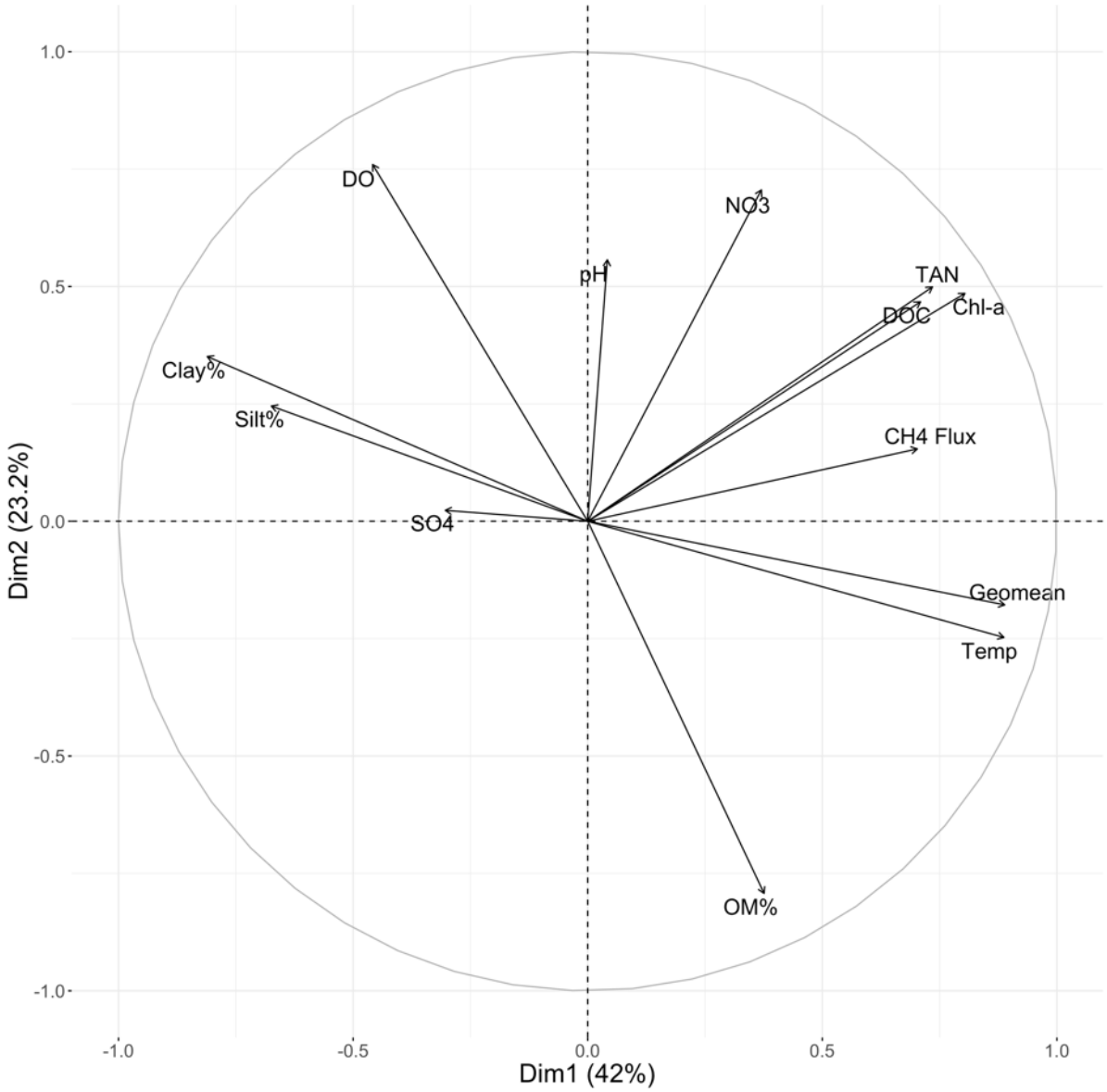

Figure 3.5: Principle components analysis showing the first two principle components (Dim1 and Dim2) of reservoir physicochemical parameters and littoral CH_4 ebullition.

3.3.3 Interannual variations in ebullitive flux from agricultural reservoirs

Relative to 2017, total annual littoral CH_4 flux significantly increased in all but one (TCR08) of the study sites monitored in the 2018 open-water season (Figure 3.6). When considering freshet meltwater (i.e. including precipitation from Nov 1st of the previous year until the end of the deployment period), the 2018 deployment season experienced less total precipitation than in 2017 (431 mm and 368 mm, respectively).

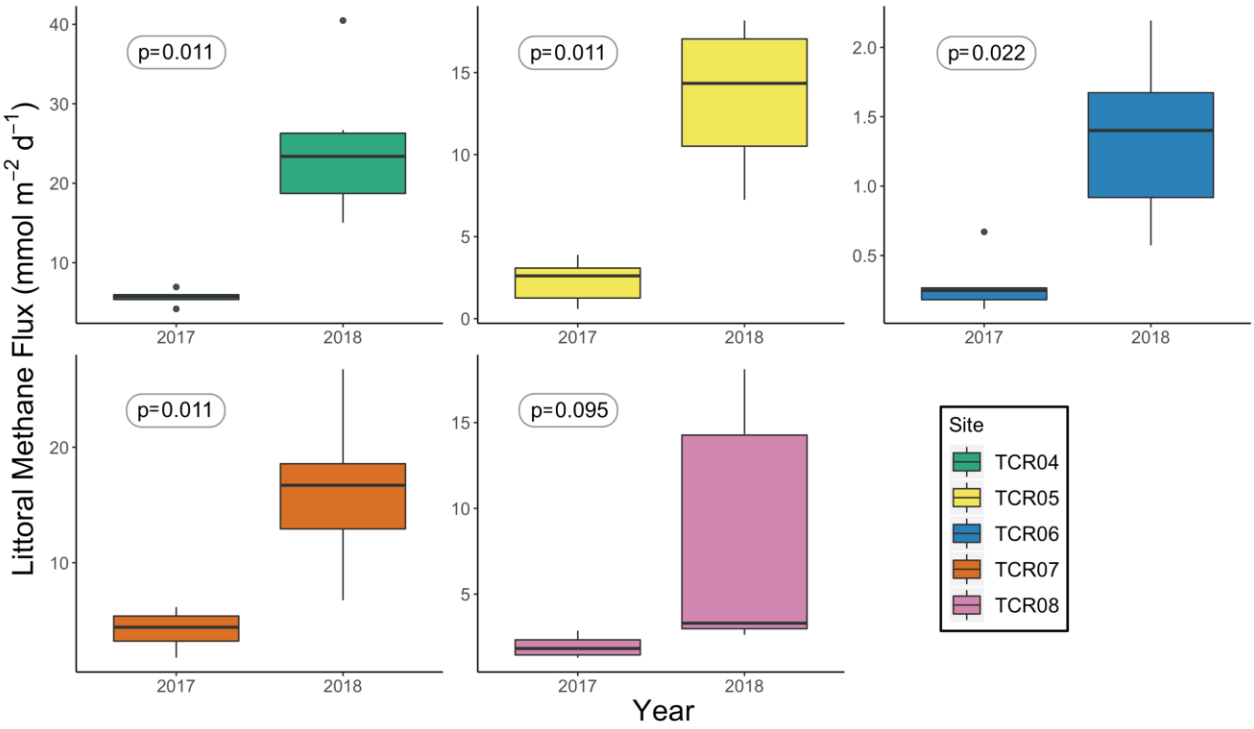

Figure 3.6: Interannual variation (2017 and 2018) of total annual littoral CH_4 flux of the study reservoirs (p-values reported from Wilcoxon-Mann Whitney tests, and Bonferroni corrected). The boxplot displays data distribution (median, two hinges [25th and 75th percentiles], two whiskers [max and min range], and outlying points).

Mean near-sediment pond temperature during the open-water season was significantly greater in 2018 than 2017 (Wilcoxon-Mann Whitney nonparametric test p = 0.024; Figure 3.7). The open-water season of 2018 demonstrated an overall greater change in hydrostatic pressure at depth — indicative of water level change — at most sites compared to 2017 (data normalized to April 25th – August 28th; to encompass the longest stretch of days recorded at all sites for both years); however, significant differences between the years were not detected (Figure 3.8). Of the two variables shown to be significantly related to littoral ebullition rates in this study, TAN concentrations were significantly greater across the five study sites in 2018 than in 2017 (Wilcoxon-Mann Whitney nonparametric test p = 0.034; Figure B.5). Changes in mean Chl *a* concentrations were not significantly different between the two monitoring seasons.

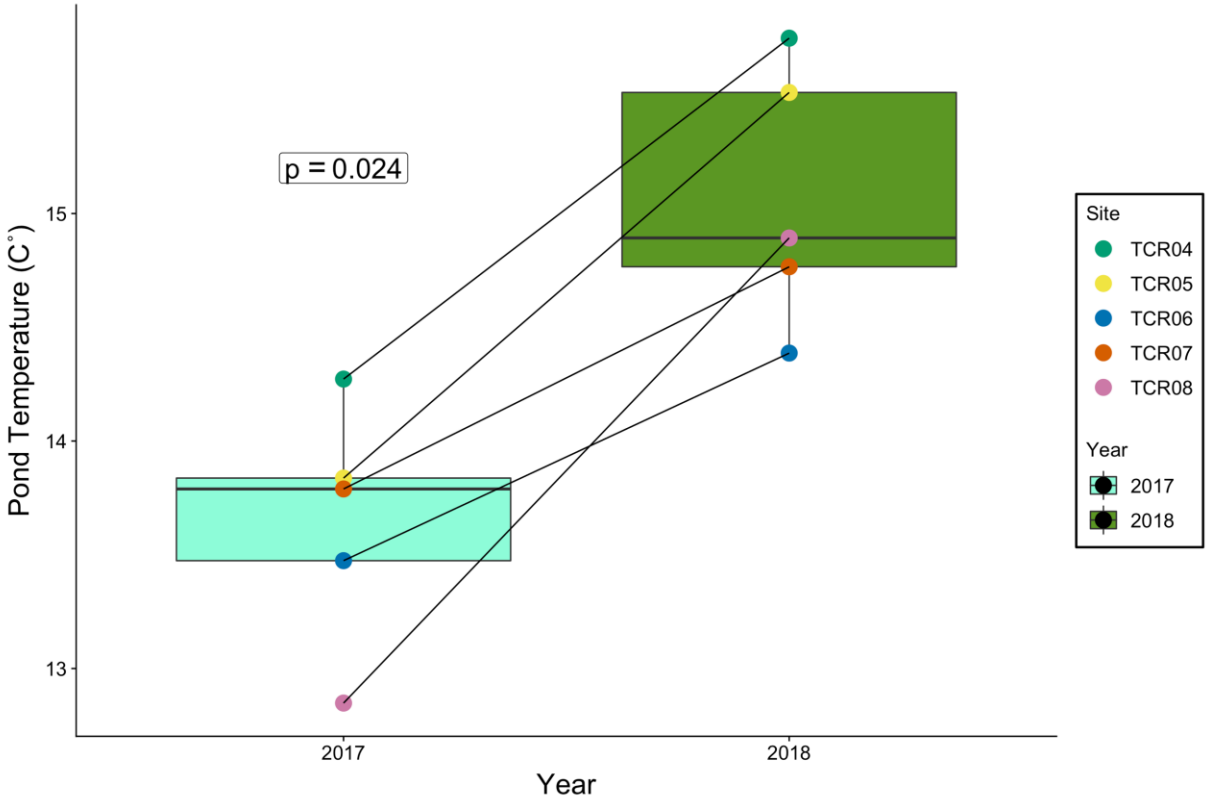

Figure 3.7: Interannual variation (2017 and 2018) of mean pond temperature near the sediments of the study reservoirs (p-value reported from Wilcoxon-Mann Whitney test, and Bonferroni corrected). The boxplot displays data distribution (median, two hinges [25th and 75th percentiles], two whiskers [max and min range], and outlying points). Individual observations are shown as points with connecting lines across years.

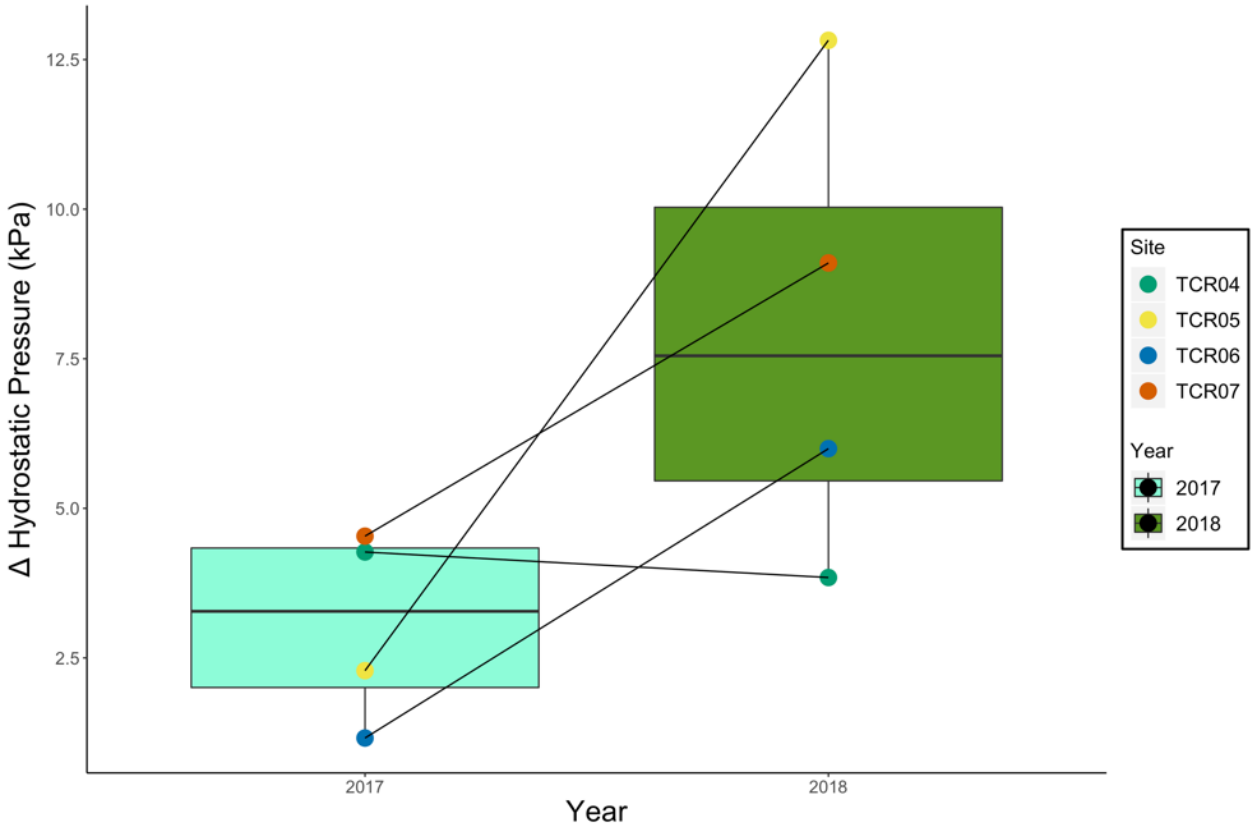

Figure 3.8: Interannual comparison of the change in hydrostatic pressure at depth (indicative of water level change) experienced for each study reservoir during the 2017 and 2018 deployment periods (data used was normalized to April 25th–August 28th; to encompass the longest stretch of days recorded for both years). The boxplot displays data distribution (median, two hinges [25th and 75th percentiles], two whiskers [max and min range], and individual observations as points with connecting lines across years).

3.3.4 Within reservoir: littoral vs. pelagic

Measurements of CH_4 flux from the pelagic zone of the reservoirs, provided by the AES, demonstrated a significantly greater flux than did the littoral zone (Wilcoxon-Mann Whitney nonparametric test $p = 0.014$; Figure 3.9). Average volumetric flux of bubbles released from the sediments was greater in the pelagic zone (577 mL m^{-2} d^{-1}) than in the littoral zone (349 mL m^{-2} d^{-1}), and the CH_4 concentrations of ebullition were also significantly greater (t-test[91] = –5.33, $p = 0.001$) from the pelagic (mean= 5.7 X 10^5 ppmv) relative to the littoral (mean= 4.0 X 10^5 ppmv).

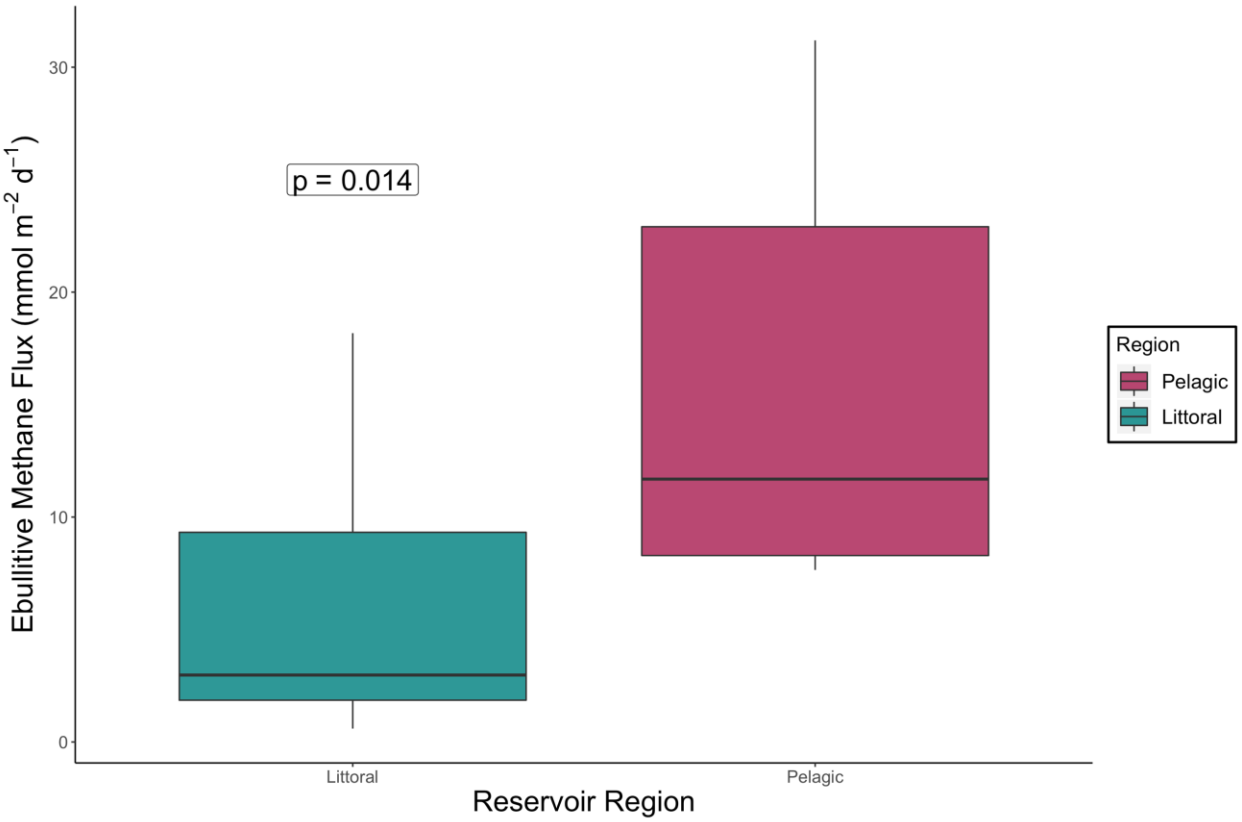

Figure 3.9: Comparison of CH_4 flux from different reservoir zones at TCR02, TCR05 and TCR08 over both 2017 and 2018 seasons (p-value reported from Wilcoxon-Mann Whitney test). The boxplot displays data distribution (median, two hinges [25th and 75th percentiles], and two whiskers [max and min range]).

Sediment organic matter content of pelagic sites was significantly greater than those from littoral sites sampled (t-test[47] = –4.77, Bonferroni corrected $p = 0.001$; Figure 3.10). Clay content, silt content, as well as Geomean, did not show significant differences between zones.

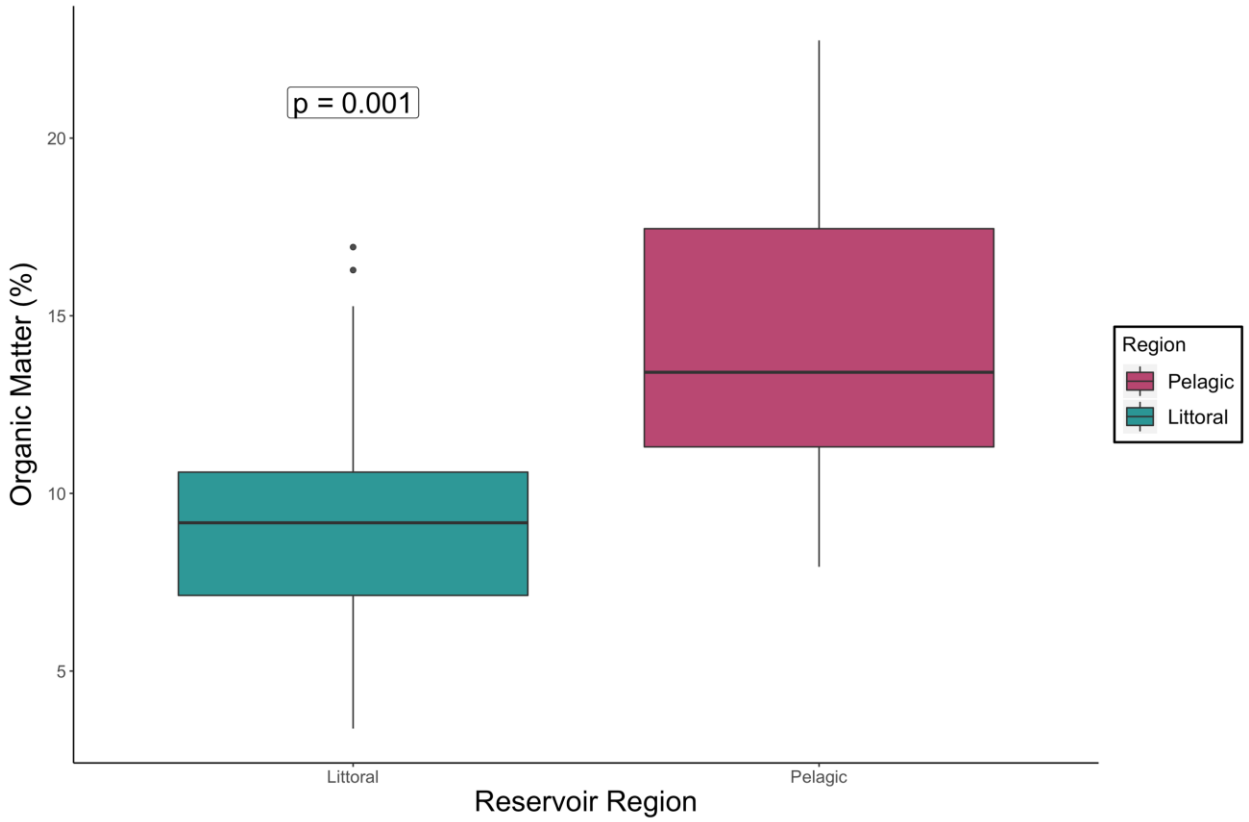

Figure 3.10: Comparison of organic matter content in the different reservoir zones at TCR02, TCR05 and TCR08 over both 2017 and 2018 seasons (p-value reported from unpaired t-test [data normal and demonstrates equal variance]). The boxplot displays data distribution (median, two hinges [25th and 75th percentiles], two whiskers [max and min range], and outlying points).

3.3.5 High temporal resolution analysis of ebullition

Total ebullitive emissions from the pelagic sites of TCR05 were more than double that of similar sites of TCR08 (173 L m^{-2} and 68.2 L m^{-2}, respectively) over the deployment period. Ebullition rates at TCR05 were more consistent over the AES deployment period; whereas TCR08 demonstrated a period of increased rates between ~ mid-June and ~ mid-September (Figure 3.11A and 3.11B). Dissolved oxygen concentrations fluctuated between 0 and 16.5 mg L^{-1} (mean: 3.9 mg L^{-1}) at TCR05, and between 0 and 17.2 mg L^{-1} (mean: 4.5 mg L^{-1}) at TCR08; however, TCR05 demonstrated more gradual seasonal changes and a shorter period of anoxia (~ early-July – mid-August) compared to TCR08 (Figure 3.11C and 3.11D). Water temperature near the sediments of the pelagic zone at TCR05 was 14.4˚C on average (range: 3.9–21˚C), while

on average TCR08 was one degree lower at 13.4˚C (range: 2.7–21.5˚C) (Figure 3.11E and 3.11F). Despite the similarity in temperature of the reservoirs, TCR08 demonstrated a period of relatively static temperatures during ~ mid-June to mid-September (similar to the period of anoxia); while TCR05 did not (Figure 3.11E and 3.11F).

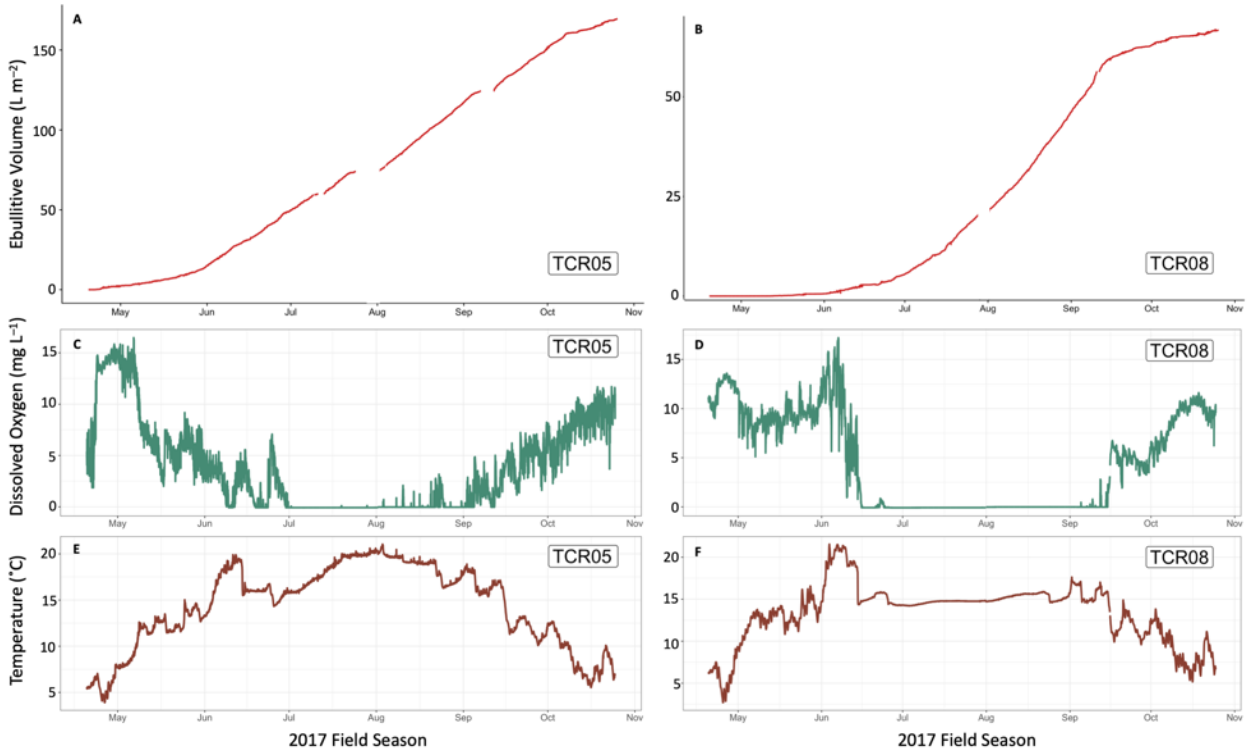

Figure 3.11: Cumulative volume (L m $^{-2}$) released via ebullition from the pelagic zone during the 2017 deployment period (gaps in data are period of non-measurement when datalogger capacity full or volume breached max chamber capacity) at TCR05 (A) and TCR08 (B); dissolved oxygen concentrations (mg L^{-1}) of the water near the sediments of the pelagic zone during the 2017 deployment period at TCR05 (C) and TCR08 (D); temperature (˚C) of the water near the sediments of the pelagic zone during the 2017 deployment period at TCR05 (E) and TCR08 (F).

Wavelet transforms of the aforementioned data records can show timescale-specific relationships between the variables that traditional correlation could not (Varadharajan and Hemond 2012; Sheppard et al. 2017). The coherence between wavelet transforms of temperature and ebullitive release over timescales of 5–20 hours (1 day) show significant synchronicity at both TCR05 (p = 0.011) and TCR08 (p = 0.005). Reservoir TCR05 also demonstrated significant synchronicity over longer timescales of ~ 8–30 days (p = 0.001) and 60–70 days (p = 0.036), while reservoir TCR08 demonstrated significant synchronicity over timescales of ~17–30 days (p = 0.005) (Figure 3.12).

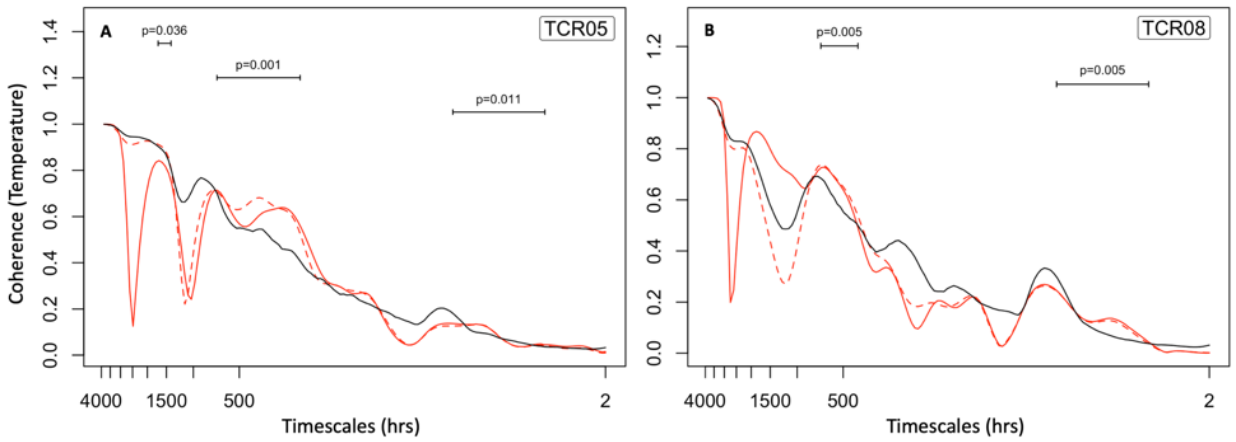

Figure 3.12: Plots of the coherence between wavelet transforms of ebullition and temperature at varying timescales at TCR05 (A) and TCR08 (B). The solid black line indicates the significant threshold (i.e. 95% confidence interval) between the two variables across the range of timescales (hours). Coherence between wavelet transformed variables is significant when either red line is above the black line; solid red line indicates default algorithm, while the dashed red line is the alternate "fast" algorithm. While the two lines are typically similar, the "fast" algorithm is used to make conclusions about significance of coherence. Periods of significant coherence indicated on plot above range of timescales.

The coherence between wavelet transforms of ebullitive flux and DO concentrations was significant (p = 0.004) only over longer timescales of ~63–104 days at TCR05. Longer timescales of coherence were not observed at TCR08; significant synchronicity instead occurred at timescales of 8–10 hours (p = 0.001) as well as 30–40 hours (p = 0.002) and ~8 days (p = 0.032) (Figure 3.13).

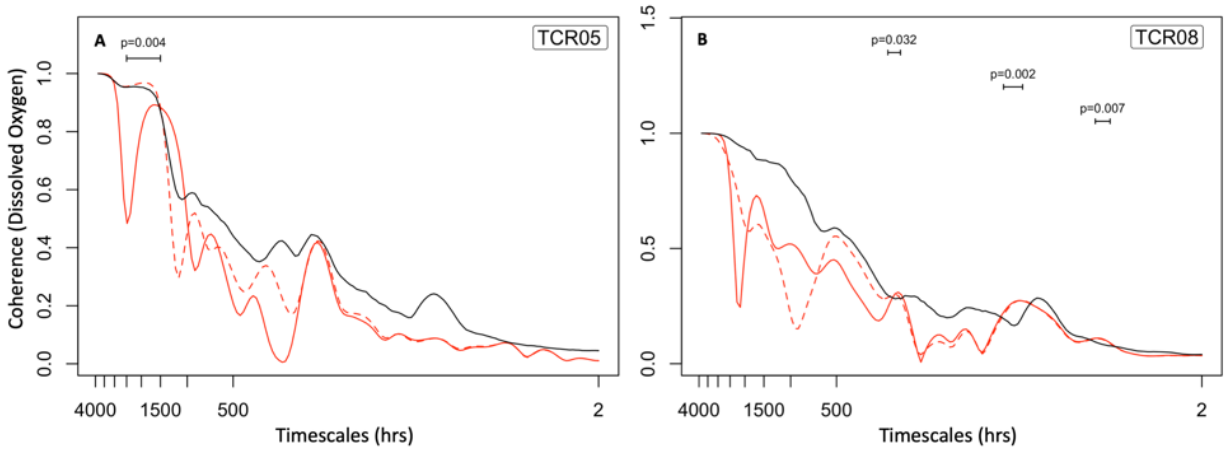

Figure 3.13: Plots of the coherence between wavelet transforms of ebullition and dissolved oxygen at varying timescales at TCR05 (A) and TCR08 (B). The solid black line indicates the significant threshold (i.e. 95% confidence interval) between the two variables across the range of timescales (hours). Coherence between wavelet transformed variables is significant when either red line is above the black line; solid red line indicates default algorithm, while the dashed red line is the alternate "fast" algorithm. While the two lines are typically similar, the "fast" algorithm is used to make conclusions about significance of coherence. Periods of significant coherence indicated on plot above range of timescales.

Atmospheric pressure data recorded hourly at a nearby Environment Canada weather station (#2886; Figure 3.1) was overlain with site-specific hydrostatic pressure observed at depth in the pelagic zone of the reservoirs (Figure 3.14). Recognizing that the HOBO logger deployed near the sediments expresses the influence of atmospheric pressure and water level, only the coherence with hydrostatic pressure is reported here. Furthermore, the coherence output for atmospheric pressure was also similar to that of hydrostatic pressure (Figure B.6). The submerged logger at TCR05 was deployed at ~70 cm above the underlying sediments, and over the season demonstrated an average hydrostatic pressure of 114.3 kPa (range: 109.9–117.2 kPa). At reservoir TCR08 the logger was deployed at ~70 cm above the underlying sediments and demonstrated an average hydrostatic pressure of 107.1 kPa (range: 99.5–110.9 kPa).

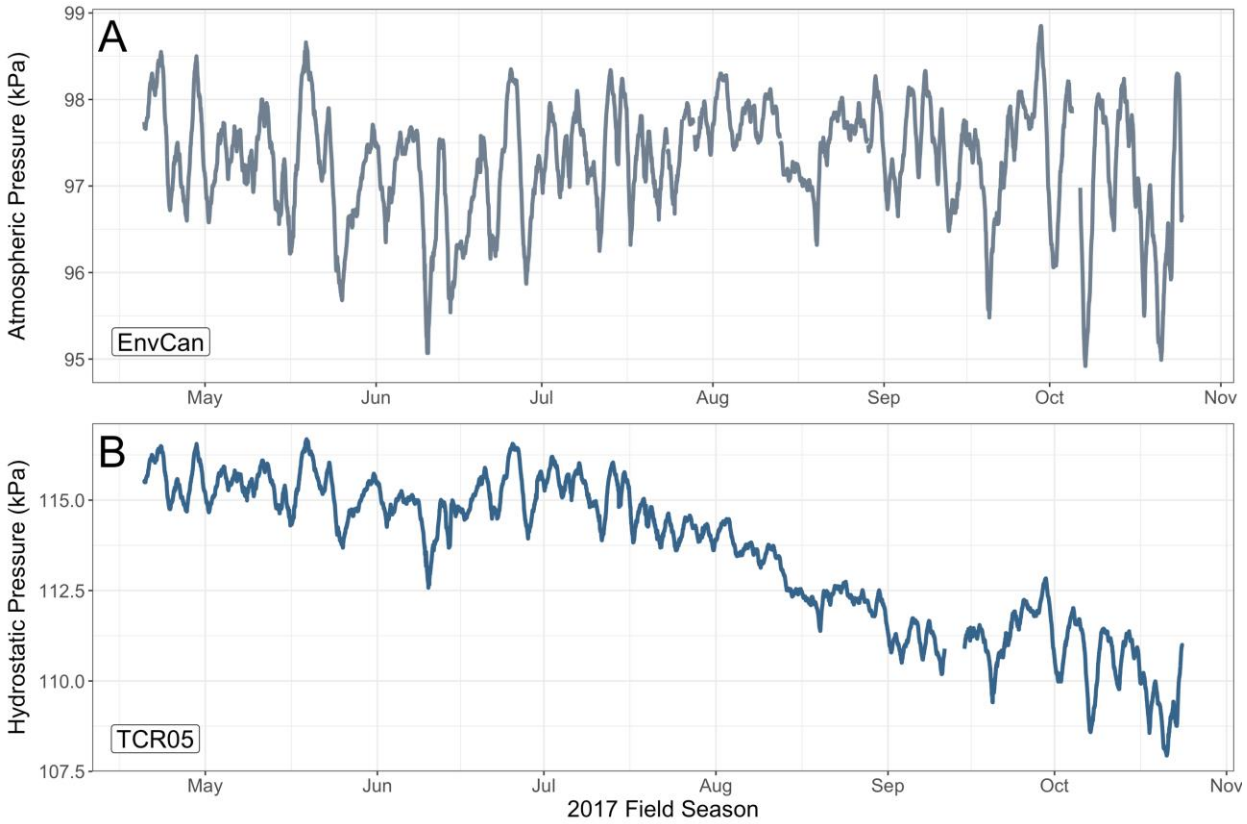

Figure 3.14: Time-series record of regional atmospheric pressure (kPa) from Environment Canada Weather Station #29886 (A), and the observed hydrostatic pressure (kPa) near the sediment-water interface of TCR05 (B) during the 2017 field season.

The coherence between wavelet transforms of ebullitive release and hydrostatic pressure overlying the sediments demonstrated one large range of significant synchronicity (p = 0.001) for timescales of 10–500 hours (~0.5–21 days) at TCR05. Reservoir TCR08 also demonstrated similar synchronicity patterns, often being at or just below the significant threshold of 0.95 (i.e. 95% confidence interval) for this timescale. Specifically, synchronicity at TCR08 was significant at timescales of 12–30 hours (p = 0.008), ~3–6 days (p = 0.001), ~12–66 days (p = 0.001) (Figure 3.15).

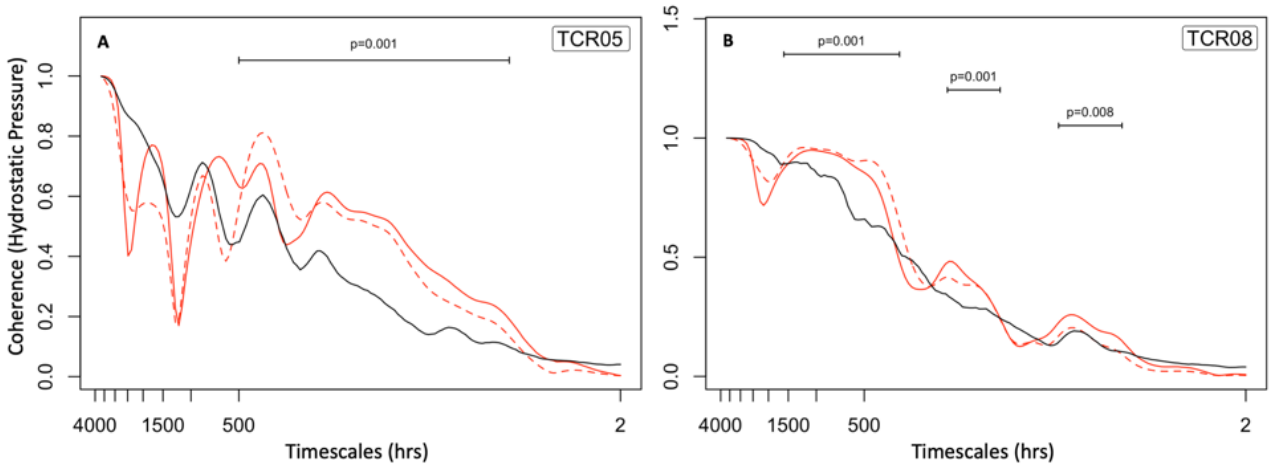

Figure 3.15: Plots of the coherence between wavelet transforms of ebullition and hydrostatic pressure at varying timescales at TCR05 (A) and TCR08 (B). The solid black line indicates the significant threshold (i.e. 95% confidence interval) between the two variables across the range of timescales (hours). Coherence between wavelet transformed variables is significant when either red line is above the black line; solid red line indicates default algorithm, while the dashed red line is the alternate "fast" algorithm. While the two lines are typically similar, the "fast" algorithm is used to make conclusions about significance of coherence. Periods of significant coherence indicated on plot above range of timescales.

3.4 Discussion

Ebullition is an important pathway for CH_4 dominated gas release to the atmosphere (Baulch et al. 2011; Stanley et al. 2016). Despite the importance of ebullition, most available CH_4 flux measurements are limited to diffusive fluxes (e.g. Beaulieu et al. 2019, Ollivier et al. 2019), likely owing to the high spatial and temporal variability of ebullition that make measurement of this process difficult (Wik et al. 2016). This paucity of observational data is one reason that broad-scale greenhouse gas dynamics of freshwater systems are to date not yet well described. Furthermore, by limiting estimates to diffusive fluxes, and thereby omitting the dominant pathway for CH_4 release (potentially upwards of 90% of a system's total CH_4 emissions [Keller and Stallard 1994; Walter et al. 2006]), the role of agricultural landscapes for GHG release to the atmosphere is likely underestimated. The results described above represent an important contribution to our understanding of ebullition at fine spatial and temporal scales in agricultural reservoirs, as well as an enhanced understanding of how these reservoirs contribute to agricultural GHG budgets. It has been suggested that CH_4 will exhibit a strong response to eutrophication patterns over the 21st century, and future nutrient loading to lakes and impoundments may dramatically increase emissions to the atmosphere, opening the possibility

that this source could surpass natural wetland emissions that dominate at present (Beaulieu et al. 2019).

3.4.1 Drivers of ebullition in agricultural reservoirs

The eight agricultural reservoirs investigated in this study demonstrated an average littoral ebullitive CH_4 flux of 2.6 (0.1–6.9) mmol CH_4 m^{-2} d^{-1} during the 2017 field season. This is an important finding as these rates are among the highest observed for lentic systems, with only those rates reported for large tropical reservoirs demonstrating characteristically higher rates (Table 3.4). Interestingly, the range in ebullition rates across the STCW study sites spanned nearly two orders of magnitude, approximately half of the ebullition range reported in global syntheses (Beaulieu et al. 2019).

Reservoirs in the STCW remove significant amounts of nutrients from their source water (Tiessen et al. 2011; Gooding and Baulch 2017). Enhanced nutrient additions can stimulate eutrophication or primary production (Schindler et al. 2012). Chlorophyll *a* has been linked to CH_4 production in lentic systems (Holgerson 2015; Deemer et al. 2016). Both Chl *a* and TAN are thought to be good indicators of autotrophic C fixation, which can lead to C deposition to sediments, and is an important determinant of total CH_4 (and CO_2) flux in lakes (DelSontro et al. 2016) and wetlands (Whiting and Chanton 1993). Ebullition rates have similarly been linked to Chl *a* (DelSontro et al. 2016; Beaulieu et al. 2019). Of the twelve reservoir physicochemical parameters measured in this study, only TAN and Chl *a* were found to be significantly correlated with littoral ebullitive CH_4 flux. In lotic systems, ebullition rates have been reported to be positively related to the proportion of fine (clay and silt) sediment particles (Baulch et al. 2011). This investigation did not find evidence that sediment properties were linked to littoral rates of CH_4 release. While the underlying mechanisms remain unclear, finer sediments (i.e. increased surface area) may provide a more ideal substrate for microbes. However, recent investigations of prairie wetlands in Manitoba and Saskatchewan (Whitfield et al. unpublished data) have also not found evidence of a statistical relationship between ebullition rates and sediment particle size.

Despite few significant relationships among littoral ebullition rates and physicochemical properties, the broad patterns suggested by the PCA are consistent with current understanding. All the variables linked to primary productivity or OM mineralization (TAN, Chl *a*, DOC, and NO_3^-) align with ebullitive CH_4 flux on PC1. The PCA also demonstrates that both SO_4^{2-} and

DO load on PC1 opposite to ebullitive CH_4 flux. Microbial CH_4 production is enhanced in anaerobic environments (Cicerone and Oremland 1988), and is reduced in the presence of high SO_4^{2-} (Pennock et al. 2010). Despite being associated with primary productivity, and serving as the substrate for methanogenesis, OM loaded more strongly on PC2. Most of the study reservoirs featured steep-sided morphology (i.e. dug-out along the mid-line of the reservoir, resulting in steep banks and deeper water near the center), resulting in greater deposition of OM downslope in pelagic zones. This morphology appears to be an important influence on spatial variability within reservoirs (see 3.4.2 below).

Overall, it appears that multiple competing factors are exerting an influence on ebullition rates in the study reservoirs, which, combined with a limited number of study sites, likely contributes to there being few significant relationships found herein. While relationships between, for instance, ebullition or diffuse flux and Chl *a* have been reported in the literature (Beaulieu et al. 2019), these are not particularly well constrained relationships, as there is large variability in the data on which the relationships are based. Additional local or landscape influences were not quantified in the analysis, but can be discussed briefly.

TCR06 had the lowest littoral flux (0.12 mmol CH_4 m^{-2} d^{-1}) of all reservoirs (and moderate OM and Chl *a*), despite being among the warmest. This reservoir is positioned and sheltered down in a depression, with the immediate landscape comprised of largely unmanaged grasses and large vegetation potentially acting as a buffer between the reservoir and surrounding untilled or unfertilized livestock pasture (during the 2017 and 2018 seasons). This may limit the amount of nutrients or remobilized C it receives. In contrast to most other reservoirs, this site showed no visible signs of primary productivity (i.e. *Lemnoideae* cover) over both seasons. TCR06 also featured high SO_4^{2-}, which can impair methanogenesis. Reservoir TCR01 (2.96 mmol CH_4 m^{-2} d^{-1}) likewise had high SO_4^{2-}, and is the largest of all reservoirs. This site is located in a larger riparian valley surrounded by steep hillslopes, and livestock watering was common at the reservoir over both years of study. Livestock disturbance to the soils in the area immediately surrounding the reservoir, and tilled cropland located upslope to the north, may have increased material trapping and benthic sediment accumulation here, compared to TCR06. During instrumentation of this site, sediments were observed to be particularly unconsolidated in comparison to other sites. Additionally, TCR01 and TCR06 were constructed in 1997 and 1990, respectively. Reservoir age can affect GHG flux, as newly immobilized C from the flooded

landscape is more efficiently processed causing the flux to decline as a reservoir matures (St. Louis et al. 2000; Barros et al. 2011).

Table 3.4: Comparison of mean, or range of, ebullitive CH_4 flux reported for lentic systems in different regions of the world.

	Flux mmol CH_4 m^{-2} d^{-1}	Location	Source
Ag Reservoirs (Littoral)	**2.6**	**Manitoba**	**This study 2017**
Ag Reservoirs (Littoral)	**12.7**	**Manitoba**	**This study 2018**
Ag Reservoirs (Pelagic)	**16.3**	**Manitoba**	**This study 2017, 2018**
Ponds	4.6	Québec	DelSontro 2016
Lakes	1.1	Québec	DelSontro 2016
	4	Switzerland	Schubert 2012
	0.02–3.71	Michigan	Bastviken 2004
	0.22–1.53	Finland	Huttunen 2003
	12.4	England	Casper 2000
	0.05–4.26	N. Hampshire	Mattson & Likens 1993
	0.49–1.49	Puerto Rico	Joyce & Jewell 2003
	0.83	Sweden	Wik 2013
Reservoirs	0.03–90.3	Zimbabwe	DelSontro 2011
	0.62–124	Panama	Keller & Stallard 1994
	5.36	Switzerland	DelSontro 2010
	0.04–22.7	Brazil	dos Santos 2006
	16.7	Czech Republic	Sajdlova 2017
	9.6	Germany	Maeck 2013

2017: Sites TCR01–TCR08; 2018: Sites TCR04–TCR08; 2017, 2018: Sites TCR02, TCR05, and TCR08

Of all eight study reservoirs, TCR04 demonstrated the highest ebullitive CH_4 flux rate, followed by TCR07. These two reservoirs demonstrate the highest Chl *a* and TAN concentrations, and experience in the field was that they are both productive, as inferred from observations of *Lemnoideae* partially or fully covering the reservoir surface at various times. Reservoir TCR07 had the highest Chl *a*, TAN, and NO_3^- concentrations, and was the only site featuring tile drainage. These two sites are also comparatively well exposed and featured warmer water temperatures (Table 3.3). For instance, the ephemeral TCR04 is the shallowest (max depth of ~1.4 m; April 2017) reservoir, and rather than being located in a somewhat hillslope and vegetation-sheltered riparian depression like most, TCR04 is largely unsheltered by virtue of its

location in the middle of a relatively flat and notably active agricultural cropland. As such, increased solar radiation into the shallow water body may be an important driver of warmer temperatures. Furthermore, TCR04 features active agricultural cropland that extends to much of the periphery of the reservoir. Over both the 2017 and 2018 seasons this cropland was observed to be more heavily tilled and worked than witnessed in others — increasing the likelihood of remobilized C and nutrient inputs into this warm and light-abundant reservoir.

3.4.2 Role of spatial and temporal variability in ebullition

Detailed observations of study reservoirs revealed characteristic differences in time and space, beyond statistically significant inter-site differences in littoral ebullition. The AES were critical in allowing for differences between littoral and pelagic rates to be discerned. Confidence in this comparison can be found based on the reliability demonstrated by the AES (R. E. J. Helmle: Chapter 2). Monitoring both the littoral and pelagic zones over the two study years in select reservoirs revealed significant variability — with pelagic ebullitive CH_4 flux being much greater, and among the highest for freshwater systems. The mean pelagic flux rate of 16.3 mmol CH_4 m^{-2} d^{-1} (range: 7.65–31.2 mmol CH_4 m^{-2} d^{-1}) was nearly three times greater than the nearby littoral zone flux rate of 6.04 mmol CH_4 m^{-2} d^{-1} (range: 0.596–18.2 mmol CH_4 m^{-2} d^{-1}) at TCR02, TCR05, and TCR08 over both 2017 and 2018 seasons. This suggests that current estimates of the role of ebullition for global CH_4 emission from freshwater systems are likely underestimated. Most measurements are performed in littoral areas with depths < 2 m, and deep areas of lakes or large reservoirs are typically not strong sources of ebullition due to the potential for dissolution or methanotrophy during transit through overlying water columns. These results demonstrate the need to characterize ebullition rates at these intermediate depths.

Reservoirs can exhibit hotspots of CH_4 emissions near the lotic-lentic interface as suspended loads slow and settle out (Delsontro et al. 2011; Maeck et al. 2013; Harrison et al. 2017). These patterns were not observable in this study (Figure B.7) as inputs to these systems are dominated by snowmelt, and lotic inputs for the majority of the open-water season are believed negligible. The hotspot of importance in these systems is the pelagic zone, a result of significantly greater amounts of OM in these deeper reaches due to the constructed reservoir design and morphology. These reservoirs are predominantly dug out such that the area along the

mid-line of the reservoir and adjacent to the earth-dam is the deepest and can act as a sink for sediments travelling downslope into these pelagic zones, as well as a repository for autochthonous C introduced at the reservoir surface. While DO concentrations were monitored in the littoral zone only during site visits (mean: 8.8 mg L^{-1}; range: 1.7–28.1 mg L^{-1}), autotrophic activity, and exposure to the overlying atmosphere likely result in shorter periods of anoxia for sediments in the shallower littoral waters. Consequently, in these study systems, CH_4 concentrations in bubbles were significantly greater (*t*-test[91] = –5.33, $p = 0.001$) and volumetric flux larger in the pelagic (5.7 X 10^5 ppmv and 577 mL m^{-2} d^{-1}, respectively) than that from the littoral (4.0 X 10^5 ppmv and 349 mL m^{-2} d^{-1}, respectively).

Notable year-to-year variability was also demonstrated in those reservoirs (TCR04–TCR08) monitored in both years. In 2018, all five reservoirs demonstrated greater littoral flux rates — four of which were significant. The reservoirs ordered from greatest to lowest in 2017 mean flux rates are TCR04, TCR07, TCR05, TCR08, and TCR06, and the amount by which each reservoir increased in 2018 flux rates follows the same order of magnitude (18.8, 12.1, 11.3, 6.07, and 1.06 mmol CH_4 m^{-2} d^{-1}, respectively) — demonstrating that higher emitters were more sensitive to greater absolute changes in interannual variability. With patterns being similar across all study reservoirs, it appears that annual variations in local hydroclimate seemed to be an important control on flux in these systems for these years. When considering freshet meltwater (i.e. including precipitation from Nov 1st of the previous year until the end of the deployment period) the 2018 deployment season experienced less total precipitation than in 2017. Experience in the field was that the region was notably dryer and reservoir water levels initially lower in spring of 2018 than in 2017 — likely due to visibly less spring freshet meltwater in 2018. As a result, the reservoirs demonstrated a greater drop in water level during the 2018 field season than in the 2017 field season (Figure 3.8).

This interannual variability likely influences the strength of relationships with potential drivers. In fact, while 2017 Chl *a* was correlated with littoral ebullition flux of CH_4, comparison to ebullition rates predicted from a regression model based on Chl *a* concentrations (Beaulieu et al. 2019) resulted in a strong tendency to overestimate rates across the eight reservoirs (Figure 3.16). Conversely, performing the same exercise according to 2018 observations suggests that predicted rates would underestimate ebullitive CH_4 flux (Figure 3.16). The higher ebullition rates in 2018 of this investigation occurred despite Chl *a* levels being lower than that of 2017 (Figure

B.5). Littoral ebullitive CH_4 flux rates in 2018 were also positively correlated with Chl *a* concentrations, but this correlation was not found to be significant (Figure B.10). These results may be demonstrating a lag-effect of ebullitive CH_4 flux being stimulated by primary productivity (i.e. increased flux rates in 2018 were a product of increased C assimilation and deposition in 2017). This is a strong indication that multi-year records may be critical to understanding the principle drivers of ebullition — highlighting a potential opportunity to establish more advanced predictive models of ebullition fluxes.

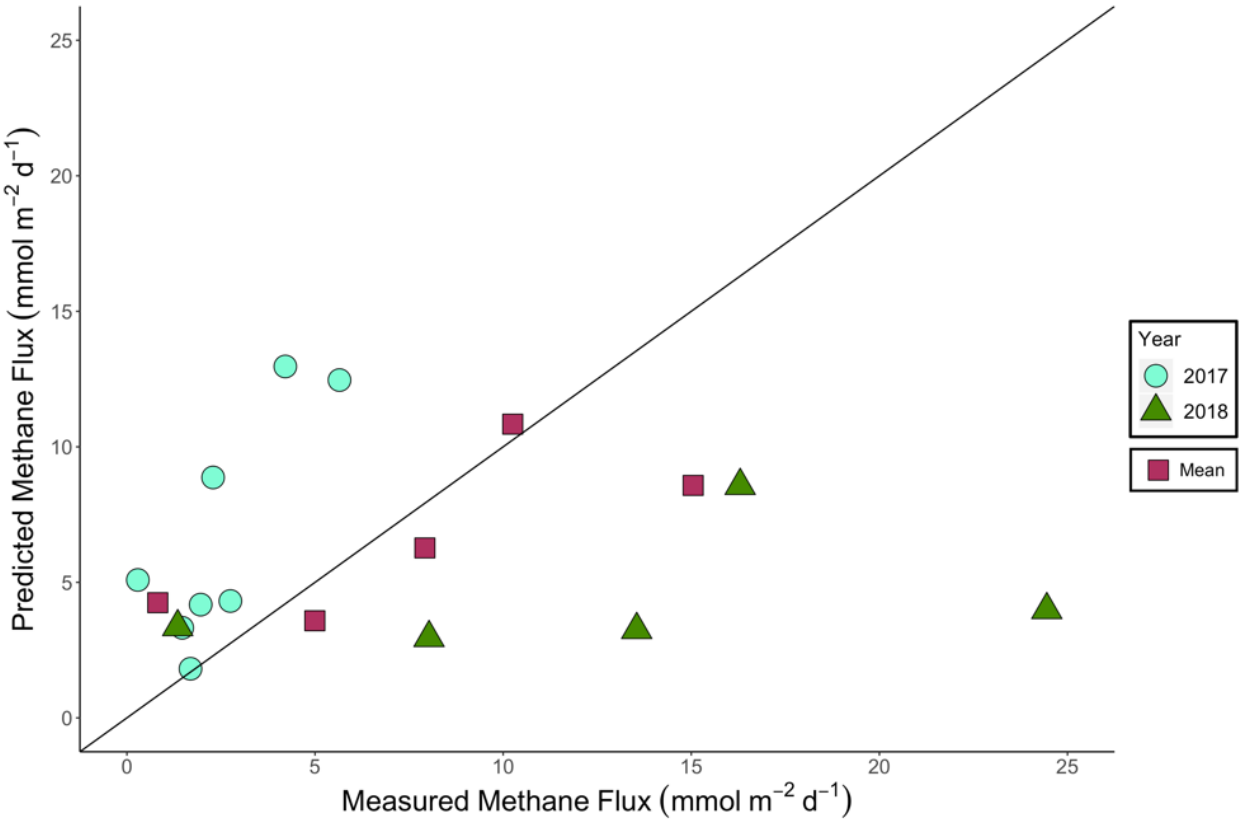

Figure 3.16: Measured and Chl *a* predicted (from Beaulieu et al. 2019 regression model) littoral ebullitive CH_4 flux for the study reservoirs in 2017, 2018, and the mean of both study years for each reservoir.

Enhanced microbiological activity within the sediments stimulating CH_4 production in 2018, when water levels were lower, could be a direct result of warmer temperatures. The greater change in hydrostatic pressure on the sediments (i.e. greater water level reduction) in most reservoirs during 2018 may also have contributed to enhanced emissions, as reduced pressure on the sediments can lead to heightened CH_4 release (Tokida et al. 2007; Beaulieu et al. 2018).

While hydropeaking (i.e. periodic drops or fluctuations in hydrostatic pressure) has been reported to enhance CH_4 emissions from large reservoirs (Harrison et al. 2017), others suggest that drawdown affects the timing of emissions, without a change in overall CH_4 yield (J. Beaulieu, pers. comm. 2019). Experimental manipulation of hydrostatic pressure via reservoir drawdown (water levels reduced 23 cm over a 10-hour period) at TCR08 in 2018 demonstrated increased flux rates compared to periods immediately preceding the drawdown (Table B.1). Reservoir TCR08 was the only reservoir for which ebullitive CH_4 release did not increase significantly in 2018. This might be partly due to the fact that this reservoir is the only multi-purpose dam where water levels are actively controlled by the landowner through reservoir drawdown each fall (J. Pankiw, pers. comm. 2017). Water level drawdown can also contribute to enhanced diffusive emissions via degassing on the outlet side of the dam (Maeck et al. 2013). While it was possible to quantify elevated rates of ebullition during manual drawdown periods, this was possible only at TCR08 owing to inoperable outlets at the remainder of the study sites. Further investigation is required to understand the role of water level management at the study sites.

The efficiency of methanogenesis is known to increase with increased temperatures (Zeikus and Winfrey 1976), but how ebullitive flux is influenced by seasonal variations of temperature is rarely studied in great detail. At TCR05 significant synchronicity between temperature and ebullitive flux was detected at larger scales of 63–70 days. Although nearing the significance threshold at similar scales, significant synchronicity with temperature was not detected at TCR08; however, this might be impacted by relatively static temperature observed across an extended period in the summer months (Figure 3.11). Temperature at this site decreased somewhat in mid-June, coincident with *Lemnoideae* coverage beginning, suggesting an important interaction with solar radiation during the peak of summer. Coherence between wavelet transforms of ebullitive emissions and near-sediment pond temperature show significant synchronicity at longer scales (~2 weeks to 1 month) at both TCR05 and TCR08, indicative of ebullitive flux (i.e. CH_4 production) increasing with seasonal increases in temperature. Both reservoirs demonstrated significant synchronicity with temperature at very short timescales (~1 day), which may reflect changes in gas solubility associated with diurnal temperature changes. During the 2018 field season, sediment temperatures were significantly higher during the day at TCR08 (Wilcoxon-Mann Whitney nonparametric test $p = 0.002$). At TCR05, daytime and nighttime temperatures averaged 14.3˚C and 14.1˚C, respectively, but were not significantly

different. This suggests that diurnal variations in sediment (or water) temperatures might be an important factor to take into account when characterizing a system in terms of CH_4 contributions. As a result, studies in which observations are limited to daytime hours, or diel studies based on several short (sub-hourly) periods of observations could be subject to bias.

While methanogenesis has been uncommonly demonstrated in aerobic conditions (Bogard et al. 2014), microbial CH_4 production primarily occurs in anaerobic environments (Conrad 1996), with again little knowledge on the temporal relationships between these two variables. Significant synchronicity between DO concentrations were detected at long timescales (~2–3 months) at TCR05, but this was not the case at TCR08 where significant synchronicity between these two variables was detected at shorter timescales (8–10 hrs, 30–40 hrs, and ~8 days) at TCR08. Further study is necessary to better understand the role of changing DO in these systems.

Over short timescales of hours to weeks, atmospheric pressure can fluctuate or drop, and these pressure fluctuations have been reported to trigger ebullition events (Tokida et al. 2007; Crawford et al. 2014). The coherence outputs between ebullition and hydrostatic pressure were notably shorter than most other instances of synchronicity. TCR05 demonstrated significance over the range of 10–500 hours (~0.5–21 days), which reflects periods of atmospheric pressure induced fluctuations on the hydrostatic pressure record (Figure 3.14). Similar trends were observed at TCR08, which also demonstrated significant synchronicity with hydrostatic pressure at longer timescales (12–66 days). While the reasons for longer periods of synchronicity at TCR08 are not definitive, it could be speculated that the reservoir's morphology and nature of the reservoir being drained each fall could play a role. Unlike TCR05, water levels decreased shortly after instrumentation at TCR08, which could be suggestive of an increased opportunity to observe coherence at scales approaching two months. Additionally, whereas TCR05 exhibited more of a step-change in rates (low initially, then higher), TCR08 demonstrated a more gradual change in ebullition rates during the first three months of observation, which might lend itself to detection of synchronicity at longer timescales given the gradual nature of water level drawdown.

3.4.3 Importance of ebullition in agricultural reservoirs and implications for design and management

It has been demonstrated that the nature of constructed reservoirs in the STCW promotes enhanced microbial production of CH_4 within the underlying sediments, although to varying degrees in different reservoirs. The results herein provide insights into holistic management or potential adaptation strategies for constructed agricultural reservoirs in a way that promotes the benefits they confer while minimizing tradeoffs associated with CH_4 release. Reservoirs acting as the highest sources of CH_4 via ebullition featured physicochemical parameters indicative of higher primary productivity, demonstrating that nutrient loading can be an important control on CH_4 flux. Reservoir TCR07 demonstrated the highest flux among the study sites; this was the only reservoir where tile drainage was used. While tile drainage has not yet seen wide uptake in MB (Kokulan et al. 2019), these results suggest that enhanced nutrient movement associated with this practice could yield higher CH_4 emissions in receiving reservoirs or other freshwaters. This parallels work of Jacinthe et al. (2012), who reported elevated GHG emissions following hydrologic events resulting in material transfers to a large agricultural reservoir. Further research should be pursued to provide more conclusive evidence, but these results suggest that avoiding locations with tile drainage might be pragmatic with respect to future siting of reservoirs. Moreover, siting of reservoirs such that they are not immediately adjacent to worked agricultural lands or subject to fertilizer inputs may also be warranted. Future research could investigate the role of buffer strips on reservoirs, or shallow natural water bodies more generally, to understand if this can be used as an additional BMP to reduce nutrient loads, and consequently CH_4 emissions. Study reservoirs featuring lower CH_4 fluxes (TCR06 and TCR01) also tended to have high SO_4^{2-} concentrations. As such there might be an opportunity to implement reservoirs to inhibit methanogenesis in addition to focusing on practices to reduce nutrient and C inputs to these systems. Identifying locations where reservoirs can feature high SO_4^{2-} concentrations, either through input of groundwater, or by forming a (terminal) basin that promotes evapoconcentration of dissolved solutes could also present an opportunity to limit methanogenesis. Targeted investigations should be carried out for all suggestions mentioned here prior to making conclusive recommendations about reservoir siting.

One potentially important finding of this study was that the ephemeral reservoir (TCR03) demonstrated lower total ebullitive CH_4 fluxes. This reservoir typically goes dry in June (L.

McEwan, pers. comm. 2017), as was observed during both years of the study, indicating a more limited period for methanogenesis to occur. If the rates for this reservoir are normalized to the open water period, it would have the second lowest mean emissions of CH_4 via ebullition (0.78 mmol m^{-2} d^{-1}). The reservoir is situated in a grove featuring mature trees as well as shrubs and tall grasses in the understory. This vegetation has access to water in the vadose zone during the early part of the growing season, thus unlike the other reservoirs, which, apart from aquatic macrophytes, are predominantly unvegetated, fixation of C by vegetation and storage in aboveground biomass within the footprint of the reservoir could be important for balancing some CH_4 emitted each spring.

While not within the scope of the current study, alternate GHG emission pathways within reservoirs (i.e. diffuse flux, vegetation flux, exposed saturated sediments) should also be investigated. Since this study demonstrated that interannual variability — a result of hydroclimate effects on water temperature and varying water level — is significant for these systems, the effects of warmer temperatures and receding water leading to exposed sediments should be also investigated. A notable next step would be to understand how GHG may be released via exposed sediments as reservoir water levels recede. Furthermore, most reservoir boundaries were dominated by *Typha* for most of the season, representing an important seasonal assimilation and subsequent input of nutrients (Whitfield et al. 2019) and C into littoral zones as these materials decay. Likewise, aquatic macrophytes can act as a conduit of GHG transfer from sediments to atmosphere (Chanton et al. 1993); thus, understanding their role in these reservoirs could lead to additional opportunities to reduce emissions of GHG (e.g. via seasonal removal of this C-based material before decay and deposition) from these systems.

Atmospheric CH_4 demonstrates a GWP_{100} that is 25 times that of CO_2 (IPCC 2014), and arguably more so when its effects via atmospheric interactions (i.e. tropospheric ozone, stratospheric water vapour) are taken into consideration (Hansen and Sato 2001). Fortunately, atmospheric CH_4 also has a relatively shorter lifetime of ~10 years relative to that of CO_2 (up to thousands of years) (Lelieveld et al. 1998; Dlugokencky et al. 2009), and reduction in its emissions creates an opportunity for quick benefits in terms of atmospheric warming. While design and management of reservoir systems such as those considered herein can be targeted to elicit reductions in CH_4 emitted via ebullition, it should be acknowledged that even with changes to management that reduce nutrient inputs to these systems, there may be significant lags in CH_4

emission due to legacy effects of considerable nutrient loading over more than three decades. In contrast, CH_4 from livestock is a dominant source of agricultural GHG emissions (Environment Canada 2019), and one with notable opportunity for reductions (Asgedom and Kebreab 2011). In light of the climate crisis, there is a need to address all aspects of agricultural GHG emissions, including indirect impacts to aquatic systems, but also through more direct emissions pathways that can have immediate impact.

3.5 Conclusions

This study is among the first to both quantify, and identify important dynamics of, the ebullitive CH_4 flux from agricultural reservoirs in the Canadian prairies. The results show that when quantifying ebullitive CH_4 flux using typical measurement techniques (manually-operated BTs in littoral zones), agricultural reservoirs are hotspots of CH_4 production and release — making them strong contributors to atmospheric CH_4 concentrations, relative to other lentic freshwater systems. Primary production, or C assimilation, was an important factor driving the range in flux exhibited across the reservoirs in this region. Furthermore, annual ebullitive flux was higher in 2018 when the reservoirs demonstrated greater absolute reductions in water level, as well as elevated water temperatures compared to those in 2017. Comparing fluxes emitted from different locations within reservoirs demonstrated that there is significantly greater flux being released from the pelagic zone of these reservoirs, likely owing to higher OM accumulation in the deeper reaches associated with reservoir design and morphology. Stronger anoxia may also be important for driving ebullition in the pelagic zones as high temporal resolution identified synchronicity between ebullitive flux and DO. Temperature at both long (seasonal) and short (diel) timescales was also synchronous with ebullition. Constructed agricultural reservoirs like those studied herein are essential tools for agricultural productivity in the face of an increasing global population and pressures for food and water security; however, it is equally essential to fully analyze GHG emissions in the face of impending climate change. This study identifies important variations of the ebullitive flux pathway that should be taken into consideration when developing research designs for comprehensive flux quantification of these systems; both spatially (across and within reservoir) and temporally (diel, seasonal, and interannual). These results demonstrate that limiting nutrient inputs to these reservoirs will be

important for limiting CH_4 flux via ebullition, but that additional considerations when siting these reservoirs (e.g. seasonal longevity), are expected to be important for retaining nutrients and water during spring to reduce downstream flooding, without establishing conditions which contribute to hotspots of CH_4 release.

3.6 Acknowledgements

I would like to acknowledge my field partner, Carlie Elliott for her hard work, determination and patience throughout both field seasons; as well as Lauren Dyck and Stephanie Witham for additional field assistance. I would like to acknowledge Dr. Helen Baulch and the entire SaskWatChE (Saskatchewan Water Chemistry and Ecology) lab group, for their assistance and support with laboratory analyses, experiments and field expeditions. Special acknowledgement to Dr. Nora Casson and her lab group (Jeremy Leathers, Hamza Amjad, Emily Kroft, and Kody Oleson) from the University of Winnipeg for field assistance; Dr. Dan Karran for his assistance with data analysis and support. I would like to acknowledge the Deerwood Soil and Water Management Association and, in particular, Les McEwan, Jim Pankiw and the landowners of STCW reservoirs. Funding for this work was provided through a grant from AAFC (Agricultural Greenhouse Gases Program) and a Faculty Start-up Grant (USask) awarded to C.J. Whitfield.

3.7 Author contributions

The bulk of the field work was performed by R.E.J Helmle and field partner Carlie Elliott, with assistance from Lauren Dyck and Stephanie Witham. R.E.J Helmle performed majority of the laboratory work as well as both data and statistical analyses, and was lead author on the manuscript, with support and contributions from C.J. Whitfield.

Chapter 4: General conclusions

4.0 Summary

With growing pressures on earth systems threatening to cross planetary boundaries (e.g. Steffen et al. 2015), coupled with increased food security challenges for the expanding global population, it is important to understand the impacts and interactions of anthropogenic activity on natural systems. It is speculated that anthropogenic activity has influenced global atmospheric CH_4 concentrations for ~3000 years (Ruddiman 2005), and this influence has increased at an alarming rate since the industrial age (Dlugokencky et al. 2011; Mitchell et al. 2013). Within the larger context of global C cycles, emissions of CH_4 to the atmosphere are of particular concern due to the strong global warming potential of this greenhouse gas, and because sources of CH_4 have outpaced sinks globally, contributing to rising concentration levels as a result of anthropogenic activity.

Agricultural practices influence atmospheric CH_4 concentrations in a number of ways (e.g. landscape manipulation [Keller et al. 1990], biomass burning [Hao and Ward 1993], fossil fuel combustion [e.g. Kirschke et al. 2013; Schwietzke et al. 2016], aggregated livestock [Wolf et al. 2017], fertilizer-soil interactions [Carlson et al. 2017]). Despite the number of CH_4 sources within agricultural landscapes, agricultural C budgets and ultimately their contributions to global atmospheric budgets remain poorly described. While ebullition is acknowledged as being the dominant pathway of CH_4 release to the atmosphere, the few existing flux measurements of agricultural reservoirs are typically limited to diffusive fluxes (Ollivier et al. 2019). This thesis aimed to improve our ability to quantify ebullitive flux in agricultural reservoirs, and to use measurements of this flux to characterize the potential for CH_4 release from agricultural reservoirs. Part of the interest in this topic stems from the fact that agricultural practices contribute to widespread land modification as well as redistribution of materials (including fertilizers) on the landscape, and understanding how these activities impact freshwater resources could contribute to improving BMPs.

In Chapter 2 an automated sensor (AES) was developed and tested to measure ebullition flux in shallow lentic aquatic systems. In both experimental and field settings the AES proved to be an effective device to measure the volume released through the process of ebullition in shallow aquatic systems — at a high temporal resolution, as well as in typically unmeasured

zones. The AES demonstrated a volume measurement error that is small, and less than or similar to operator errors (conducted in a controlled setting) associated with manually-operated traps often used to measure ebullition. The AES also provided gas concentration samples comparable to those extracted from traditional sediment gas concentration sampling techniques. As a result, the sensors provide reliable records of ebullition similar to those typically used, but can also provide an advanced look at GHG dynamics of freshwater systems (i.e. deployment in pelagic zones, temporal trends at high resolution). These instruments provide advantages in characterizing the spatial and temporal nature of ebullition, while also improving capacity to quantify fluxes of specific gases when compared to existing methods.

For use in agricultural reservoirs, and in similar systems, the low-maintenance AESv2 (with its ability to self-purge, energy efficiency, and wireless data transmission potential) could be a relatively cost-friendly option for measuring ebullitive flux with greater detail than previous techniques. Along with the abilities mentioned above, AESv2 exhibits a number of improvements over AESv1 (i.e. shorter total length, smaller air-water interface in collection chamber). While the AESv2 developed for this study proved effective to accurately measure gas volumes in the laboratory, as well as in the field, the upgraded circuit board was prone to failure after varying amounts of deployment time, most likely due to a low-cost release solenoid used for the self-purging mechanism which caused a voltage kick-back that paused data logging. As a result, most AESv2 data records were short and unusable for the comparative (spatial and temporal) analyses performed in Chapter 3. Future versions of the AES (currently in development) seek to rectify this issue via upgraded circuit boards with integrated protective measures and a high-quality release solenoid. Further enhancement of the AES also presents opportunity for upgrades such as the addition of both CO_2 and CH_4 concentration sensors — which would provide detailed analysis on the trends and concentration dynamics of these ebullitive gases at high temporal resolutions, while also reducing laboratory analytical costs. An upgraded AES, with the ability to accurately measure both volumetric fluxes, and GHG concentrations, at high temporal resolutions for extended unmanned periods would be highly valuable for future freshwater GHG emissions research, as this would allow fluxes of individual gases to be quantified in near real-time.

In Chapter 3 the sensors were used alongside traditional techniques to both quantify and identify dynamics of the ebullitive CH_4 flux from agricultural reservoirs in STCW. The results

clearly demonstrate that agricultural reservoirs can be hotspots of CH_4 production and release. Primary production, or C assimilation, was an important factor driving the range in flux exhibited across the reservoirs in this region. Notably, ebullitive CH_4 flux from these systems was higher than reported for most freshwater systems. Furthermore, while quantification of ebullitive CH_4 flux from these systems is critical for developing accurate GHG budgets, this study demonstrates that analyzing different dynamics of the ebullitive flux (i.e. interannual variations, within-reservoir variations) is just as important, as these variations can be significant. Interannual variation was attributed to the effects of annual variations in local hydroclimate on both water temperature and water level (i.e. hydrostatic pressure on the sediments) in these systems. Perhaps more importantly, deployment and utilization of the novel AES permitted quantifying CH_4 release as ebullition from the typically unmonitored pelagic zones, which were found to have rates up to three-fold higher than did littoral zones. Given the limitations of other methods used to quantify ebullition, this finding provides a strong rationale to investigate ebullition of the nutrient rich, productive, freshwaters of the prairies, including for instance, the lakes of southern Saskatchewan, that feature moderate depths and bank morphology not entirely dissimilar to the steep sided reservoirs that were common to many of the study sites. Furthermore, while the study sites investigated herein may have comparatively steeper banks and deeper pelagic zones than those of natural small lentic systems, including pothole wetlands that were once ubiquitous in this landscape and for which these reservoirs serve to replace, the findings of this study could be applied more broadly across the landscape in similar systems (i.e. ponds, wetlands, ditch-pools etc.) that share similar properties.

The detailed temporal investigations described in this thesis (i.e. deployment of AES and associated high-resolution time-series variables monitored) also contributed to illustrating notable differences between sites. Two relatively nearby reservoirs (TCR05 and TCR08) are both situated at the bottom of the Manitoba escarpment and appear rather similar in terms of their contributing areas. The detailed records obtained at these reservoirs demonstrate how the dynamics of physicochemical parameters (i.e. ebullitive CH_4 flux, temperature) can surprisingly vary non-uniformly among different reservoirs over the course of a season. Developing an enhanced understanding of the dynamics and interactions within these systems will be an important tool for understanding (and potentially predicting) how ebullition might change under future climate conditions.

4.1 Implications for the use and management of reservoirs

Constructed agricultural reservoirs like those studied herein are useful tools for agricultural productivity in the face of increasing global population and pressures for food and water security; however, it is becoming increasingly important to develop more sound GHG emissions estimates (from agriculture and other industries) in the face of impending climate change. Agriculturists often create small reservoirs to reduce flood damage and/or aid agricultural practices, and constructed reservoirs can be important components of the C cycle (Soumis et al. 2004). These reservoirs slow hydrologic flow paths by storing water, but often have considerably higher sedimentation rates shortly following reservoir construction — leading to storage of large amounts of C that was destined for transport elsewhere (Stallard 1998). It has been long speculated that large amounts of C are being stored and processed within lentic systems — potentially accounting for missing portions of C in global budgets (Mulholland et al. 1982; Kempe 1984). This study contributes to addressing this issue by providing data driven insights on the CH_4 contributions of these lentic systems to agricultural GHG budgets, and therefore advances the capacity to quantify agricultural contributions to global atmospheric GHG budgets.

The results of this study demonstrated that strategic implementation and subsequent management of these reservoirs and surrounding lands in ways that reduce primary productivity, or C assimilation, in the reservoirs could yield reduced CH_4 emissions. Given the importance of primary productivity for ebullition rates, both in this study and in broader regional analyses, reservoirs constructed with buffer zones (a BMP accepted as a tool for other aquatic systems in the region) immediately surrounding them could serve as a simple technique to integrate CH_4 emission mitigation strategies into more holistic water resource management strategies. Furthermore, planning for reservoir construction (i.e. morphology and location) such that OM does not accumulate in the anoxic deeper regions might be suggested to mitigate the significantly greater flux being released from pelagic zones. Sites conducive to establishing ephemeral reservoirs could be important for minimizing saturated periods when anoxia develops, but also in supplying water to vegetation capable of long-term storage of C as aboveground biomass. Additional investigations on the effect that reservoir water volume (i.e. pressure on sediments and temperature) has on CH_4 flux would be beneficial, as these systems demonstrated significant interannual variability — a result of hydroclimate effects on water temperature and varying

water level. Insights gained from this research could help inform holistic implementation and management strategies of agricultural reservoirs that allow continued use of the benefits they confer, while mitigating trade-offs associated with ebullitive CH_4 release to the atmosphere.

While this research yielded an enhanced understanding of the dynamics of ebullitive CH_4 release, this work will benefit from a more complete picture of system behaviour with respect to GHG budgets. While some suggestions are made here on possible mitigative approaches to reservoir design and management, such approaches will necessarily be informed by additional study of diffusive water-atmosphere GHG exchange that will help to provide a more comprehensive understanding of the behaviour of these systems and their role as hotspots of GHG exchange. Future studies will benefit from increasing the number of sensors deployed, as ebullition has demonstrated high variability over small spatial scales. Moreover, there are additional auxiliary GHG emission pathways, with their own respective temporal and spatial dynamics (i.e. vegetation mediated, newly exposed saturated sediments, diffuse fluxes) that warrant investigation. Developing full GHG budgets incorporating all potential pathways will be an important next step for characterizing these systems in terms of their atmospheric GHG contributions to the atmosphere. This more comprehensive analysis is necessary to permit consideration of possible trade-offs that could be used to guide reservoir implementation and management strategies.

References

Abril, G., F. Guérin, S. Richard, and others. 2005. Carbon dioxide and methane emissions and the carbon budget of a 10-year old tropical reservoir (Petit Saut, French Guiana). Global Biogeochem. Cycles **19**: 1–16. doi:10.1029/2005GB002457

Addison, P. 2002. The Illustrated Wavelet Transform Handbook,.

Asgedom, H., and E. Kebreab. 2011. Beneficial management practices and mitigation of greenhouse gas emissions in the agriculture of the Canadian Prairie: A review. Agron. Sustain. Dev. **31**: 433–451. doi:10.1007/s13593-011-0016-2

Barros, N., J. J. Cole, L. J. Tranvik, Y. T. Prairie, D. Bastviken, V. L. M. Huszar, P. Giorgio, and F. Roland. 2011. Carbon emission from hydroelectric reservoirs linked to reservoir age and latitude. Nat. Geosci. **4**: 593–596. doi:10.1038/ngeo1211

Bastviken, D., J. Cole, M. Pace, and L. Tranvik. 2004. Methane emissions from lakes : Dependence of lake characteristics , two regional assessments , and a global estimate. Global Biogeochem. Cycles **18**: 1–12. doi:10.1029/2004GB002238

Bastviken, D., L. J. Tranvik, J. A. Downing, P. M. Crill, and A. Enrich-Prast. 2011. Freshwater Methane Emissions Offset the Continental Carbon Sink. Science (80-.). **331**: 50–50. doi:10.1126/science.1196808

Battin, T. J., S. Luyssaert, L. A. Kaplan, A. K. Aufdenkampe, A. Richter, and L. J. Tranvik. 2009. The boundless carbon cycle. Nat. Geosci. **2**: 598–600. doi:10.1038/ngeo618

Baulch, H. M., P. J. Dillon, R. Maranger, and S. L. Schiff. 2011. Diffusive and ebullitive transport of methane and nitrous oxide from streams: Are bubble-mediated fluxes important? J. Geophys. Res. Biogeosciences **116**. doi:10.1029/2011JG001656

Beaulieu, J. J., D. A. Balz, M. K. Birchfield, and others. 2018. Effects of an Experimental Water-level Drawdown on Methane Emissions from a Eutrophic Reservoir. Ecosystems **21**: 657–674. doi:10.1007/s10021-017-0176-2

Beaulieu, J. J., T. DelSontro, and J. A. Downing. 2019. Eutrophication will increase methane emissions from lakes and impoundments during the 21st century. Nat. Commun. **10**: 3–7. doi:10.1038/s41467-019-09100-5

Bogard, M. J., P. A. del Giorgio, L. Boutet, M. C. G. Chaves, Y. T. Prairie, A. Merante, and A. M. Derry. 2014. Oxic water column methanogenesis as a major component of aquatic CH4 fluxes. Nat. Commun. **5**: 5350. doi:10.1038/ncomms6350

Boon, P. I., and A. Mitchell. 1995. Methanogenesis in the sediments of an Australian freshwater wetland: Comparison with aerobic decay, and factors controlling methanogenesis. FEMS Microbiol. Ecol. **18**: 175–190. doi:10.1016/0168-6496(95)00053-5

Bridgham, S. D., H. Cadillo-Quiroz, J. K. Keller, and Q. Zhuang. 2013. Methane emissions from wetlands: Biogeochemical, microbial, and modeling perspectives from local to global scales. Glob. Chang. Biol. **19**: 1325–1346. doi:10.1111/gcb.12131

Bubier J.L., MooreT.R., R. N. T. 1993. Methane Emissions from Wetlands in the Midboreal Region of Northern Ontario , Canada. Ecol. Soc. Am. **74**: 2240–2254.

Canada, E. and C. C. 2019. National Inventory Report 1990–2017: Greenhouse Gas Sources and Sinks in Canada.

Carlson, K. M., J. S. Gerber, N. D. Mueller, and others. 2017. Greenhouse gas emissions intensity of global croplands. Nat. Clim. Chang. **7**: 63–68. doi:10.1038/nclimate3158

Carpenter, S. R., N. F. Caraco, D. L. Correll, R. W. Howarth, A. N. Sharpley, and V. H. Smith. 1998. Nonpoint pollution of surface waters with phosphorus and nitrogen. Ecol. Appl. **8**: 559–568.

Chanton, J. P., G. J. Whiting, J. D. Happell, and G. Gerard. 1993. Contrasting rates and diurnal patterns of methane emission from emergent aquatic macrophytes. Aquat. Bot. doi:10.1016/0304-3770(93)90040-4

Cicerone, R. J., and R. S. Oremland. 1988. Biogeochemical Aspects of Atmophseric Methane. Global Biogeochem. Cycles **2**: 299–327.

Cole, J. J., Y. T. Prairie, N. F. Caraco, and others. 2007. Plumbing the global carbon cycle: Integrating inland waters into the terrestrial carbon budget. Ecosystems **10**: 171–184. doi:10.1007/s10021-006-9013-8

Comas, X., L. Slater, and A. Reeve. 2007. Is situ monitoring of free-phase gas accumulation and release in peatlands using ground penetrating radar (GPR). Geophys. Res. Lett. **34**: 1–5. doi:10.1029/2006GL029014

Conrad, R. 1996. Soil microorganisms as controllers of atmospheric trace gases (H2, CO, CH4, OCS, N2O, and NO). Microbiol. Rev. **60**: 609–40. doi:https://doi.org/10.1007/978-3-642-61096-7_11

Crawford, J. T., E. H. Stanley, S. A. Spawn, J. C. Finlay, L. C. Loken, and R. G. Striegl. 2014. Ebullitive methane emissions from oxygenated wetland streams. Glob. Chang. Biol. **20**:

3408–3422. doi:10.1111/gcb.12614

Daelman, M. R. J., E. M. van Voorthuizen, U. G. J. M. van Dongen, E. I. P. Volcke, and M. C. M. van Loosdrecht. 2012. Methane emission during municipal wastewater treatment. Water Res. doi:10.1016/j.watres.2012.04.024

Dean W.E., and E. Gorham. 1998. Magnitude and Signifigance of Carbon Burial in Lakes, Reservoirs, and Peatlands. Geology **26**: 535–538. doi:10.1130/0091-7613(1998)026<0535

Deemer, B. R., J. A. Harrison, S. Li, and others. 2016. Greenhouse Gas Emissions from Reservoir Water Surfaces : A New Global Synthesis. Bioscience **66**: 949–964. doi:10.1093/biosci/biw117

DelSontro, T., L. Boutet, A. St-Pierre, P. A. del Giorgio, and Y. T. Prairie. 2016. Methane ebullition and diffusion from northern ponds and lakes regulated by the interaction between temperature and system productivity. Limnol. Oceanogr. **61**. doi:10.1002/lno.10335

Delsontro, T., M. J. Kunz, T. Kempter, A. Wüest, B. Wehrli, and D. B. Senn. 2011. Spatial heterogeneity of methane ebullition in a large tropical reservoir. Environ. Sci. Technol. **45**: 9866–9873. doi:10.1021/es2005545

Delwiche, K. B., and H. F. Hemond. 2017. Methane Bubble Size Distributions, Flux, and Dissolution in a Freshwater Lake. Environ. Sci. Technol. **51**: 13733–13739. doi:10.1021/acs.est.7b04243

Denfeld, B. A., H. M. Baulch, P. A. del Giorgio, S. E. Hampton, and J. Karlsson. 2018. A synthesis of carbon dioxide and methane dynamics during the ice-covered period of northern lakes. Limnol. Oceanogr. Lett. **3**: 117–131. doi:10.1002/lol2.10079

Dlugokencky, E. J., L. Bruhwiler, J. W. C. White, and others. 2009. Observational constraints on recent increases in the atmospheric CH4 burden. Geophys. Res. Lett. **36**: 3–7. doi:10.1029/2009GL039780

Dlugokencky, E. J., E. G. Nisbet, R. Fisher, and D. Lowry. 2011. Global atmospheric methane: Budget, changes and dangers. Philos. Trans. R. Soc. A Math. Phys. Eng. Sci. **369**: 2058–2072. doi:10.1098/rsta.2010.0341

Downing, J. A. 2010. Emerging global role of small lakes and ponds : little things mean a lot. Limnetica **29**: 9–24.

Downing, J. A., and J. J. Cole. 2006. The global abundance and size distribution of lakes , ponds , and impoundments. Limnol. Oceanogr. **51**: 2388–2397.

Downing, J. A., J. J. Cole, C. M. Duarte, and others. 2012. Global abundance and size distribution of streams and rivers. Inl. Waters **2**: 229–236. doi:10.5268/IW-2.4.502

Dudgeon, D., A. H. Arthington, M. O. Gessner, Z. Kawabata, R. J. Naiman, D. J. Knowler, and C. Le. 2006. Freshwater biodiversity : importance , threats , status and conservation challenges. Biol. Rev. **81**: 163–182. doi:10.1017/S1464793105006950

Dunbabin, M., and A. Grinham. 2010. Experimental Evaluation of an Autonomous Surface Vehicle for Water Quality and Greenhouse Gas Emission Monitoring. 5268–5274.

Falkowski, P. 2000. The Global Carbon Cycle: A Test of Our Knowledge of Earth as a System. Science (80-.). **290**: 291–296. doi:10.1126/science.290.5490.291

Fendinger, N. J. N. J., D. D. D. D. Adams, and D. E. D. . Glotfelty. 1992. The role of gas ebullition in the transport of organic contaminants from sediments. Sci. Total Environ. **112**: 189–201. doi:10.1016/0048-9697(92)90187-W

Frouzova, J., M. Tušer, and P. Stanovsky. 2015. Quantification of methane bubbles in shallow freshwaters using horizontal hydroacoustical observations. Limnol. Oceanogr. Methods **13**: 609–616. doi:10.1002/lom3.10051

Galloway, J. N., Z. Dianwu, V. Thomson, and L. H. Chang. 1996. Nitrogen Mobilization in the United States of America and the People's Republic of China. Atmos. Environ. **30**: 1551–1561. doi:https://doi.org/10.1016/1352-2310(95)00456-4

Glaser, P. H., J. P. Chanton, P. Morin, D. O. Rosenberry, D. I. Siegel, O. Ruud, L. I. Chasar, and A. S. Reeve. 2004. Surface deformations as indicators of deep ebullition fluxes in a large northern peatland. Global Biogeochem. Cycles **18**. doi:10.1029/2003GB002069

Glozier, N. E., J. A. Elliott, B. Holliday, J. Yarotski, and B. Harker. 2006. Water Quality Characteristics and Trends in a Small Agriculutral Watershed: South Tobacco Creek, Manitoba 1992-2001. 100.

Gooding, R. M., and H. M. Baulch. 2017. Small Reservoirs as a Beneficial Management Practice for Nitrogen Removal. J. Environ. Qual. **46**: 96. doi:10.2134/jeq2016.07.0252

Goossens, D. 2008. Techniques to measure grain-size distributions of loamy sediments: A comparative study of ten instruments for wet analysis. Sedimentology **55**: 65–96. doi:10.1111/j.1365-3091.2007.00893.x

Greinert, J., and B. Nützel. 2004. Hydroacoustic experiments to establish a method for the determination of methane bubble fluxes at cold seeps. Geo-Marine Lett. **24**: 75–85.

doi:10.1007/s00367-003-0165-7

Gupta, H. V., H. Kling, K. K. Yilmaz, and G. F. Martinez. 2009. Decomposition of the mean squared error and NSE performance criteria: Implications for improving hydrological modelling. J. Hydrol. **377**: 80–91. doi:10.1016/j.jhydrol.2009.08.003

Hansen, J. E., and M. Sato. 2001. Trends of measured climate forcing agents. Proc. Natl. Acad. Sci. U. S. A. doi:10.1073/pnas.261553698

Harrison, J. A., B. R. Deemer, M. K. Birchfield, and M. T. O'Malley. 2017. Reservoir Water-Level Drawdowns Accelerate and Amplify Methane Emission. Environ. Sci. Technol. acs.est.6b03185. doi:10.1021/acs.est.6b03185

Harrison, J. A., R. J. Maranger, R. B. Alexander, A. E. Giblin, P. J. Emilio, S. P. Seitzinger, D. J. Sobota, and W. M. Wollheim. 2009. The regional and global significance of nitrogen removal in lakes and reservoirs. Biogeochemistry **93**: 143–157. doi:10.1007/s10533-008-9272-x

Holgerson, M. A. 2015. Drivers of carbon dioxide and methane supersaturation in small , temporary ponds. Biogeochemistry **124**: 305–318. doi:10.1007/s10533-015-0099-y

Holgerson, M. A., and P. A. Raymond. 2016. Large contribution to inland water CO2 and CH4 emissions from very small ponds. Nat. Geosci. **9**. doi:10.1038/ngeo2654

Hope, J., Harker, D.B., & and Townley-Smith, L. 2002. Long Term Land Use Trends For Water Quality Protection: Ten Years of Monitoring in the South Tobacco Creek Watershed.

Horn, M. A., C. Matthies, K. Ku, A. Schramm, and H. L. Drake. 2003. Hydrogenotrophic Methanogenesis by Moderately Acid-Tolerant Methanogens of a Methane-Emitting Acidic Peat. Appl. Environ. Microbiol. **69**: 74–83. doi:10.1128/AEM.69.1.74

Huttunen, J. T., J. Alm, A. Liikanen, S. Juutinen, T. Larmola, T. Hammar, J. Silvola, and P. J. Martikainen. 2003. Fluxes of methane, carbon dioxide and nitrous oxide in boreal lakes and potential anthropogenic effects on the aquatic greenhouse gas emissions. Chemosphere **52**: 609–621. doi:10.1016/S0045-6535(03)00243-1

IPCC. 2014. Climate Change 2014: Synthesis Report,.

Jacinthe, P. A., G. M. Filippelli, L. P. Tedesco, and R. Raftis. 2012. Carbon storage and greenhouse gases emission from a fl uvial reservoir in an agricultural landscape. Catena **94**: 53–63. doi:10.1016/j.catena.2011.03.012

Janssen, P. H. M., and P. S. C. Heuberger. 1995. Calibration of Process-Orientated Models. Ecol.

Modell. **83**: 55–66. doi:https://doi.org/10.1016/0304-3800(95)00084-9

Keller, M., M. E. Mitre, and R. F. Stallard. 1990. Consumption of atmospheric methane in soils of central Panama: Effects of agricultural development. Global Biogeochem. Cycles. doi:10.1029/GB004i001p00021

Keller, M., and R. F. Stallard. 1994. Methane emission by bubbling from Gatun Lake, Panama. J. Geophys. Res. **99**: 8307–8319. doi:10.1029/92JD02170

Kellner, E., A. J. Baird, M. Oosterwoud, K. Harrison, and J. M. Waddington. 2006. Effect of temperature and atmospheric pressure on methane (CH4) ebullition from near-surface peats. Geophys. Res. Lett. **33**. doi:10.1029/2006GL027509

Kelly, C. A., J. W. M. Rudd, R. A. Bodaly, and others. 1997. Increases in Fluxes of Greenhouse Gases and Methyl Mercury following Flooding of an Experimental Reservoir. Environ. Sci. Technol. **31**: 1334–1344. doi:10.1021/es9604931

Kempe, S. 1984. Sinks of the Anthropogenically Enhanced Carbon Cycle in Surface Fresh Waters. Geophys. Res. **89**: 4657–4676.

Kirschke, S., P. Bousquet, P. Ciais, and others. 2013. Three decades of global methane sources and sinks. Nat. Geosci. **6**. doi:10.1038/ngeo1955

Kling, G., G. Kipphut, and M. Miller. 1991. Arctic lakes and streams as gas conduits to the atmosphere: implications for tundra carbon budgets. Science (80-.). **251**: 298–301. doi:10.1126/science.251.4991.298

Kokulan, V., M. L. Macrae, D. A. Lobb, and G. A. Ali. 2019. Contribution of Overland and Tile Flow to Runoff and Nutrient Losses from Vertisols in Manitoba, Canada. J. Environ. Qual. **48**: 959. doi:10.2134/jeq2019.03.0103

Krinner, G. 2003. Impact of lakes and wetlands on boreal climate. J. Geophys. Res. **108**. doi:10.1029/2002JD002597

Leifer, I., J. R. Boles, B. P. Luyendyk, and J. F. Clark. 2004. Transient discharges from marine hydrocarbon seeps: Spatial and temporal variability. *Environmental Geology*. 1038–1052.

Lelieveld, J., P. J. Crutzen, and F. J. Dentener. 1998. Changing concentration, lifetime and climate forcing of atmospheric methane. Tellus, Ser. B Chem. Phys. Meteorol. doi:10.3402/tellusb.v50i2.16030

Liu, Y., W. Yang, Z. Yu, I. Lung, J. Yarotski, J. Elliott, and K. Tiessen. 2014. Assessing Effects of Small Dams on Stream Flow and Water Quality in an Agricultural Watershed. J. Hydrol.

Eng. **19**: 1–14. doi:10.1061/(ASCE)HE.1943-5584.0001005.

St. Louis, Vincent L.; Kelly, Carol A.; Duchemin, Eric.; Rudd, John W.M.; Rosenberg, D. M. 2000. Reservoir Surfaces as Sources of Greenhouse Gases to the Atmosphere : A Global Estimate. Bioscience **50**: 766–775.

Maeck, A., T. Delsontro, D. F. McGinnis, H. Fischer, S. Flury, M. Schmidt, P. Fietzek, and A. Lorke. 2013. Sediment trapping by dams creates methane emission hot spots. Environ. Sci. Technol. **47**: 8130–8137. doi:10.1021/es4003907

Martins, P. D., D. W. Hoyt, S. Bansal, and others. 2017. Abundant carbon substrates drive extremely high sulfate reduction rates and methane fluxes in Prairie Pothole Wetlands. Glob. Chang. Biol. **23**: 3107–3120. doi:10.1111/gcb.13633

McCarty, G. W., and J. C. Ritchie. 2002. Impact of soil movement on carbon sequestration in agricultural ecosystems. Environ. Pollut. **116**: 423–430.

McClain, M. E., E. W. Boyer, C. L. Dent, and others. 2003. Biogeochemical Hot Spots and Hot Moments at the Interface of Terrestrial and Aquatic Ecosystems. Ecosystems **6**: 301–312. doi:10.1007/s10021-003-0161-9

Mitchell, L., E. Brook, J. E. Lee, C. Buizert, and T. Sowers. 2013. Constraints on the late Holocene anthropogenic contribution to the atmospheric methane budget. Science (80-.). doi:10.1126/science.1238920

Mulholland, B. P. J., J. W. Elwood, and E. S. Division. 1982. The role of lake and reservoir sediments as sinks in the perturbed global carbon cycle. Tellus **34**: 490–499.

Ollivier, Q. R., D. T. Maher, C. Pitfield, and P. I. Macreadie. 2019. Punching above their weight: Large release of greenhouse gases from small agricultural dams. Glob. Chang. Biol. **25**: 721–732. doi:10.1111/gcb.14477

Ostrovsky, I. 2003. Methane bubbles in Lake Kinneret: Quantification and temporal and spatial heterogeneity. Limnol. Oceanogr. **48**: 1030–1036. doi:10.4319/lo.2003.48.3.1030

Ostrovsky, I., D. F. McGinnis, L. Lapidus, and W. Eckert. 2008. Quantifying gas ebullition with echosounder: the role of methane transport by bubbles in a medium-sized lake. Limnol. Oceanogr. Methods **6**: 105–118. doi:10.4319/lom.2008.6.105

Pennock, D., T. Yates, A. Bedard-Haughn, K. Phipps, R. Farrell, and R. McDougal. 2010. Landscape controls on N2O and CH4 emissions from freshwater mineral soil wetlands of the Canadian Prairie Pothole region. Geoderma **155**: 308–319.

doi:10.1016/j.geoderma.2009.12.015

Percival, D.B., Walden, A. T. 2000. Wavelet Methods for Time Series Analysis, Cambridge University Press.

Phoenix, G. K., R. E. Booth, J. R. Leake, D. J. Read, J. P. Grime, and J. A. Lee. 2003. Effects of enhanced nitrogen deposition and phosphorus limitation on nitrogen budgets of semi-natural grasslands. Glob. Chang. Biol. **9**: 1309–1321. doi:10.1046/j.1365-2486.2003.00660.x

Premke, K., K. Attermeyer, J. Augustin, and others. 2016. The importance of landscape diversity for carbon fluxes at the landscape level: small-scale heterogeneity matters. WIREs Water **3**: 601–617. doi:10.1002/wat2.1147

Reuman, D. C. ., T. L. . Anderson, J. A. . Walter, L. Zhao, and L. W. Sheppard. 2019. wsyn: Wavelet Approaches to Studies of Synchrony in Ecology and Other Fields. R package version 1.0.1. https://CRAN.R-project.org/package=wsyn

Ricão Canelhas, M., B. A. Denfeld, G. A. Weyhenmeyer, D. Bastviken, and S. Bertilsson. 2016. Methane oxidation at the water-ice interface of an ice-covered lake. Limnol. Oceanogr. **61**: S78–S90. doi:10.1002/lno.10288

Riera, J. L., J. E. Schindler, T. K. Kratz, and C. Lake. 1999. Seasonal dynamics of carbon dioxide and methane in two clear-water lakes and two bog lakes in northern Wisconsin , U . S . A . Can. J. Fish. Aquat. Sci. **56**: 265–274.

Rudd, J. W. M., A. Furutani, R. J. Flett, and R. D. Hamilton. 1976. Factors controlling methane oxidation in shield lakes : The role of nitrogen fixation and oxygen concentration. Limnol. Oceanogr. **21**.

Rudd, J. W. M., and R. D. Hamilton. 1978. Methane cycling in a eutrophic shield lake and its effects on whole lake metabolism. Limnol. Oceanogr. **23**: 337–348.

Rudd, J. W. M., R. Harris, C. A. Kelly, and R. E. Hecky. 1993. Are Hydroelectric Reservoirs Significant Sources of Greenhouse Gases ? Ambio **22**: 246–248.

Ruddiman, W. F. 2005. How did humans first alter global climate? Sci. Am. **292**: 34–41.

Sanders, I. A., C. M. Heppell, J. A. Cotton, G. Wharton, A. G. Hildrew, E. J. Flowers, and M. Trimmer. 2007. Emission of methane from chalk streams has potential implications for agricultural practices. Freshw. Biol. **52**: 1176–1186. doi:10.1111/j.1365-2427.2007.01745.x

Schimel, D. 1995. Terrestrial ecosystems and the carbon cycle. Glob. Chang. Biol. **1**: 77–91. doi:10.1111/j.1365-2486.1995.tb00008.x

Schindler, D. W., and W. F. Donahue. 2006. An impending water crisis in Canada's western prairie provinces. Proc. Natl. Acad. Sci. U. S. A. **103**: 7210–6. doi:10.1073/pnas.0601568103

Schindler, D. W., R. E. Hecky, and G. K. McCullough. 2012. The rapid eutrophication of Lake Winnipeg: Greening under global change. J. Great Lakes Res. **38**: 6–13. doi:10.1016/j.jglr.2012.04.003

Schubert, C. J., T. Diem, and W. Eugster. 2012. Methane emissions from a small wind shielded lake determined by eddy covariance, flux chambers, anchored funnels, and boundary model calculations: A comparison. Environ. Sci. Technol. **46**: 4515–4522. doi:10.1021/es203465x

Schumacher, B. Methods for the determination of total organic carbon (TOC) in soils and sediment.

Schwietzke, S., O. A. Sherwood, L. M. P. Bruhwiler, and others. 2016. Upward revision of global fossil fuel methane emissions based on isotope database. Nature **538**: 88–91. doi:10.1038/nature19797

Segers, R. 1998. Methane production and methane consumption--a review of processes underlying wetland methane fluxes [Review]. Biogeochem. **41**: 23–51. doi:10.1023/A:1005929032764

Sheppard, L. W., J. R. Bell, R. Harrington, and D. C. Reuman. 2016. Changes in large-scale climate alter spatial synchrony of aphid pests. Nat. Clim. Chang. **6**: 610–613. doi:10.1038/nclimate2881

Sheppard, L. W., E. J. Defriez, P. C. Reid, and D. C. Reuman. 2019. Synchrony is more than its top-down and climatic parts: Interacting Moran effects on phytoplankton in British seas. PLoS Comput. Biol. **15**: 1–25. doi:10.1371/journal.pcbi.1006744

Sheppard, L. W., P. C. Reid, and D. C. Reuman. 2017. Rapid surrogate testing of wavelet coherences. EPJ Nonlinear Biomed. Phys. **5**: 1. doi:10.1051/epjnbp/2017000

Slater, L., X. Comas, D. Ntarlagiannis, and M. R. Moulik. 2007. Resistivity-based monitoring of biogenic gases in peat soils. Water Resour. Res. **43**: 1–13. doi:10.1029/2007WR006090

Soumis, N., E. Duchemin, R. Canuel, and M. Lucotte. 2004. Greenhouse gas emissions from reservoirs of the western United States. Global Biogeochem. Cycles **18**: 1–11. doi:10.1029/2003GB002197

Stallard, R. F. 1998. Terrestrial sedimentation and the carbon cycle: Coupling weathering and

erosion to carbon burial. Global Biogeochem. Cycles **12**: 231–257. doi:10.1029/98GB00741

Stanley, E. H., N. J. Casson, S. T. Christel, J. T. Crawford, L. C. Loken, and S. K. Oliver. 2016. The ecology of methane in streams and rivers: Patterns, controls, and global significance. Ecol. Monogr. **86**: 146–171. doi:10.1890/15-1027.1

Steffen, W., K. Richardson, J. Rockström, and others. 2015. Planetary boundaries : Guiding changing planet. Science (80-.). doi:10.1126/science.1259855

Syvitski, J. P. M., C. J. Vo, A. J. Kettner, and P. Green. 2005. Impact of Humans on the Flux of Terrestrial Sediment to the Global Coastal Ocean. Science (80-.). **308**: 376–381.

Tangen, B. a, R. G. Finocchiaro, and R. a Gleason. 2015. Effects of land use on greenhouse gas fluxes and soil properties of wetland catchments in the Prairie Pothole Region of North America. Sci. Total Environ. **533**: 391–409. doi:10.1016/j.scitotenv.2015.06.148

TCMW. 2004. Tobacco Creek Model Watershed: People, landscape, planning, action.

Themelis, N. J., and P. A. Ulloa. 2007. Methane generation in landfills. Renew. Energy. doi:10.1016/j.renene.2006.04.020

Tiessen, K. H. D., J. A. Elliott, M. Stainton, J. Yarotski, D. N. Flaten, and D. a. Lobb. 2011. The effectiveness of small-scale headwater storage dams and reservoirs on stream water quality and quantity in the Canadian Prairies. J. Soil Water Conserv. **66**: 158–171. doi:10.2489/jswc.66.3.158

Tokida, T., T. Miyazaki, M. Mizoguchi, O. Nagata, F. Takakai, A. Kagemoto, and R. Hatano. 2007. Falling atmospheric pressure as a trigger for methane ebullition from peatland. Global Biogeochem. Cycles **21**: 1–8. doi:10.1029/2006GB002790

Tremblay, A., M. Lambert, and L. Gagnon. 2004. Do hydroelectric reservoirs emit greenhouse gases? Environ. Manage. **33**: 509–517. doi:10.1007/s00267-003-9158-6

Tubiello, F. N., M. Salvatore, R. D. Cóndor Golec, and others. 2014. Agriculture , Forestry and Other Land Use Emissions by Sources and Removals by Sinks.

Varadharajan, C., and H. F. Hemond. 2012. Time-series analysis of high-resolution ebullition fluxes from a stratified, freshwater lake. J. Geophys. Res. Biogeosciences **117**: 1–15. doi:10.1029/2011JG001866

Varadharajan, C., R. Hermosillo, and H. F. Hemond. 2010. A low-cost automated trap to measure bubbling gas fluxes. Limnol. Oceanogr. Methods **8**: 363–375.

doi:10.4319/lom.2010.8.363

Venkiteswaran, J. J., S. L. Schiff, V. L. St. Louis, C. J. D. Matthews, N. M. Boudreau, E. M. Joyce, K. G. Beaty, and R. A. Bodaly. 2013. Processes affecting greenhouse gas production in experimental boreal reservoirs. Global Biogeochem. Cycles **27**: 567–577. doi:10.1002/gbc.20046

Walter, K. M., S. A. Zimov, J. P. Chanton, D. Verbyla, and F. S. C. Iii. 2006. Methane bubbling from Siberian thaw lakes as a positive feedback to climate warming. Nature **443**: 71–75. doi:10.1038/nature05040

Washburn, L., C. Johnson, C. C. Gotschalk, and E. Thor Egland. 2001. A gas-capture buoy for measuring bubbling gas flux in oceans and lakes. J. Atmos. Ocean. Technol. **18**: 1411–1420. doi:10.1175/1520-0426(2001)018<1411:AGCBFM>2.0.CO;2

Webb, J. R., N. M. Hayes, G. L. Simpson, P. R. Leavitt, H. M. Baulch, and K. Finlay. 2019. Widespread nitrous oxide undersaturation in farm waterbodies creates an unexpected greenhouse gas sink. Proc. Natl. Acad. Sci. **116**: 9814–9819. doi:10.1073/pnas.1820389116

Wei Min Hao, and D. E. Ward. 1993. Methane production from global biomass burning. J. Geophys. Res.

Weyhenmeyer, C. E. 1999. Methane Emissions from Beaver Ponds: Rates, patterns, and transport mechanisms. Global Biogeochem. Cycles **13**: 1079–1090.

Weyhenmeyer, G. A., S. Kosten, M. B. Wallin, L. J. Tranvik, E. Jeppesen, and F. Roland. 2015. Significant fraction of CO2 emissions from boreal lakes derived from hydrologic inorganic carbon inputs. Nat. Geosci. **8**: 933–936. doi:10.1038/ngeo2582

Whitfield, C. J., J. Aherne, and H. M. Baulch. 2011. Controls on greenhouse gas concentrations in polymictic headwater lakes in Ireland. Sci. Total Environ. **410**–**411**: 217–225. doi:10.1016/j.scitotenv.2011.09.045

Whitfield, C. J., N. J. Casson, R. L. North, and others. 2019. The effect of freeze-thaw cycles on phosphorus release from riparian macrophytes in cold regions. Can. Water Resour. J. **44**: 160–173. doi:10.1080/07011784.2018.1558115

Whitfield, C. J., T. A. Seabert, J. Aherne, and S. A. Watmough. 2010. Carbon dioxide supersaturation in peatland waters and its contribution to atmospheric efflux from downstream boreal lakes. J. Geophys. Res. Biogeosciences **115**: 1–10. doi:10.1029/2010JG001364

Whiting, G. J., and J. P. Chanton. 1993. Primary production control of methane emission from wetlands. Nature **364**: 794.

Wik, M., B. F. Thornton, D. Bastviken, J. Uhlbäck, and P. M. Crill. 2016. Biased sampling of methane release from northern lakes: A problem for extrapolation. Geophys. Res. Lett. **43**: 1256–1262. doi:10.1002/2015GL066501

Wilson, J. O., P. M. Crill, K. B. Bartlett, D. I. Sebacher, C. Robert, R. L. Sass, and R. C. Harriss. 1989. Seasonal Variation of Methane Emissions from a Temperate Swamp Seasonal variation of methane emissions from a temperate swamp. Biogeochemistry **8**: 55–71. doi:10.1007/BF02180167

Wolf, J., G. R. Asrar, and T. O. West. 2017. Revised methane emissions factors and spatially distributed annual carbon fluxes for global livestock. Carbon Balance Manag. **12**. doi:10.1186/s13021-017-0084-y

Yarotski, J. 1996. South Tobacco Creek Pilot Project: Effect of Headwater Storage on Runoff Peaks.

Zehnder, A. J. B., and W. Stumm. 1988. Geochemistry and Biogeochemistry of anaerobic habitats, *In* A.J.B. Zehnder [ed.], Biology of anaerobic microorganisms. Wiley.

Zeikus, J. G., and M. R. Winfrey. 1976. Temperature limitation of methanogenesis in aquatic sediments. Appl. Environ. Microbiol.

Appendix A: Supplementary information chapter 2 (A novel sensor for automated high temporal resolution measurement of ebullition from shallow lentic systems)

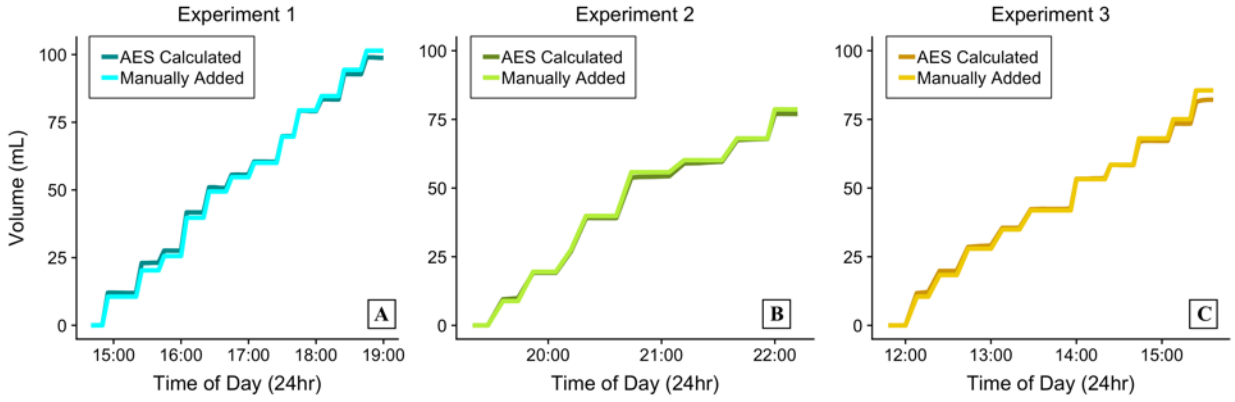

Figure A.2: Time-series comparison of the manually added volume (mL) with the AES calculated volume output (mL) over the duration of trials one (A), two (B), and three (C).

Appendix B: Supplemental information chapter 3 (Methane flux from agricultural reservoirs: rates and drivers of ebullition)

Table B.1: Comparison table of CH_4 flux at TCR08 prior to and during 2018 reservoir drawdown experiment.

	3rd Period Prior AES = 1 day	**2nd Period Prior** AES = 1 day BT = 13.1 days	**1st Period Prior** AES = 1 day BT = 6.1 days	**During DD** AES = 0.4 day BT = 0.94 day
AESv1_Stn1	111	156	90	942.9
AESv1_Stn2	—	—	—	1581.2
AESv1_Stn3	—	—	—	679.1
BT1A	—	34.8	589.8	1086.5
BT1B	—	18.1	76.8	846.3
BT2D	—	67	41.1	87.9
BT3E	—	37.4	131.3	428.5
BT3F	—	45.1	175.1	357.1

*All values are in (mL m^{-2} d^{-1})

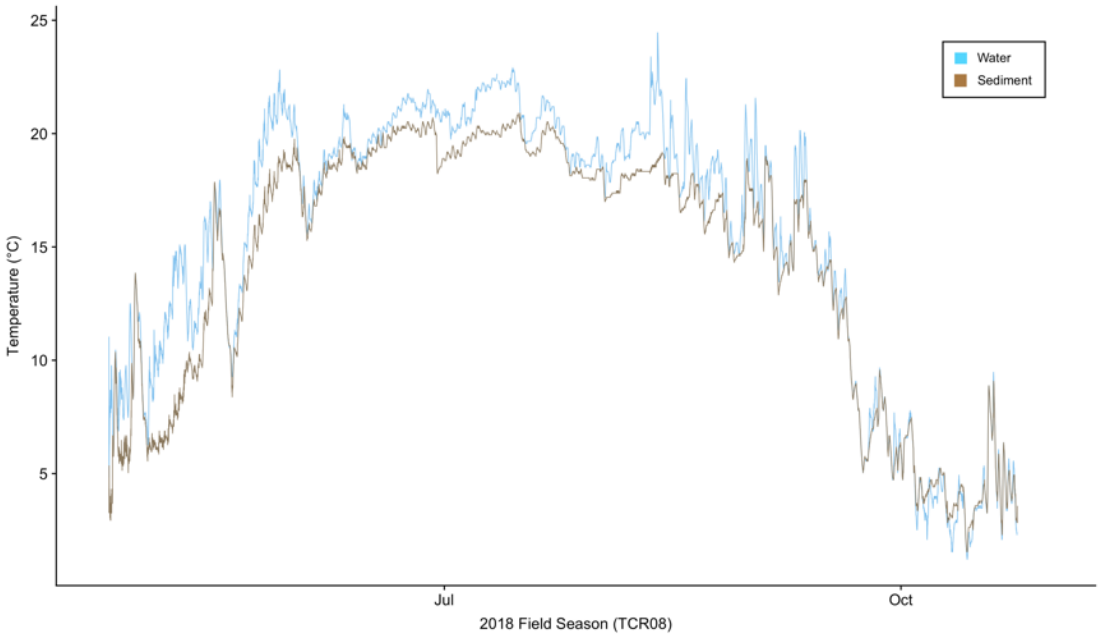

Figure B.1: Plot demonstrating seasonal record comparison of HOBO temperature pendant logger (UA-002-08) inserted directly into the sediments, with HOBO temperature logger (U20L-04) at TCR08 in 2018.

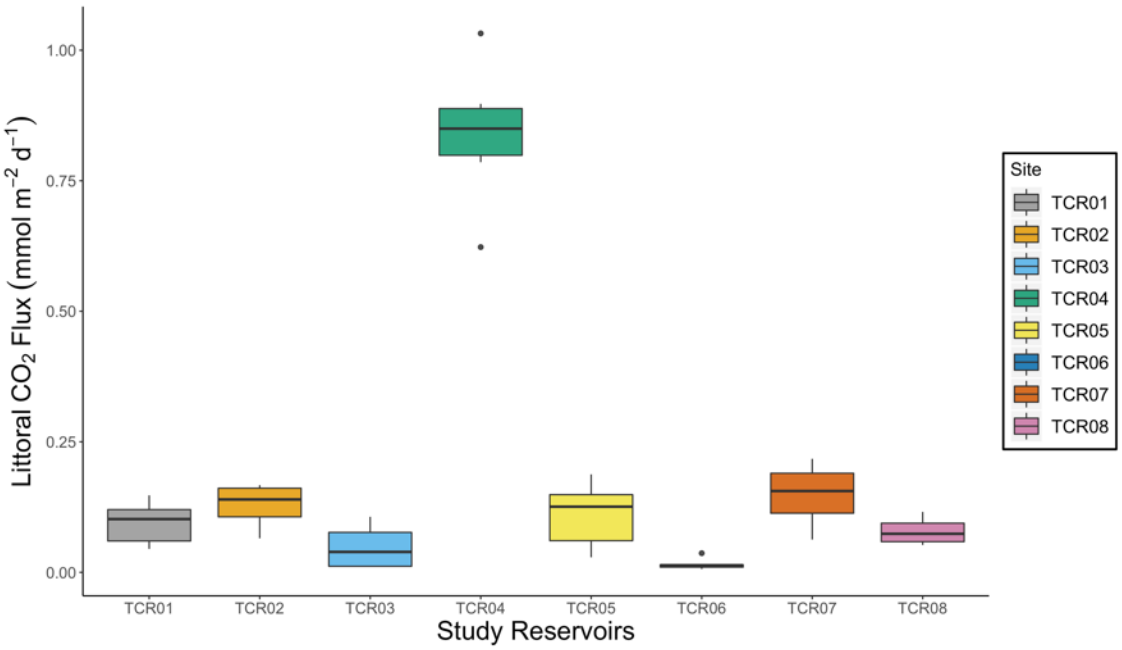

Figure B.2: Boxplots of the range in total littoral CO_2 flux via ebullition in 2017. The boxplot displays data distribution (median, two hinges (25^{th} and 75^{th} percentiles), two whiskers (max and min range), and outlying points).

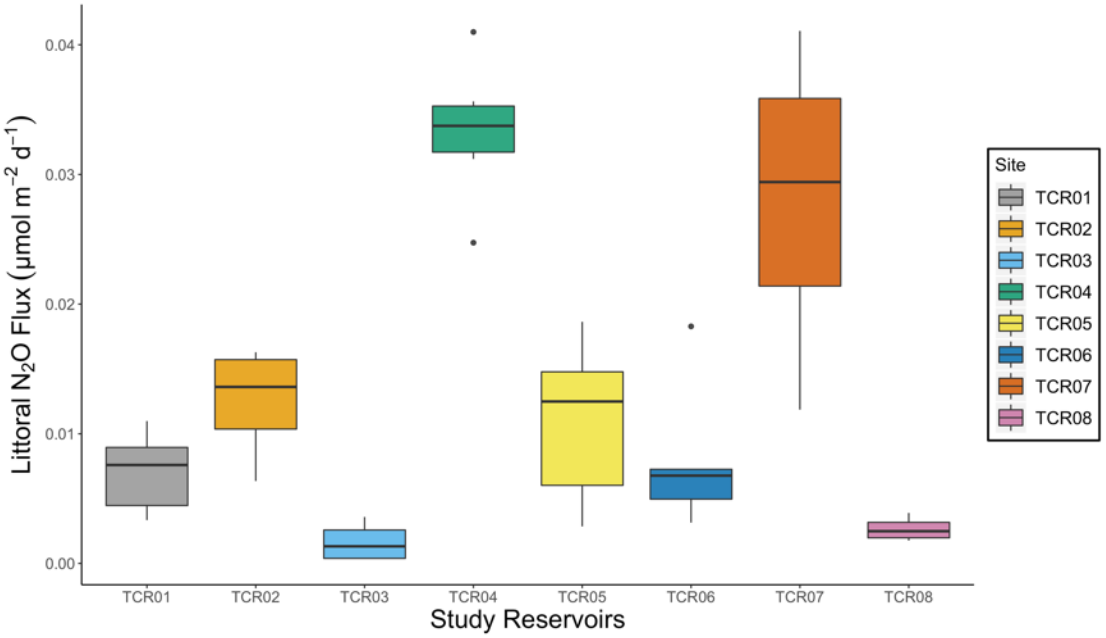

Figure B.3: Boxplots of the range in total littoral N_2O flux via ebullition in 2017. The boxplot displays data distribution (median, two hinges (25^{th} and 75^{th} percentiles), two whiskers (max and min range), and outlying points).

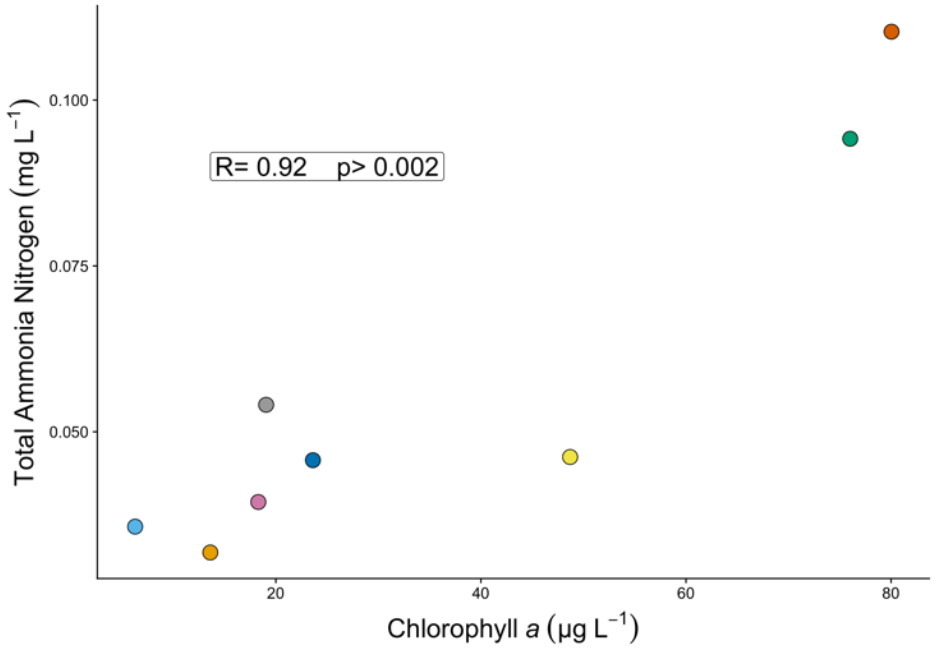

Figure B.4: Scatterplot of select water chemistry parameters (chlorophyll *a* and TAN) linked to primary productivity.

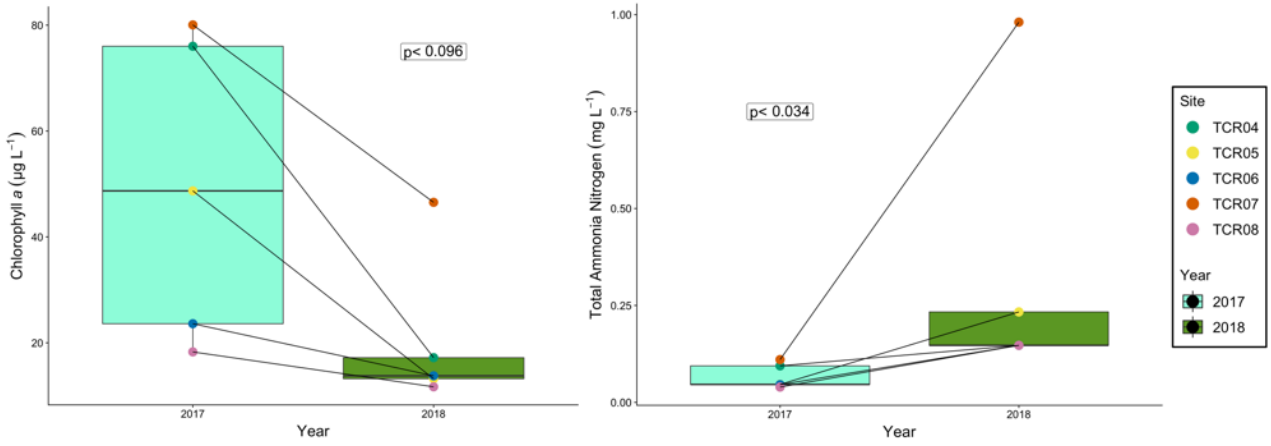

Figure B.5: Interannual variation (2017 and 2018) of mean open-water chlorophyll *a* (left panel) and total ammonia nitrogen concentrations (right panel) of the study reservoirs; *p*-values Bonferroni corrected. The boxplot displays data distribution (median, two hinges (25th and 75th percentiles), two whiskers (max and min range), and outlying points).

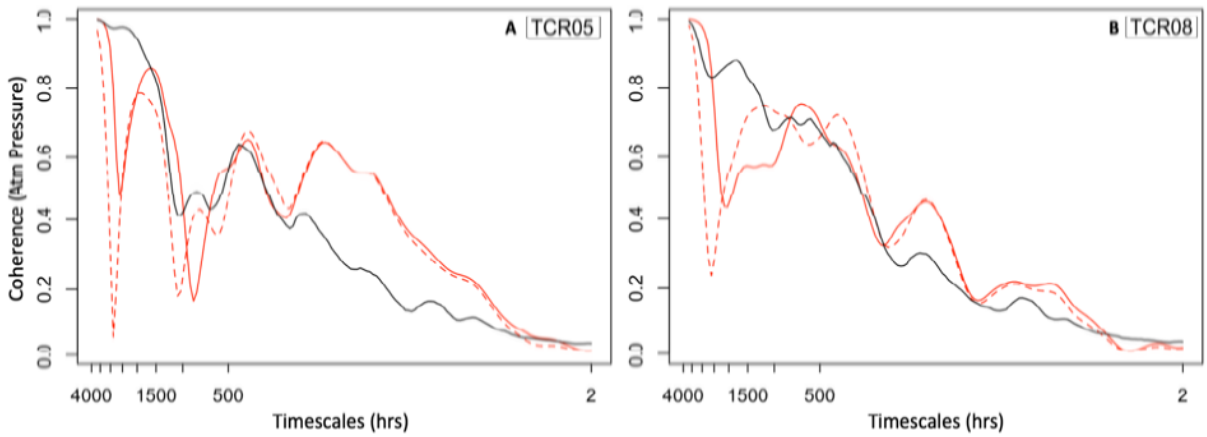

Figure B.6: Plots of the coherence between wavelet transforms of ebullition and atmospheric pressure at varying timescales at TCR05 (A) and TCR08 (B). The solid black line indicates the significant threshold (i.e. 95% confidence interval) between the two variables across the range of timescales (hours). Coherence between wavelet transformed variables is significant when either red line is above the black line; solid red line indicates default algorithm, while the dashed red line is the alternate "fast" algorithm. While the two lines are typically similar, the "fast" algorithm is used to make conclusions about significance of coherence.

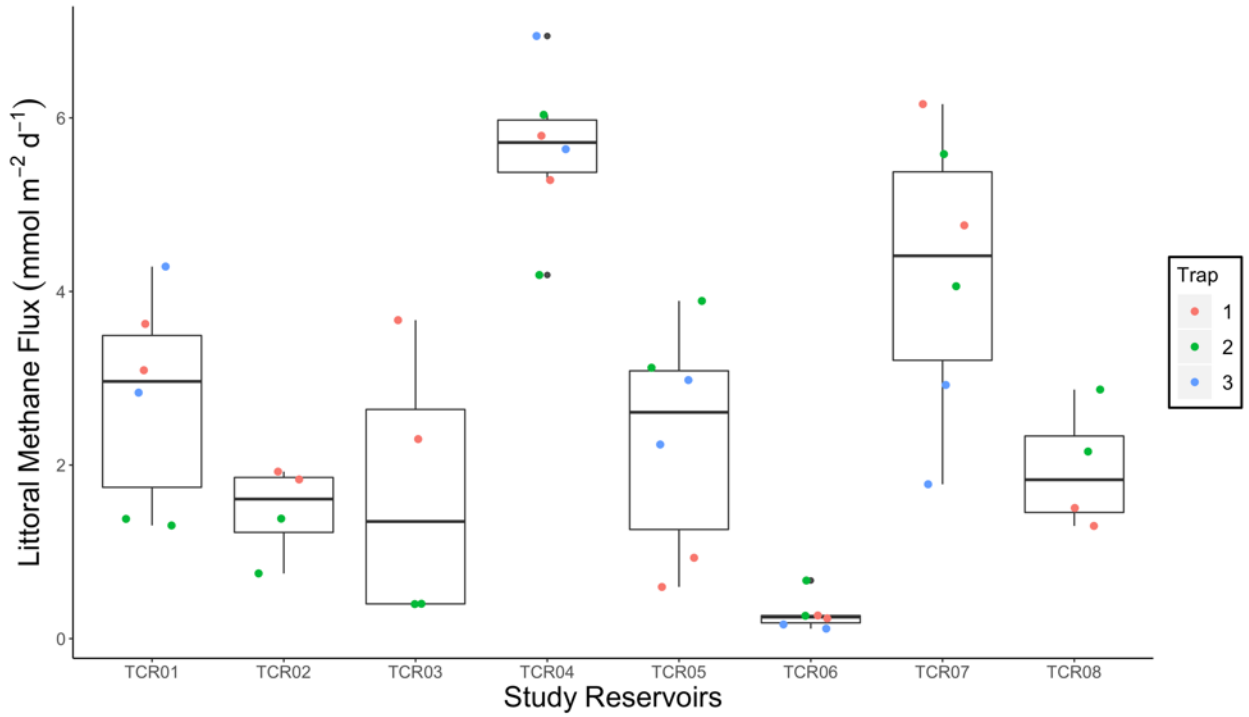

Figure B.7: Boxplots of the range in total annual littoral CH_4 flux demonstrated in 2017; demonstrating location range of flux within reservoir; near dam outlet, middle of reservoir and reservoir inlet are Trap 1, Trap 2 and Trap 3, respectively. The boxplot displays data distribution (median, two hinges (25^{th} and 75^{th} percentiles), two whiskers (max and min range), and outlying points).

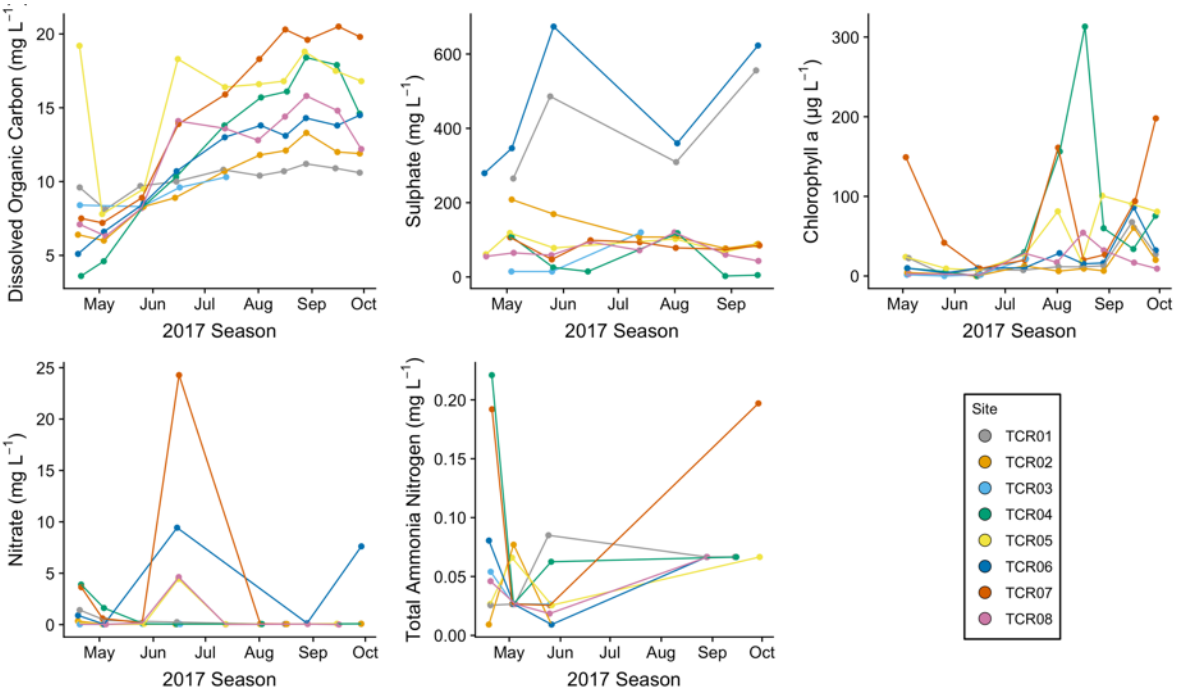

Figure B.8: Seasonal trend of select core analytes at all 2017 study sites.

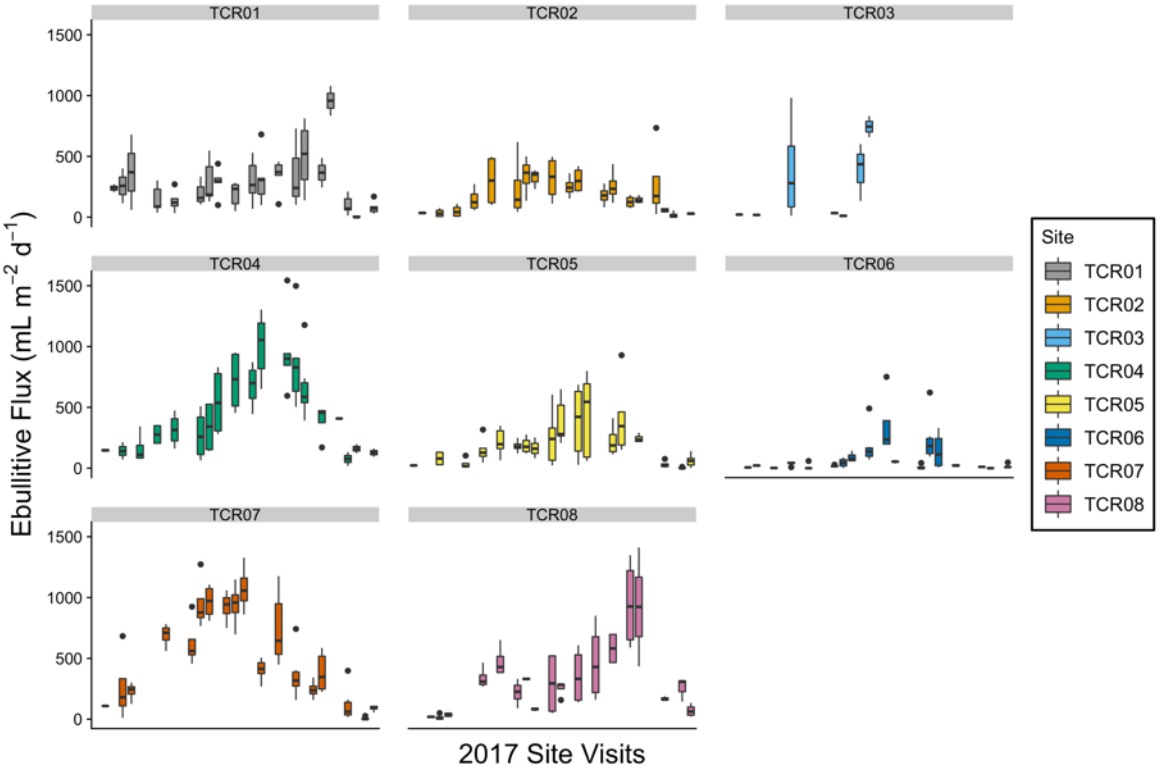

Figure B.9: Range in littoral ebullitive flux during each site visit, over the 2017 deployment season. The boxplot displays data distribution (median, two hinges (25th and 75th percentiles), two whiskers (max and min range), and outlying points).

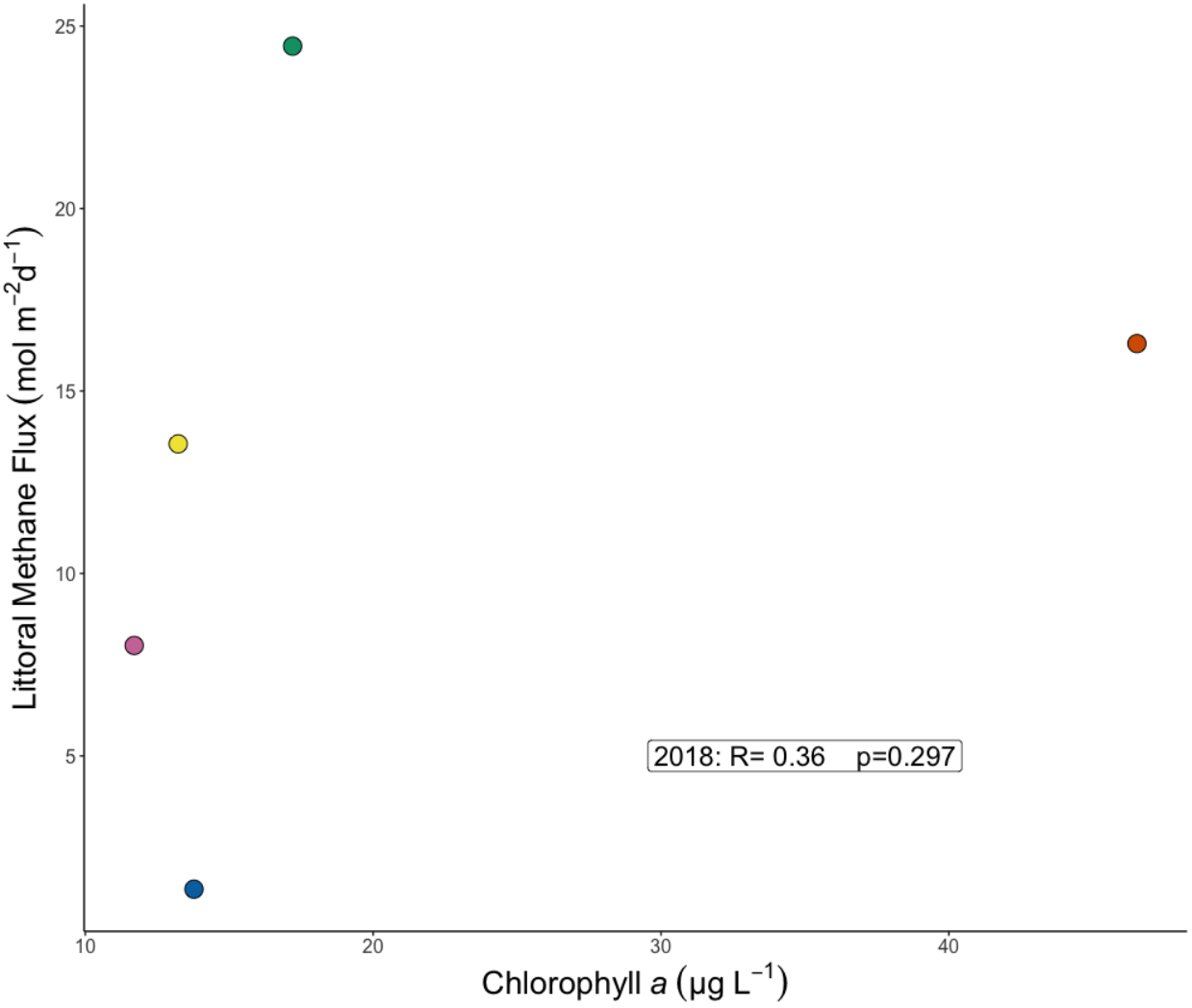

Figure B.10: Scatterplot of littoral ebullitive CH_4 and chlorophyll *a* during the 2018 field season.